Acta Orthopaedica

Microarchitectural adaptations in aging and osteoarthrotic subchondral bone tissues

Ming Ding

Supplementum no 340 Volume 81 February 2010

Orthopaedic Research Laboratory
Department of Orthopaedics
Aarhus University Hospital
Faculty of Health Sciences
Aarhus University
Denmark
2009

Microarchitectural adaptations in aging and osteoarthrotic subchondral bone tissues

Ming Ding

ACTA ORTHOPAEDICA SUPPLEMENTUM NO. 340, VOL. 81, 2010

informa
healthcare

Contact address

Ming Ding, M.D., Ph.D.
Associate Professor
Orthopaedic Research Laboratory
Department of Orthopaedics O
Odense University Hospital
Institute of Clinical Research
University of Southern Denmark
J.B. Winsloewsvej 15, 3rd floor
DK-5000 Odense C, Denmark
Phone: + 45 6541 3598, Fax: +45 6541 4558
ming.ding@ouh.regionsyddanmark.dk

Denne afhandling er i forbindelse med nedenstående anførte tidligere offentliggjorte artikler af Det Sundhedsvidenskabelige Fakultet ved Aarhus Universitet antaget til offentligt at forsvares for den medicinske doktorgrad.
Aarhus Universitet, den 5. november 2009
Søren Mogensen
Dekan

Forsvaret finder sted fredag den 26. februar 2010, kl. 14.00 præcis i Auditorium 424, Anatomisk Institut, Aarhus Universitet.

 ISSN 1745–3674. Printed in Sweden
DOI 10.3109/17453671003619037

Printed in Sweden
Wallin & Dalholm
2010

List of Papers

This thesis is based on the following 9 publications, which will be referred to in the text by their Roman numerals (I–IX):

I. Ding M, Odgaard A, Hvid I. Accuracy of cancellous bone volume fraction measured by micro-CT scanning. J Biomech 1999; 32: 323-326. [**49**]

II. Ding M, Hvid I. Quantification of age-related changes in the structure model type and trabecular thickness of human tibial cancellous bone. Bone 2000; 26: 291-295. [**47**]

III. Ding M, Odgaard A, Linde F, Hvid I. Age-related variations in the microstructure of human tibial cancellous bone. J Orthop Res 2002a; 20: 615-621. [**51**]

IV. Ding M, Odgaard A, Danielsen CC, Hvid I. Mutual associations among microstructural, physical and mechanical properties of human cancellous bone. J Bone Joint Surg (Br) 2002b; 84-B: 900-907. [**48**]

V. Ding M, Danielsen CC, Hvid I. Bone density does not reflect mechanical properties in early-stage arthrosis. Acta Orthop Scand 2001; 72: 181-185. [**42**]

VI. Ding M, Odgaard A, Hvid I. Changes in the three-dimensional microstructure of human tibial cancellous bone in early osteoarthritis. J Bone Joint Surg (Br) 2003; 85(6): 906-912. [**50**]

VII. Ding M, Danielsen CC, Hvid I. Age-related three-dimensional microarchitectural adaptations of subchondral bone tissues in guinea pig primary osteoarthrosis. Calcif Tissue Int 2006; 78(2): 113-122. [**44**]

VIII. Ding M, Danielsen CC, Hvid I. Effects of hyaluronan on three-dimensional microarchitecture of subchondral bone tissues in guinea pig primary osteoarthrosis. Bone 2005; 36(3): 489-501. [**43**]

IX. Ding M, Danielsen CC, Hvid I. The effects of bone remodeling inhibition by alendronate on three-dimensional microarchitecture of subchondral bone tissues in Guinea pig primary osteoarthrosis. Calcif Tissue Int 2008; 82: 77-86. [**45**]

Preface

This thesis is based on the investigations performed at the Orthopaedic Research Laboratory, Department of Orthopaedics, Aarhus University Hospital, and Faculty of Health Sciences, Aarhus University, Denmark during a senior research fellowship in the period 1999 to 2003. All experimental investigations were carried out at Orthopaedic Research Laboratory (Department of Orthopaedics, Aarhus University Hospital) in close collaboration with Department of Connective Tissue Biology (Institute of Anatomy, Aarhus University). The publications of articles, in the period of 1999 to 2008, were made mainly at the Orthopaedic Research Laboratory (Aarhus University Hospital), and the manuscripts of the last 3 publications were prepared at the Orthopaedic Research Laboratory (Odense University Hospital).

I would like to express my profound gratitude to Professor Ivan Hvid for introducing me to the field of orthopaedic research and for his enthusiastic support, stimulating criticism, and inspiring atmosphere. I wish to express my gratitude to Professor Otto Sneppen for his everlasting support during the experiments. I wish to thank all my scientific co-authors: Associate Professors Carl Christian Danielsen, Anders Odgaard and Frank Linde for their invaluable time and many pleasant hours of discussion and for their great contribution to the studies.

I am very grateful to Associate Professor Michel Dalstra for valuable advice in mechanical test, and to Eva Mikkelsen, Jane Pauli and Anette Milton for their skilful technical assistance. I would like to thank the entire Orthopaedic Research Laboratory staff and the Department of Orthopaedics for an inspiring atmosphere. A special thank goes to Professor Søren Overgaard and Director Chief Consultant Niels Dieter Röck, Department of Orthopaedics, Odense University Hospital for their great support during my position as associate professor in Odense since January 2004.

My warmest thanks should go to my wife Na Lin and our children Yanyan and Oliver for their never-ending love and support throughout the work.

Financial supports for these studies were kindly granted by the Danish Health Research Council; the Danish Rheumatism Association; the Orthopaedic Research Foundation; Aarhus University Hospital; the Institute of Clinical Medicine, Aarhus University; Peter Ryholts Legat; Rektorkollegiet; Hørslevfonden; Helga og Peter Kornings Fond, Denmark. Thanks to the European Commission Research Directorates (5th Framework) for a Senior Fellowship.

Ming Ding

Structure of the thesis

This review concentrates on human aging and osteoarthrosis-related three-dimensional (3D) microarchitectural and mechanical adaptations, bone collagen and mineral qualities of subchondral bone tissues. The review consists of an appraisal of recent investigations, methodological considerations and results of own studies: study I to study IX. Furthermore, recent studies on the property changes of normal aging and the most common age-related musculoskeletal degenerative diseases – osteoarthrosis, osteoporosis and rheumatoid arthritis are highlighted and summarized in the discussion section. The conclusion and summary based on own studies are presented, and suggestions for future studies are also proposed.

Contents

Abstract

The human skeleton optimizes its microarchitecture by elaborate adaptations to mechanical loading during development and growth. The mechanisms for adaptation involve a multistep process of cellular mechanotransduction stimulating bone modelling, and remodeling resulting in either bone formation or resorption. This process causes appropriate microarchitectural changes tending to adjust and improve the bone structure to its prevailing mechanical environment.

Normal individual reaches peak bone mass at age between 25 and 30 years, and thereafter bone mass declines with age in both genders. The bone loss is accompanied by microarchitectural deterioration resulting in reduced mechanical strength likely leading to fragility fractures. With aging, inevitable bone loss occurs, which is frequently the cause of osteoporosis; and inevitable bone and joint degeneration happens, which often results in osteoarthrosis. These diseases are among the major health care problems in terms of socio-economic costs.

The overall goals of the current series of studies were to investigate the age-related and osteoarthrosis (OA) related changes in the 3-D microarchitectural properties, mechanical properties, collagen and mineral quality of subchondral cancellous and cortical bone tissues. The studies included mainly two parts. For human subjects: aging- (I–IV) and early OA-related (V–VI) changes in cancellous bone properties were assessed. For OA guinea pig models (VII–IX), three topics were studied: firstly, the spontaneous, age-related development of guinea pig OA; secondly, the potential effects of hyaluronan on OA subchondral bone tissues; and thirdly, the effects on OA progression of an increase in subchondral bone density by inhibition of bone remodeling with a bisphosphonate. These investigations aimed to obtain more insight into the age-related and OA-related subchondral bone adaptations.

Microarchitectural adaptation in human aging cancellous bone

The precision of micro-CT measurement is excellent. Accurate 3-D micro-CT image datasets can be generated by applying an appropriate segmentation threshold. A fixed threshold may be used to obtain reliable volume fraction data, and this fixed threshold may be determined from the Archimedes-based volume fraction of a subgroup of specimens (I).

Based on accurately generated micro-CT datasets, age-related microarchitectural changes of human tibial cancellous bone have been demonstrated (II, III). Apart from connectivity, all measured microarchitectural properties correlate significantly with age. However, age-related changes in the properties of human tibial cancellous bone do not follow the same pattern, nor do they occur at the same age. The observed increase of anisotropy and the constant nature of connectivity suggest an important bone remodeling mechanism that normal aging tibia may adapt trabecular volume orientation. Namely, that the aging trabeculae align preferentially to the primary loading direction to compensate bone loss (III). Age-related changes in trabecular thickness and structure type become significant first after 80 years of age. The plate-like structure reflects high mechanical stress whereas rod-like structure reflects low mechanical stress (II). Trabecular structure type and bone volume fraction correlates strongly. Trabecular structure type together with anisotropy correlates well with the Young's modulus. The most effective microarchitectural properties for predicting the mechanical properties of cancellous bone seem to differ with age (IV).

Microarchitectural adaptation in human osteoarthrotic subchondral bone

In early human OA subchondral cancellous bone, none of the mechanical properties of cancellous bone can be predicted by the measured physical/compositional properties (V). The increased trabecular thickness and density, but relatively decreased connectivity suggests a mechanism of bone remodeling in early OA as a process of filling trabecular cavities. This process leads to a progressive change of trabeculae from rod-like to plate-like, the opposite to that of normal ageing. The increase in bone tissue accompanied with deteriorated microarchitecture in early-stage OA cancellous bone does not account for the loss of mechanical properties, which suggests deterioration in the quality of OA cancellous bone (VI).

Microarchitectural adaptation in guinea pig osteoarthrotic subchondral bone

Age-related pronounced changes of the microarchitecture and bone matrix composition of the subchondral bone tissues in guinea pig have been demonstrated. These changes do not appear to follow the same pattern as in normal aging and may have different influences on the resulting mechanical properties (VII).

Intra-articular injection of hyaluronan effectively protects against cartilage degeneration in guinea pig primary OA. The decrease of subchondral bone density and thickness and change of trabecular structure toward rod-like result in more compliant subchondral bone and thereby reduces cartilage stress during impact loading. Moreover, hyaluronan maintains the mechanical properties of cancellous bone likely through increasing its mineralization. Early administration of hyaluronan is effective for intervention of OA initiation and progression, and short-term early HA treatment is sufficient to maintain treatment effects in OA guinea pig model (VIII).

The inhibition of bone remodeling by ALN leads to significant increase of subchondral bone mass and bone mineral content, and marked changes of microarchitecture. Furthermore, the resulting increased bone mass accelerates articular cartilage degeneration at the medial condyle and, to some extent, at the lateral condyle. These results suggest that increased subchondral bone density promotes OA progression and call for circumspection in using bone density–enhancing drugs for intervention of primary OA (IX).

Conclusion

Age-related musculoskeletal diseases increase as a result of increase in the elderly population and a change in lifestyle. Over the last a few decades, much significant research on the properties has been carried out on diseases such as age-related bone fracture, prosthetic loosening, bone remodeling, and degenerative bone diseases on both axial central vertebra and peripheral trabecular bone. We have now achieved a great deal of knowledge on normal aging- and diseases-related changes in bone properties and quality. This knowledge is of major importance for the understanding of degenerative bone diseases, and for the design, fixation, survival of joint prosthesis, functional adaptation of host bone; and for application of biomaterials regarding interface reaction, fracture repair and defect healing. Understanding the microarchitectural properties, mechanical adaptations, and collagen and mineral qualities of subchondral bone tissues highlighted in these studies may help to gain more insights into the pathogenesis of degenerative bone diseases and to target and develop novel approaches for the intervention and treatment.

Key words:

Three-dimensional reconstruction; microarchitectural properties; microarchitectural adaptation; micro-CT; mechanical properties; collagen; mineral; aging; osteoarthrosis; osteoporosis; rheumatoid arthritis; subchondral bone tissues; bone quality; human; guinea pig

Definitions

Three-dimensional microarchitectural properties

Cancellous bone

From accurately segmented 3-D reconstruction of micro-CT imaging datasets, detailed microarchitectural (or microstructural) parameters of cancellous bone (trabecular bone, or spongy bone) can be quantified based on novel, unbiased, assumption-free 3-D methods. These microarchitectural characteristics are summarized as the followings (see more detail in the text).

- ***Architectural anisotropy (DA):*** Reflects preferential orientation of trabeculae, namely, its main direction and the degree of dispersion around it. Anisotropy can be quantified based on a 3-D volume method: star volume distribution (SVD), or mean intercept length method (MIL). Primary degree of anisotropy (DA_{1-3}) is calculated as the eigenvalue of the primary direction divided by the eigenvalue of the tertiary direction; secondary degree of anisotropy (DA_{1-2}) is calculated as the eigenvalue of the primary direction divided by the eigenvalue of the secondary direction; tertiary degree of anisotropy (DA_{2-3}) is calculated as the eigenvalue of the secondary direction divided by the eigenvalue of the tertiary direction. Unit: dimensionless.
- ***Connectivity density (CD):*** Reflects the fundamental property of 3-D trabecular networks, and is quantified in an unbiased and model-free manner by the Euler number from 3-D images using a topological approach. Connectivity density is standardized by total specimen volume. Unit: mm^{-3}.
- ***Bone volume fraction (BV/TV, or Vv):*** A dimensionless unit, and is calculated as bone volume of a specimen divided by its total volume. Unit: percent.
- ***Porosity (p):*** Calculated as "1 – cancellous bone volume fraction". Porosity is defined as void volume per unit volume of whole bone (total specimen volume), i.e. the sum of its total volume minus trabecular volume. "p" is used to designate porosity, a dimensionless ratio. Unit: percent.
- ***Structure model index (SMI):*** Cancellous bone structure type can be assessed by calculating the structural model index. This technique is able to quantify the type of structure, such as plate, rod or spherical objects, and mixtures of plates and rods. The SMI is calculated from 3-D image analysis using a differential analysis of the triangulated bone surface of the structure. The SMI characterizes a 3-D bone structure composed of a certain amount of plates and rods. The SMI is defined as a value between 0 and 3. In an ideal plate structural model, the SMI value is 0, and in an ideal cylindrical rod structure, the SMI value is 3, independent of the physical dimensions of the structure. Thus, the SMI lies between 0 and 3 when a structure consists of both plates and rods of equal thickness, depending on the volume ratio of rods and plates. Unit: dimensionless.
- ***Trabecular thickness (TbTh*):*** The mean trabecular thickness of cancellous bone is calculated directly from 3-D micro-CT images independent of an assumed structure type. The volume-based local thickness is determined as the diameter of the maximal sphere that includes every point and that can be fitted completely inside the structure. This technique allows quantification of the mean thickness of any structure, e.g., geometrical objects like plates, cylinders, or balls. Sometimes, asterisk is used to designate the true value from 3D method. Unit: μm.
- ***Trabecular separation (TbSp*):*** Calculated as mean distance between trabeculae. Unit: μm.
- ***Bone surface density (BS/TV):*** Calculated as bone surface area of the specimen divided by its total volume. Unit: mm^{-1} or mm^2/mm^3.
- ***Bone surface-to-volume ratio (BS/BV):*** Calculated as bone surface area of the specimen divided by bone volume of the specimen. Unit: mm^{-1} or mm^2/mm^3.
- ***Mean trabecular volume (MTV):*** Calculated as the total bone volume of the specimen divided by its "connectivity+1". Unit: $μm^3$.
- ***Mean marrow space volume (MMSV):*** Calculated as the total marrow space volume of the specimen divided by its "connctivity+1". Unit: $μm^3$.
- ***Trabecular number (TbN):*** 3-D trabecular number is calculated from micro-CT images. Volume-weighted mean 3-D trabecular number is calculated as the diameter of the maximal sphere that fills into the background of the mid-axis-transformed object. Unit: mm^{-1}.

Cortical bone

Similarly, from accurately segmented 3-D reconstruction micro-CT imaging datasets, meaningful microarchitectural parameters of cortical bone (or compact bone) can be quantified as well. These microarchitectural characteristics are summarized as the followings.

- ***Bone volume fraction (BV/TV):*** Calculated as bone volume of a specimen divided by its total cortical bone volume. Unit: percent.
- ***Cortical bone porosity (cavity/perforation):*** Calculated as "1 – cortical bone volume fraction". Like cancellous bone porosity, cortical porosity is defined as void volume per unit volume of whole bone (total specimen volume), i.e. the sum of its total volume minus cortical bone volume. "p" is used to designate porosity, a dimensionless ratio. Unit: percent.
- ***Thickness of cortex (CtTh*):*** The mean cortical thickness

is calculated directly from 3-D micro-CT image datasets using the volume-based local thickness methods. Unit: μm.
- ***Bone surface density (BS/TV):*** Calculated as cortical bone surface area of the specimen divided by its total volume. Unit: mm^{-1} or mm^2/mm^3.
- ***Cortical cross-sectional area:*** The cross sectional area of cortical bone is calculated from entire micro-CT 2-D image slices as the mean value obtained from the midshaft cortical bone or subchondral cortical bone. Unit: mm^2.

Physical/compositional properties

- ***Tissue density*** (ρ_{tiss})***:*** Reflects the mineralized bone tissue (material) density, determined from Archimedes' principle, and calculated as dry weight of the specimen divided by the volume of bone matrix excluding marrow space. Unit: g/cm^3.
- ***Apparent density*** (ρ_{app})***:*** Reflects the mineralized bone apparent (structural) density, and calculated as dry weight of specimen divided by the total volume of specimen. Unit: g/cm^3
- ***Apparent ash density*** (ρ_{ash})***:*** Reflects the mineralized bone non-organic density, and is calculated as ash weight divided by the total volume of specimen. Unit: g/cm^3
- ***Mineral concentration*** (C_{min})***:*** Calculated as the total mineral content (ash weight) of the specimen divided by the total dry weight of the specimen. Unit: percent.
- ***Collagen density*** (ρ_{coll})***:*** Reflects the bone organic density, and calculated as total collagen weight divided by the total volume of specimen. Unit: g/cm^3
- ***Collagen concentration*** (C_{coll})***:*** Calculated as the total collagen weight of the specimen divided by the total dry weight of the specimen. Unit: percent.
- ***Collagen/Mineral ratio (C/M):*** Calculated as the percent collagen of the specimen divided by the percent mineral of the specimen, reflecting degree of mineralization. Unit: dimensionless.

Mechanical properties

Any material with a linear elastic component under uniaxial loading can be described by a proportional relationship between change in load and change in length of the material. During mechanical testing, a force-deformation curve is obtained. This curve can be converted to stress and strain curve using the cross-sectional area of the specimen for normalization of load to stress and the original length of the specimen for normalization of deformation to strain.

- ***Ultimate stress (bone strength,*** σ***):*** Determined from destructive testing, and calculated from the first point with maximal stress. Unit: MPa.
- ***Young's modulus (elastic modulus, or normalized stiffness, E):*** Reflects the stiffness of a material, determined from both non-destructive and destructive tests, and calculated as the tangent to the loading curve of the stress-strain diagram at a given axial strain. Unit: MPa.
- ***Ultimate strain*** (ε)***:*** Determined from destructive testing, and calculated from the first point with maximal stress. Unit: percent.
- ***Failure energy (fracture toughness, F):*** Determined from destructive testing, and calculated as the area underneath the compression curve between zero strain and ultimate strain. Unit: kJ/cm^3.

Introduction

Skeleton optimizes its microarchitecture by elaborate adaptations to mechanical loading during development and growth. The mechanisms for adaptation involve a multistep process of cellular mechanotransduction stimulating bone modeling and remodeling resulting in either bone formation or resorption. This process causes appropriate microarchitectural changes tending to adjust and improve the bone structure to its prevailing mechanical environment [**178**]. This general concept of "bone functional adaptation" to mechanical loading is well known as Wolff's law [**193**] that has been supported by much experimental and observational data [**60**]. One important proposal of the Wolff's law is that the architecture of cancellous bone determines its mechanical properties. Therefore, it is a prerequisite that the architectural variables relate directly to the mechanical properties and as determinants of mechanical properties.

Normal individual reaches peak bone mass at age between 25 and 30 years, and thereafter bone mass declines with age in both genders [**124, 127**]. Bone loss patterns differ for men and women. In men, decreased formation may be the principal factor, and bone loss attributes to generalized attenuation of trabecular bone. In women, increased resorption seems to be the principal factor, and bone loss attributes to the total removal of individual trabeculae. These different patterns of bone loss suggest differences in bone remodeling between both genders as a consequence of aging [**1**].

The bone loss acceleration is accompanied by microarchitectural changes, and reduced mechanical strength is the typical result from the bone mass loss and microarchitectural deterioration in both genders. The reductions in mechanical strength and bone mass are disproportionate, i.e. in normal aging, the reduction in mechanical strength has a greater extent than bone tissue loss itself would suggest [**99, 143, 147**]. Furthermore, trabecular bone becomes increasingly brittle and tends to easily fracture with less energy. This tendency is suggested to be driven by the need for remodeling to repair fatigue damage. Unfortunately, most remodeling events fail to replace all the bone that they remove [**119**].

Basic Multicellular Unit-based (BMU) bone remodeling by resorption and formation drifts can add bone and reshape the trabeculae and cortex to strengthen them. Bone remodeling affects bone collagen fiber orientation, trabecular preferential orientation (architectural anisotropy), connectivity (multiple connections within trabecular network), degree of mineralization, and the amount of unrepaired fatigue damage. These factors, like bone density, are also important determinants of bone strength and stiffness [**59**].

Age-related musculoskeletal diseases increase as a result of increase in the elderly population and a change in lifestyle [**126, 142**]. These diseases, such as osteoarthrosis (OA) [**12**], osteoporosis (OP) [**155, 172**], and fragility fracture [**119, 125**], are among the major health care problems in terms of socioeconomic costs. A thorough understanding of age-related microarchitectural adaptation of bone tissues is crucial for diagnosis, prophylaxis, and treatment of these age-related musculoskeletal diseases; for design, fixation, and survival of joint prosthesis, and functional adaptation of host bone; and for application of biomaterials regarding interface reaction, fracture repair and defect healing.

In vivo and *in vitro* imaging techniques for assessing bone microarchitecture

Bone mineral density (BMD) is one of the determinants of bone strength and fracture risk. Quantitative assessment of macrostructural characteristics, such as geometry and shape of bones, and microarchitectural features, such as trabecular volume fraction, architectural anisotropy, and connectivity, may improve our ability to estimate bone strength. Methods for quantitatively assessing macrostructure include conventional radiographs, dual-energy x-ray absorptiometry (DXA) and computed tomography (CT), particularly volumetric quantitative computed tomography (vQCT). Methods for non-invasive assessing microarchitecture of trabecular bone include high-resolution computed tomography (hrCT), micro-computed tomography (micro-CT), high-resolution magnetic resonance (hrMR), micromagnetic resonance (micro-MR), synchrotron radiation computed tomography (SR-CT). vQCT, hrCT and hrMR are generally applicable *in vivo* as clinical tools for assessment of bone diseases; micro-CT and micro-MR are applicable both *in vivo* in patients and in animals, and *in vitro* for animal sample and human bone biopsy as well; and SR-CT is applicable *in vitro*. During the last decades, great progresses in imaging techniques have been achieved allowing us to monitor bone microarchitectural changes *in vivo* in a non-invasive manner and *in vitro* with high accuracy. Imaging can reach a high resolution as micrometer or even nanometer scale. However, more efforts are demanded to improve imaging techniques [**63**] (Figure 1).

Bone microarchitectural characteristics

Bone has a complex structure. Cancellous bone 3-D microarchitectural characteristics can be described by its bone volume fraction, connectivity density, architectural anisotropy, structure type, trabecular thickness, and surface den-

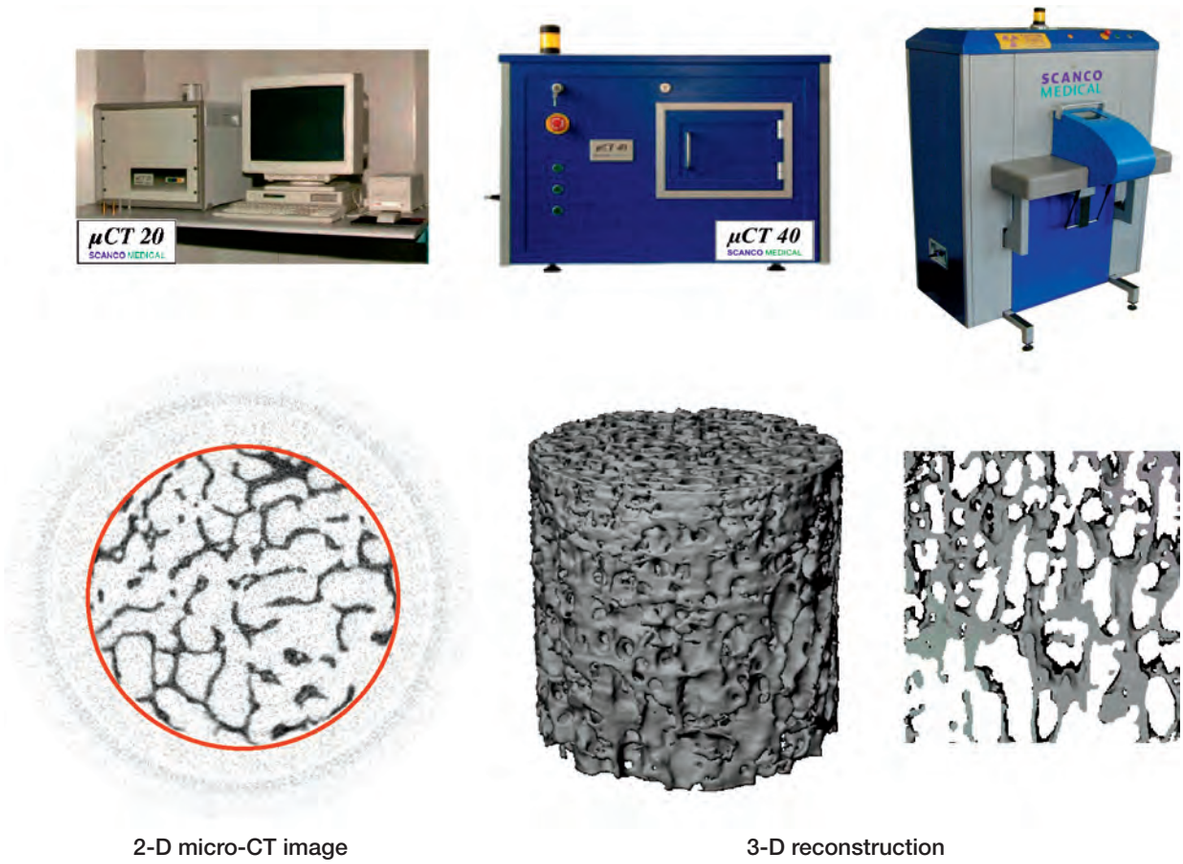

Figure 1. Micro-CT scanning and 3-D reconstruction of cancellous bone
Human cancellous bone specimen is micro-CT scanned with µCT 20, µCT 40 or vivaCT (Scanco Medical AG., Brüttisellen, Switzerland). After segmentation of micro-CT images by applying accurate optimal threshold, 3-D reconstruction is made. From 3-D micro-CT imaging datasets, microarchitectural parameters are computed based on true, unbiased, assumption-free 3-D methods (I, II, III).

sity. Bone volume fraction (BV/TV, or Vv), or bone mineral density (BMD) is the single most important parameter in describing trabecular microarchitecture. Connectivity density (CD) describes a multiple connection in a given trabecular network, based on a topological approach, it allows unbiased quantification of connectivity. Architectural anisotropy describes the preferential orientation of trabeculae. The degree of anisotropy (DA) was defined as the eigenvalue of the primary direction divided by the eigenvalue of the tertiary direction [**72**]. Structure model index (SMI) expresses cancellous bone structure type [**83**]. This technique quantifies the type of structure, such as plates, rods and spherical objects or mixtures of plates and rods. Furthermore, the decomposition of rod and plate is available recently. Trabecular thickness (TbTh) is calculated directly from 3-D micro-CT image datasets independent of an assumed structure type. The volume-based local thickness is determined as the diameter of the maximal sphere that includes every point and that could be fitted completely inside the structure [**82**]. Surface density (BS/TV) is derived from the ratio of bone surface to its total sample volume, and this parameter is important during active bone remodeling.

Other microarchitectural parameters, such as bone surface area, bone surface-to-volume ratio (bone surface area per bone volume), porosity (1-volume fraction), mean trabecular volume, mean marrow space volume, and trabecular number can also be computed from 3-D datasets. Moreover, any other microarchitectural feature may be quantified from 3-D reconstructions of cancellous bone specimens as long as an explicit definition of the property can be given [**131**]. These well-validated 3-D methods provide detailed and versatile description of cancellous bone microarchitecture (Figure 2).

Like cancellous bone, meaningful cortical microarchitectural characteristics can be described by its thickness of cortex, cortical cross-sectional area, cortical porosity, etc (Figure 3). These properties together with cortical area moment of inertia, crystallinity and the presence of microdamage (microcracks) contribute to bone's mechanical competence, integrity and resistance to fracture.

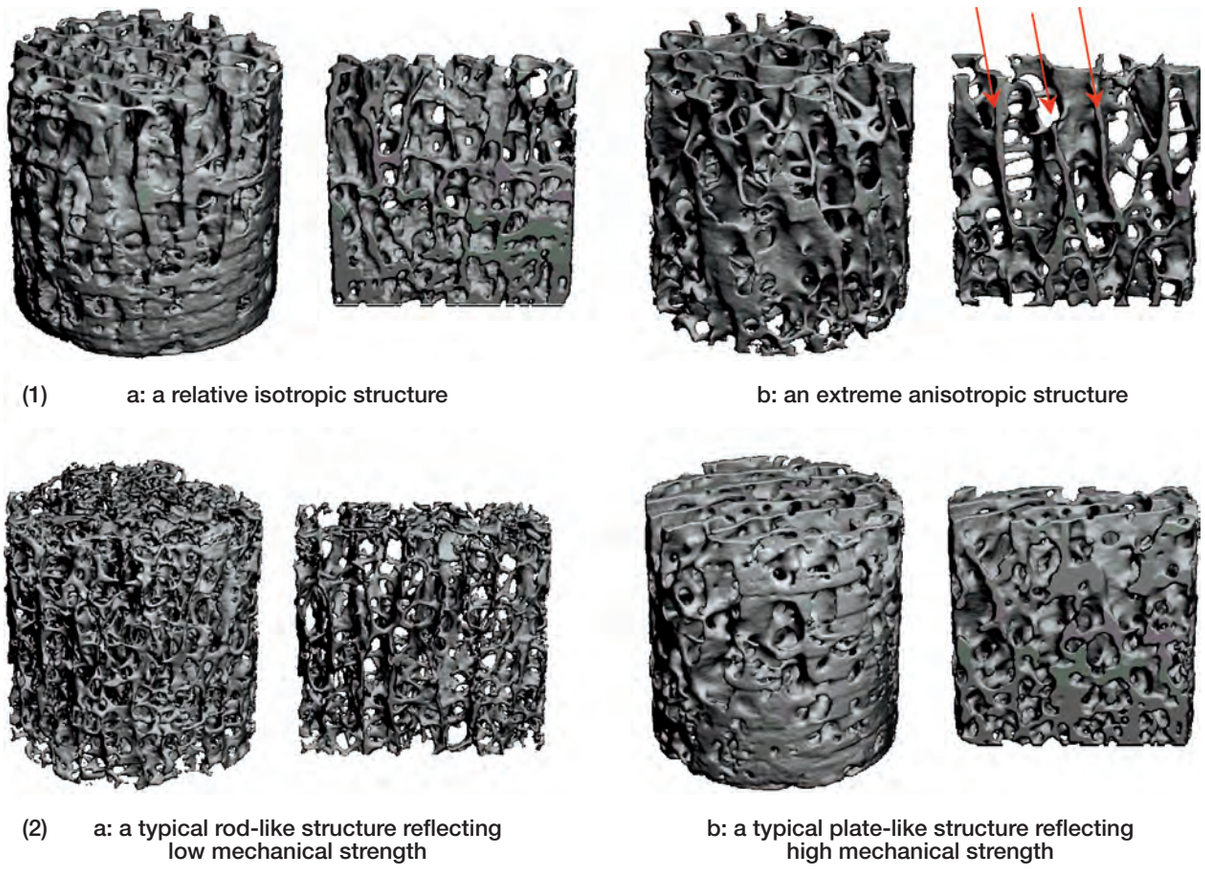

Figure 2. Microarchitectural characteristics of cancellous bone

(1) Architectural anisotropy is calculated using Mean intercept length (MIL) [41]; or Star volume distribution (SVD) [27]. Degree of anisotropy (DA) indicates preferential orientation of trabeculae (b: arrows) (IV).

(2) Structure model index (SMI, a quantification of how plate-like, rod-like or a combination of plate and rod the structure is) is based on a differential analysis of the triangulated bone surface of a structure ([12]) (II).

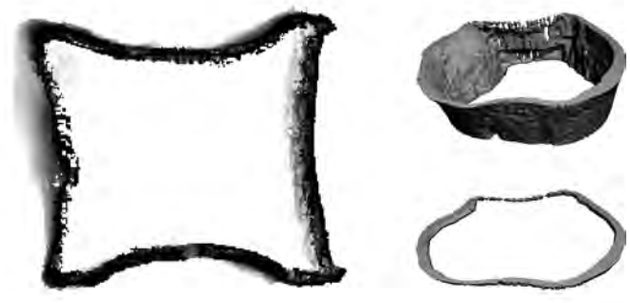

Figure 3. 3-D reconstruction of human vertebral cortical bone (left) and guinea pig proximal cortical bone (right) from micro-CT images

After applying accurate optimal threshold to segment micro-CT images, 3-D reconstruction is made. From 3-D micro-CT imaging datasets, meaningful microarchitectural parameters can be calculated based on true, assumption-free 3-D methods (VIII).

Bone collagen and mineral

Bone has been viewed as a two-phase porous composite material with two primary constituents: mineral and collagen. In structurally normal bone, the mineral provides stiffness and strength, whereas the collagen affords ductility and toughness. However, neither the specific interaction between mineral and collagen is well-revealed, nor the precise characteristics of the mineral and collagen that confer to each its characteristic behavior are completely understood [**196**]. The contribution of the mineral phase to bone's mechanical properties and integrity has been generally recognized, and bone collagen has long been considered secondly to mineral with regard to skeletal fragility. Nevertheless, mounting evidence suggests that the age- and disease-related alterations in collagen content, or changes to inter- and intra-fibrillar collagen cross-linking, can diminish failure energy (fracture toughness), and increase fracture risk [**13**]. In contrast to collagen, much less is known about the contributions of other extracellular matrix components to bone quality. It is assumed that the interactions of type

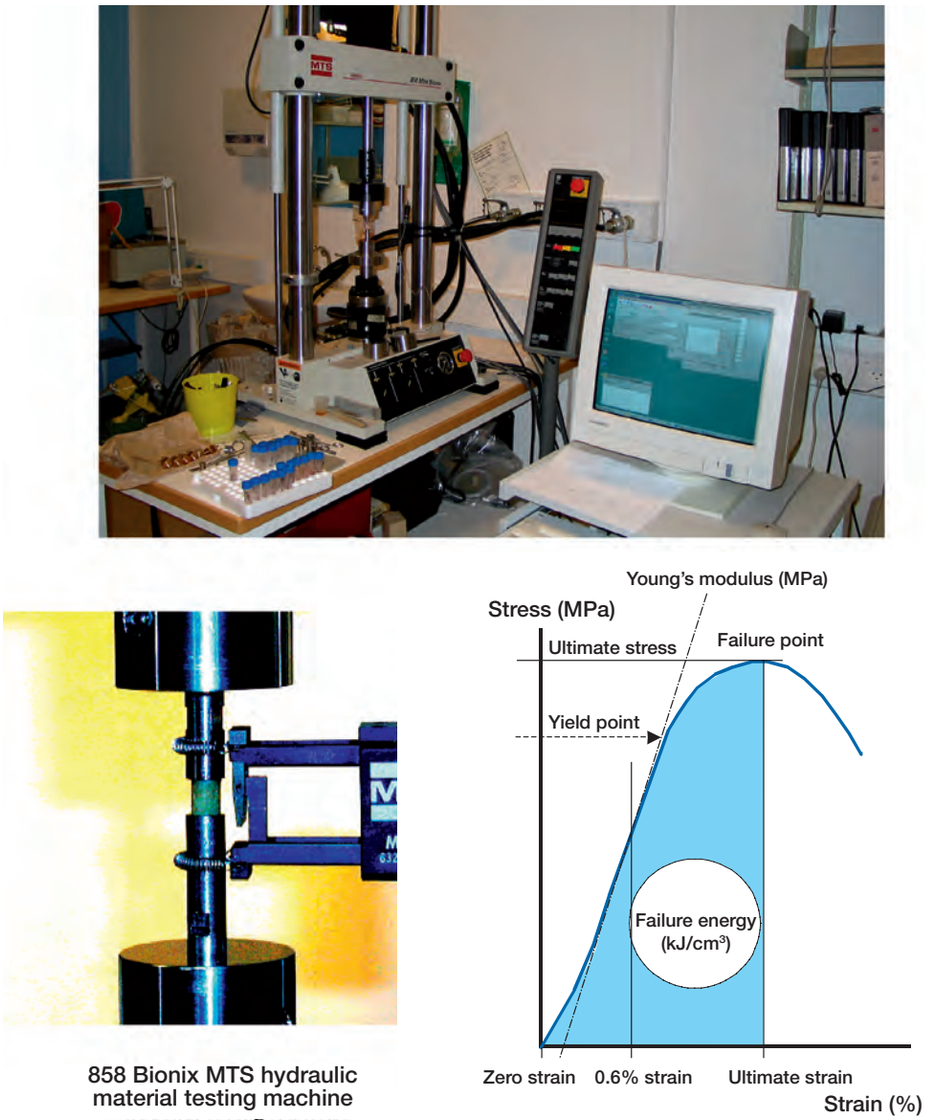

Figure 4. Compression mechanical properties of cancellous bone

Cancellous bone specimen is tested between upper and lower testing columns in an 858 Bionix MTS hydraulic material testing machine (MTS Systems Co., Minneapolis, Minnesota, USA) with 1 kN cell. Load and deformation data are recorded and converted to stress and strain data to calculate mechanical properties. Right: A typical stress-strain curve from a destructive test. Ultimate stress and ultimate strain are derived from the first maximum of the curve, Young's modulus is determined as the tangent to the point on the loading curve intersecting the 0.6% strain line, failure energy (fracture toughness) as the area underneath the compression curve between zero strain and ultimate strain (IV,V)[7]. The linear portion of the stress strain curve is called the elastic region. After the yield point, the curve became nonlinear and corresponded to the plastic region. In the elastic region there is a proportional deformation with increasing load applied, and when the load is removed, bone returns to its original shape.

I collagen with the mineral and the contribution of the orientations of the collagen fibers maybe crucial when the bone is subjected to mechanical forces [**184**].

Bone's mechanical properties

There are several types of mechanical tests, e.g. axial compression test [**109, 112**], tensile test [**157**], three-, or four-point bending test [**177**], combined test of cartilage and bone [**40, 41**], reduced platen test [**84**], and shear test of femur head [**169**] etc. Any material with a linear elastic component under uniaxial loading can be described by a proportional relationship between change in load and change in length of the material. During mechanical testing, a force-deformation curve is obtained, and is converted to stress and strain curve using the cross-sectional area of the specimen for normalization of load to stress and the original length of the specimen for normali-

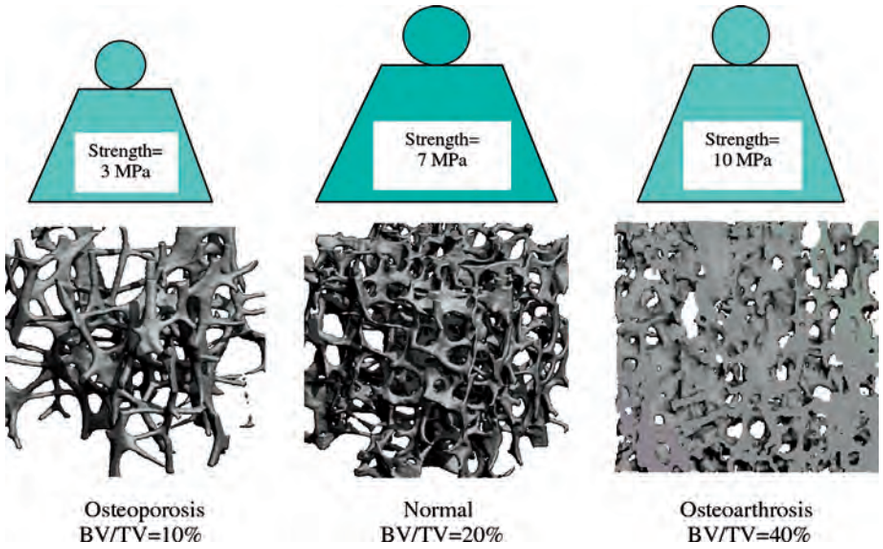

Figure 5. Strength of cancellous bone
Osteoporotic cancellous bone (left) has lest mechanical strength, lowest density, and abnormal bone quality; Normal cancellous bone (middle) has normal mechanical strength, normal density, and normal bone quality; Osteoarthrotic cancellous bone (right) has relatively reduced mechanical strength relative to highest density, and deteriorated bone quality (VI).

zation of deformation to strain. In general, Young's modulus reflects the stiffness of a material, and is calculated as the tangent to the loading curve of the stress-strain diagram at a given axial strain. Ultimate stress is calculated from the first point with maximal stress. Ultimate strain (percent deformation) is calculated from the first point with maximal stress. Failure energy is calculated as the area underneath the compression curve between zero strain and ultimate strain (Figure 4). The energy required to cause bone failure is also known as fracture toughness, i.e. toughness is a quantitative measure of bone quality in terms of its susceptibility to fracture. Thus, understanding age-related changes in the strength and toughness of bone is necessary to elucidate the underlying mechanisms of age-related bone fractures [**187**].

Bone strength, the key mechanical property, is dependent upon numerous, interrelated factors, and on both the bone quantity and the bone quality [**59, 189**]. Bone strength is determined by both its material properties and its structural properties. Material properties include bone's degree of mineralization, crystallinity, collagen characteristics, and osteocyte viability that have substantial impacts on bone strength. Structural properties include the diameter and thickness of the cortices, the cortical porosity, the connectivity and anisotropy of the trabecular network, the trabecular thickness and spacing, and the presence of trabecular stress risers and microdamages that impact bone strength in diverse manners. Bone remodeling activity has either directly or indirectly impacts on all of these processes [**27**].

Bone quality

Bone is a living material capable of self-repair. Bone is a complex tissue and its principal function is to resist mechanical forces and withstand fractures. The term "bone quality" has been used in the literature for more than 15 years, but its precise definition remains unclear. There are generally two views of the term "bone quality" in the literature. Some people consider bone quality to represent the sum of all characteristics of bone that affect the ability of bone to resist fracture (i.e., all aspects of bone size, shape, and material properties). The others refer bone quality as the factors that resist fracture but are not accounted for by bone mass or quantity [**81, 189**]. Regardless the controversy of precisely defining bone quality, the different determinants of bone quality are interrelated, in particular the mineral and collagen, although analysis of separate roles of collagen and mineral in bone strength is difficult. Bone density alone is not a surrogate for fracture prevalence and occurrence of osteoporosis, and does not completely explain the therapeutic efficacy of emerging treatments. Non invasive assessment using imaging techniques has recently received increasing attention to improve our understanding of the complexity of bone quality (Figure 5).

Bone microdamage (microcrack)

Bone microdamage is typically defined as bone matrix failure detectable histologically by light microscopy in the form of microcracks. Microcracks have been defined as cracks that

can be detected using optical microscopy and are usually of the order of 30–100 μm in length. Accumulation of microdamage in any material or structure causes a reduction in elastic modulus [**14**]. Animal and postmortem human studies show that microdamage accumulation in bone reduces the elastic modulus of the tissue, decreases bone strength, and increases energy dissipation when bone is loaded. Decreased strength and stiffness are likely to increase fracture risk, but the extent to which microdamage accumulation may increase the risk of fracture is unclear.

Aims of the studies

The overall goals of the study were to investigate the age-related and OA-related changes in the 3-D microarchitectural properties, mechanical properties, collagen and mineral qualities of both cancellous and cortical bone tissues.

The study included mainly two parts. For human subjects: we investigated aging- and early OA-related changes of the properties. Study I aimed to assess the accuracy of volume fracture measurements from micro-CT and to establish micro-CT segmentation techniques, thus to generate accurate 3-D micro-CT datasets for further analysis of bone microarchitecture . Study II & III focused on the normal age-related changes in the microarchitecture of human peripheral cancellous bone by means of the novel 3-D methods. Study IV evaluated the mutual associations among various microarchitectural properties, mechanical properties, and compositional properties. Study V assessed the association between mechanical properties and physical properties and quality changes in early-stage osteoarthrotic subchondral cancellous bone. Study VI investigated the microarchitectural changes and quality changes in subchondral cancellous bone in early human OA.

Investigations using guinea pig models aimed to obtain more insight into the age-related and OA-related subchondral bone adaptations. Study VII assessed the spontaneous, age-related development of guinea pig OA, and quantified age-related microarchitectural adaptations of subchondral bone tissues in guinea pig primary knee osteoarthrosis development that covers the entire range of OA progress from initiation to severe stage. Study VIII evaluated potential effects of hyaluronic acid (HA) on 3-D microarchitecture, mechanical properties, and collagen/mineral quality of subchondral bone tissues in guinea pig primary osteoarthrosis. Study IX studied the effects on OA progression by increasing subchondral bone density through inhibition of bone remodeling with a bisphosphonate alendronate (ALN). We evaluated the effects of bone remodeling inhibition on 3-D microarchitecture, mechanical properties and collagen/mineral of bone tissues in guinea pig primary osteoarthrosis.

Research questions/hypotheses

In these investigations, specific research questions or hypotheses were posted.

Study I: We hypothesized that a fixed threshold might be determined from the Archimedes-based volume fraction of a subgroup of specimens, and thus provide guidelines for micro-CT image segmentation.

Study II & III: We hypothesized that significant age-related microarchitectural changes occurred in human peripheral cancellous bone, and different parameter had different age-related changing pattern and most of microarchitectural changes happened after 60 years of age. The aging trabeculae align more strongly to the primary direction – parallel to the tibial longitudinal loading axis.

Study IV: We tested the hypothesised that the type of trabecular structure, plate or rod, significantly related to the mechanical properties of cancellous bone and also was a good predictor for mechanical properties of cancellous bone. There were mutual associations among various properties of human normal peripheral cancellous bone.

Study V: We postulated that significant changes in mechanical and physical properties and quality even occurred in early-stage osteoarthrotic subchondral cancellous bone, thus that the normal relationship between mechanical and physical/compositional properties could not be applied to early stage osteoarthrotic cancellous bone.

Study VI: We hypothesised that significant microarchitectural changes, in addition to changes in density, occurred in subchondral cancellous bone in early OA. Thus, the normal relationship between mechanical and microstructural properties could not be applied to cancellous bone in early OA.

Study VII: We proposed there were age-related progressive changes in three-dimensional (3-D) microarchitectural and mechanical properties, bone collagen, and mineral of subchondral bone tissues in a primary guinea pig model that covered the entire range of OA progression from initiation to the severe stage.

Study VIII: We tested the hypothesis that HA protected against cartilage degeneration, decreased subchondral bone density and changes its 3-D microarchitecture so that subchondral bone became more compliant and thereby reduced cartilage stress during impact loading.

Study IX: In contrast, by increase subchondral bone density by inhibition of bone remodeling using alendronate (ALN), we tested the hypothesis that increased bone density in subchondral bone tissues led to significant articular cartilage damage.

Methodological considerations

Assessments of bone samples

Human aging and OA

The following procedures were used to assess human bone samples (Figure 6).

The following procedures were used to assess guinea pig bone samples (Figure 7).

Human cancellous bone samples and design

Normal bone samples (I– IV)

Forty human autopsy proximal tibiae were removed and stored at -20°C. These tibiae, one from each donor, aged 16 to 85 years (mean 57, S.D. 19), were without macroscopic pathological changes, and the individuals did not have a history of musculoskeletal diseases. All of these donors (10 females and 30 males) were Caucasian. The tibiae were collected consecutively

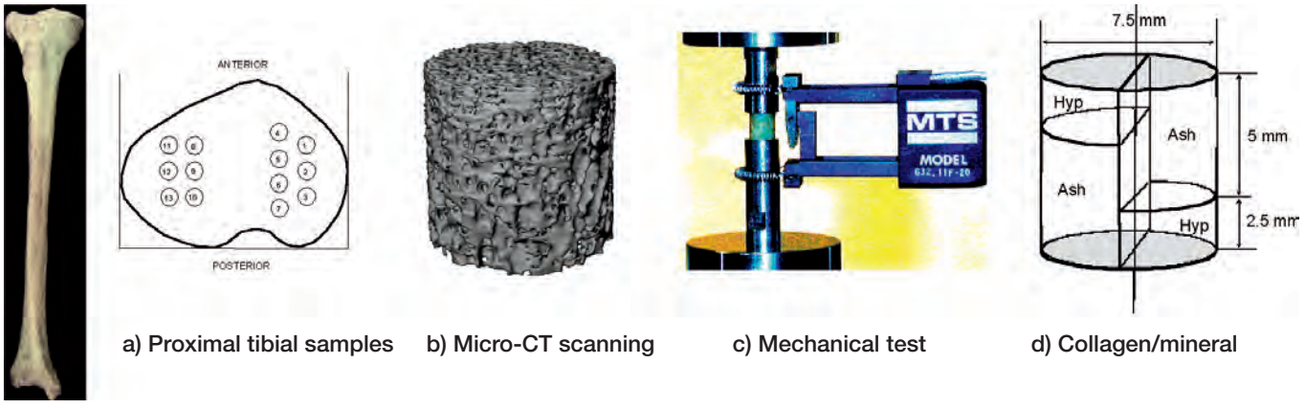

Figure 6. Typical procedure for assessing human bone samples
a) cylindrical cancellous bone samples were removed from standardized locations of proximal tibia, b) micro-CT scanned, c) tested mechanically in compression, and d) finally subjected to duplicate determination of bone collagen and mineral [38].

Figure 7. Typical procedure for assessing guinea pig bone samples
The proximal tibiae of the guinea pigs were harvested. After removing soft tissue carefully, the proximal 4 mm of tibiae were micro-CT scanned for quantification of 3-D microarchitecture of subchondral bone plate. Then a first cut was made 0.5 mm beneath subchondral bone plate and a further cut distally was made to produce a 3 mm thick cancellous-cortical bone complex specimen. This complex was micro-CT scanned to quantify the microarchitecture of subchondral cancellous and cortical bones. The cartilage-bone complex including subchondral plate was embedded for histological analysis for assessment of cartilage damages. Reduced platen test was first performed on cancellous bone only using an individual testing anvil (diameter ranging from 1.2 to 4.5 mm) that fitted to individual cross sectional area of cancellous bone, and then compression test was done on remaining cortical bone to determine the mechanical properties. Finally, bone collagen and mineral were determined for each bone sample (VII).

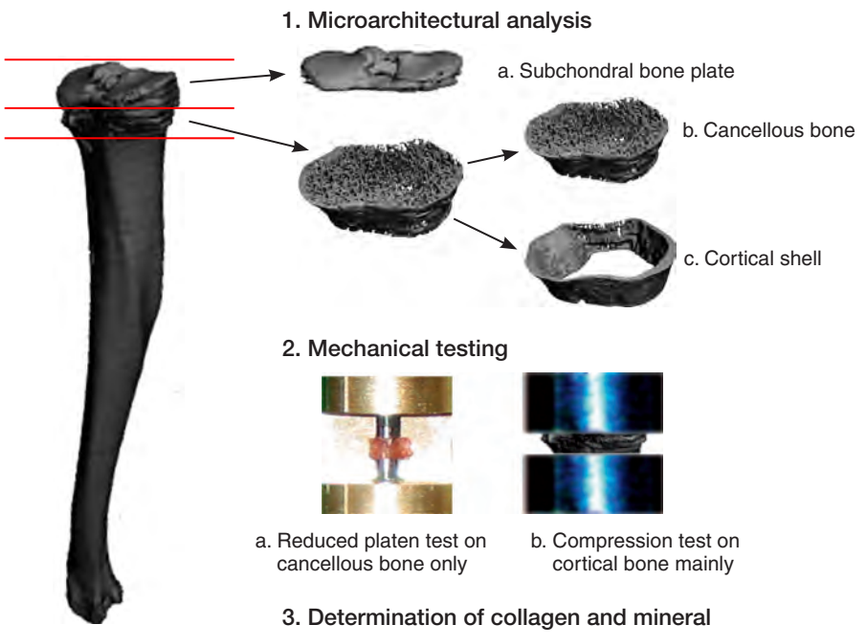

when they satisfied the selection criteria, i.e. the patients were not immobilized for more than 2 weeks before they died rather suddenly either due to trauma or due to acute disease, i.e. they had been active at a normal level until two weeks before death. These selection criteria minimized any potential effects of other factors on bone property and quality.

Two specimens were removed from standardised locations on both medial condyle and lateral condyle of each tibia, yielding a total of 160 specimens used in studies I–IV. All specimens were drilled out of frozen bone using a trephine with an inner diameter of 7.5 mm. The axis of the cylindrical specimens corresponded to the longitudinal axis of the tibia, i.e. the main loading direction. A standardized plastic template was used to assume identical locations for all specimens. The specimens were cut 1 mm beneath the subchondral bone plate and at the distal end to produce specimens with a diameter and length of 7.5 mm by the technique described previously [39]. All specimens were stored frozen in sealed plastic tubes at -20°C.

Osteoarthrotic bone samples (V–VI):

Subchondral cancellous bone specimens were produced from 10 human early-stage OA proximal tibiae [7 males, 3 females, mean age 73 (range: 63–81 years)], and 10 normal human age- and gender-matched proximal tibiae served as the control group [7 males, 3 females, mean age 72 (range: 58–85 years)]. All donors were Caucasian and one post-mortem tibia was removed from each donor.

The degree of OA was defined according to Mankin's criteria [**116**] and degeneration of cartilage was assessed histologically. Early-stage OA had the presence of macroscopically fibrillated cartilage. The cartilage surface (superficial zone) of the medial condyle in OA tibiae had visible degeneration with slight fissures, whereas there was an intact cartilage surface on the lateral condyle. The normal tibiae did not show macroscopical pathology and had intact cartilage surfaces; they had no history of musculoskeletal diseases. The donors with normal tibiae had all died rather suddenly from either trauma or acute disease that met the criteria mentioned above.

Three cylindrical specimens were drilled out from each medial and lateral condyle of a tibia using a 7.5 mm inner-diameter trephine thus that the axis of the specimen corresponded to the longitudinal axis of the tibia, and used in studies V–VI. These specimens were cut 1 mm beneath the subchondral bone plate and then further cut at the distal end to create 7.5 mm long cylindrical specimens. A total of 120 specimens were produced, and they were stored in plastic tubes at -20°C. The early OA specimens were allocated to medial OA and lateral control groups, and the normal specimens were allocated to normal medial and normal lateral groups, and 30 specimens were examined in each group (Figure 6).

These studies were approved by the Department of Orthopaedics and Institute of Forensic Medicine, Aarhus University Hospital, Denmark.

Experimental animal and designs – guinea pig primary osteoarthrosis

Male Charles River strain outbred Dunkin-Hartley guinea pigs with specified ages were purchased at 2 months before the study (HB Lidköpings Kaninfarm, Lidköping, Sweden). These guinea pigs were acclimated for a period of 2 months, housed 2–3 together in an environmentally controlled cage with size 100 × 100 × 90 cm^3 with water and standard guinea pig chow containing 18% protein, 0.9% calcium, 0.7% phosphorus and 600 IU/kg vitamin D3 (Altromin Standard Guinea Pig Chow #3020, Lage, Germany) *ad libitum*. Physical well-being and activity were checked daily, and body weight was measured weekly. At sacrifice, the left tibiae of the guinea pigs were dissected and kept in sealed plastic bags at -20°C, and the right tibiae were used in another study. All procedures were in accordance with approved Danish Animal Research guidelines, under the project protocol approved by the Danish Animal Experiments and Inspectorates (Study no. J.nr. 2000/ 561-329).

Effects of age on OA development (VII)

Fifty guinea pigs were 3, 6, 9, 12, and 24 months of age at sacrifice, ten in each age group. These animals were used to investigate spontaneous age-related progression of OA subchondral bone tissues.

Effects of hyaluronan treatment (VIII)

Fifty-six male guinea pigs were randomly divided into 5 groups based on their ages and body weight. The treatments started in all groups when the guinea pigs were 6.5 months of age. Three groups received intra-articular injections in both knee joints of HA 0.4 mg/kg/week and two groups received vehicle (0.1 ml physiological saline/week) for 5 weeks. Thereafter, the guinea pigs were left untreated until they were 9 months old. At this age, two groups (2.5-month groups, n = 2 × 10), an HA group and a saline group, were sacrificed. For the remaining three groups, 2 groups received once more the same treatment regimen (HA or saline injections for 5 weeks as before) starting when the guinea pigs were 9.5 months old, and one HA group was left untreated. The latter 3 groups (5.5-month groups, n = 3 × 12) were sacrificed when the guinea pigs were 12 months old.

Effects of alendronate treatment (IX):

Sixty-six male guinea pigs were randomly divided into 6 groups with similar ages and body weights. The treatments started in all groups when the guinea pigs were 6.5 months of age. Two groups received ALN 10 µg/kg, two groups received ALN 50 µg/kg, and two groups received vehicle (1 ml physiological saline) subcutaneously twice a week for 9 weeks. At 9 months of age, one 10 µg/kg group, one 50 µg/kg group and one control group (9-week groups, n = 3 × 10) were sacrificed. The remaining three groups received once more the same treatment regimen starting when the guinea pigs were

9.5 months old (ALN 10 µg/kg, ALN 50 µg/kg, or saline injections for an additional 8 weeks). The latter 3 groups (17-week groups, n = 3 × 12) were sacrificed when the guinea pigs were 12 months old. Physical well-being and activity of guinea pigs were checked daily, and their body weights were measured weekly. At the completion of the experiment, the guinea pigs were killed and the left tibiae of the guinea pigs were dissected and kept in sealed plastic bags at -20°C. The right tibiae were used in another study (Figure 7).

Power calculation: Error of first kind (2α), which is the level of significance or the risk of identical results if in fact they differ, was selected to 5%, SD is 50%. The minimal relevant difference (D=MIREDIF) not to be overlooked between test groups was selected to 60%. Error of the second kind (β), which is the risk of concluding that two effects are identical if in fact the difference is below the MIREDIF (false negative result), was chosen to be 20%. Based on these assumptions, at least 10 experimental subjects should be included in each experiment [**138**].

Experimental methods

1) Micro computed tomography (µCT) scanning

Human normal and early OA cancellous bone samples (I–IV & VI)

The cylindrical specimens obtained from proximal tibiae were scanned using a high resolution microtomographic system (µCT 20, Scanco Medical AG., Brüttisellen, Switzerland). These samples were scanned in a standard resolution mode, resulting in 3-D reconstruction of cubic voxel size of 22 × 22 × 22 μm^3. Scanning time for each specimen was approximately 3 hours. Each 3-D image data set consisted of approximately 350 micro-CT slide images (512 × 512 pixels) with 16-bit grey levels. The total data size (raw data and image data) was 450 Mb, unsegmented image size of 76 Mb, and 38 Mb in segmented form. Micro-CT images were segmented using individual optimal thresholds [**49**]. The segmented images were then purified after thresholding to remove the noise particles unconnected to the main structure [**132**]. To obtain accurate 3-D data sets, micro-CT images were segmented using optimal thresholds thus that the bone volume fraction of the datasets corresponded to Archimedes' based volume fraction [**49**].

Guinea pig subchondral bone samples (VII–IX)

A high resolution micro-CT system (µCT 40, Scanco Medical AG., Brüttisellen, Switzerland) was used to scan proximal tibial specimens (Figure 1), resulting in 3-D reconstruction of cubic voxel sizes 16 × 16 × 16 μm^3. Each 3-D image dataset consisted of approximately 400 micro-CT slide images for the proximal tibia and 300 slice images for subchondral bone tissue (1024 × 1024 pixels) with 16-bit-gray-levels. Two scans were done. The first scan was on the 4 mm of proximal tibia to quantify 3-D microstructure of subchondral plate. Then the proximal tibia was sawed 0.5 mm beneath the subchondral bone plate and a further cut was made distally to produce 3 mm thick cancellous-cortical bone specimen using a LEITZ Microtome 1600 (Ernst Leitz Wetzlar GmbH, Wetzlar, Germany). The second scan was done on this specimen to quantify 3-D microarchitecture of cancellous and cortical bones (Figure 7). The cartilage-bone complex including the subchondral plate was used for histological analysis for assessing the degree of cartilage degeneration (Mankin's score).

2) Accuracy and precision of micro-CT measurement (I)

The above mentioned 160 normal human cancellous bone specimens (Study 1) were scanned with a high resolution microtomographic system (µ-CT 20, Scanco Medical AG., Brüttisellen, Swizerland) to assess the accuracy and precision of micro-CT method. Each 3-D image data set consisted of approximately 350 micro-CT slide images (512 × 512 pixels) with 16-bit-gray-levels and the voxel size was 22 × 22 × 22 μm^3. A detailed description of this system can be found elsewhere [**159**].

After scanning, the 3-D data sets were segmented by using individual global thresholds, above this threshold all pixels are considered bone, and below this threshold all pixels are considered non-bone. Two methods were applied to segment the micro-CT data.

Method I: The threshold of each data set was determined using an adaptive method determined by micro-CT software, where the gray level data set is segmented at different levels, e. g. 50 different thresholds. The threshold, where the volume fraction changes the least, i. e. the steepest gradient of gray levels, is chosen as the threshold for the data set.

Method II: A second segmentation was performed using individual thresholds forcing BV/TV (bone voxels per total specimen voxels) to the Archimedes-based volume fractions.

The mean thresholds from methods I and II were applied separately to segment 20 randomly selected micro-CT image data (10 from low density, volume fraction 9.8% to 20%; and 10 from high density, volume fraction 30% to 39.8%), and volume fractions were calculated from the segmented 3-D data. Furthermore, the connectivity densities of these 20 specimens were determined [**132**]. After scanning, an accurate protocol was conducted for measuring Archimedes-based cancellous bone volume fraction as suggested [**165**], with a slight modification.

3) Microarchitectural analysis

Human cancellous bone samples (I–IV & VI)

From the segmented accurate 3-D micro-CT data sets, microarchitectural properties were calculated based on true, unbiased and assumption-free 3-D methods.

The quantification of architectural anisotropy was based on a 3-D volume method: star volume distribution (SVD) [**21, 134, 135**]. The SVD describes the typical distribution of cancellous bone around a typical point in a trabecula, and the

result of an SVD analysis may be expressed by the SVD fabric tensor [**135**].

To exclude the effects of artificial edges on the SVD measure, the SVD examination points were placed randomly at least 2 mm away from any specimen surface. The specific choice of 2 mm was made after considering the architecture of the cylindrical specimens. The SVD was determined in 3-D space for 500 random orientations for 300 random points within the trabeculae of each specimen, and the SVD fabric tensor was determined [**135**].

Eigenvalues of the fabric tensors were designated by τ_1, τ_2, and τ_3, where $\tau_1 > \tau_2 > \tau_3$. The fabric tensors were normalized by dividing by $\tau_1 + \tau_2 + \tau_3$, so that $\tau_1 + \tau_2 + \tau_3 = 1$. Here the eigenvalue τ_1 reflects the relative anisotropy strength of the primary direction, τ_2 the secondary direction, and τ_3 the tertiary direction. The *degree of anisotropy (DA)* was defined as the eigenvalue of the primary direction divided by the eigenvalue of the tertiary direction [**72**]. The anisotropy types of the specimens can be visualized in the Woodcock diagram [**58**].

The unbiased Euler number contribution of a region of interest (ROI) to the universal Euler number was developed by Odgaard and Gundersen [**132**]:

$$\Delta\chi(V) = \chi(V) - 1/2\ \Sigma\chi(F) + 1/4\ \Sigma\chi(E) - 1/8\ \Sigma\chi(P)$$

where $\chi(V)$ is the Euler number of the 3-D specimen, $\chi(F)$ is the Euler number of one of the six specimen faces, $\chi(E)$ is the Euler number of one of the 12 specimen edges, and $\chi(P)$ is the Euler number of one of the 8 specimen corners; for details the reader is referred to (132). The minimal parallelepiped specimen is a single voxel. The Euler number contribution of any irregular ROI to the universal Euler number can simply be determined by summing $\Delta\chi(V)$ over all voxels in the ROI. Knowing the Euler number contribution of the ROI, the connectivity or the number of redundant trabeculae in the ROI can be approximated by $ß_1 = -\Delta\chi(V)$. A single trabecula is ignored using this approximation [**132**]. Knowing the connectivity and the ROI volume, the *connectivity density (CD)* is easily calculated as:

$$CD = \Delta\chi(V)/\Delta V$$

where ΔV is the volume of a region of interest. The mean trabecular volume (MTV) and the mean marrow space volume (MMSV) are given by

$$MTV = (\Delta V \times Vv) / [\Delta\chi(V) + 1]$$
$$MMSV = [\Delta V \times (1–Vv)] / [\Delta\chi(V) + 1]$$

where Vv is the bone volume fraction of a region of interest.

Structure model index (SMI, a measure of predominant shapes in the structure, i.e. plate-like, rod-like or a combination of plate and rod) [**83**] was based on a differential analysis of the triangulated bone surface of a structure. The SMI quantification is especially important for an *a priori* unknown or changing structure, such as aging, bone remodeling and disease. The SMI value is zero for an ideal flat plate structure, and the SMI value is 3 for an ideal cylindrical rod structure [**83**].

From the 3-D micro-CT data sets, *trabecular thickness* (TbTh*, mm) [**82**], *bone volume fraction* (BV/TV or Vv, bone volume per total specimen volume, %) was determined in a cylindrical volume-of-interest, which was only slightly smaller than the specimen (0.1 mm margin excluded) [**49**]. *Bone surface-to-volume ratio* in mm^{-1} (BS/BV, bone surface area per bone volume), *bone surface density* in mm^{-1} (BS/TV, bone surface area per total volume of specimen), *mean trabecular volume* (MTV, μm^3), *mean marrow space volume* (MMSV, μm^3), and *trabecular separation* (TbSp*, mm) were also calculated [**131**].

Guinea pig bone samples (VII–IX)

a) 3-D microarchitectural properties of subchondral bone plate: Subchondral plate was defined as starting from the calcified cartilage-bone junction and ending at the marrow space [**16**]. To obtain accurate 3-D datasets of subchondral bone plate, micro-CT images were segmented using optimal thresholds [**49**]. Specifically, we calculated the total specimen volume of the 3 mm specimen from micro-CT images due to its irregular shape and measured dry weight of the specimen using a Mettler AT250 balance (Mettler Instrumentations AG, Greifensee, Switzerland) after defatting in an alcohol and acetone 1:1 mixture, and determining submerged weight in water based on the Archimedes's principle [**39**]. Then the calculated bone volume fraction was matched to micro-CT determined "threshold–volume fraction pattern" to get the correct optimal threshold for each specimen. Finally, a mean optimal threshold derived from the 3 mm thick specimens was applied for segmenting subchondral plate, cancellous and cortical bone image datasets, since these bone tissues have similar bone quality and hence the same bone threshold level. The meaningful microarchitectural parameters for the subchondral bone plate, i.e. *plate volume fraction* (BV/TV, bone volume per total plate volume, %), *plate thickness* (TbTh*, μm), *plate surface density* (BS/TV, plate surface to total plate volume, mm^{-1}), and *plate perforation* (mean pore size, μm) were calculated. These calculations were done first on total subchondral plate, then on the medial and lateral condyles [**43**] (Figure 8).

b) 3-D microarchitectural properties of subchondral cancellous bone: Subchondral cancellous bone was defined as cancellous bone region beneath the thin layer of the subchondral plate. The subchondral cancellous bone was segmented using the optimal threshold described above to get accurate 3-D datasets. The cancellous bone was defined and separated from the cortical shell. The microstructural properties were calculated based on true, unbiased and assumption-free 3-D methods. *Bone volume fraction* (BV/TV, %)[**49**], and *trabecu-*

a. 3-D microarchitectural quantification of subchondral bone plate: total, medial and lateral

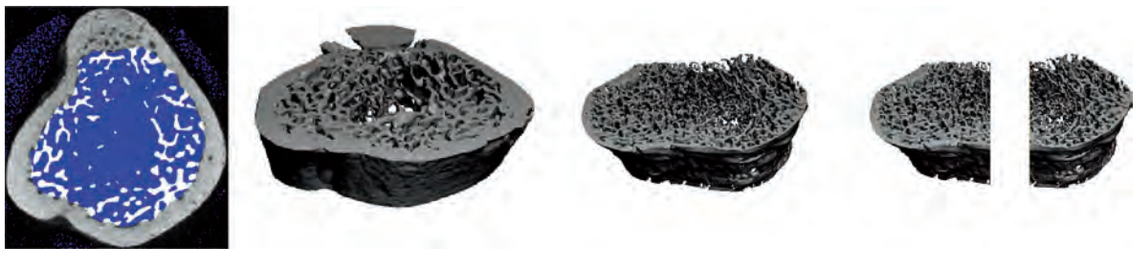

b. 3-D microarchitectural quantification of subchondral cancellous bone: total, medial and lateral

c. 3-D microarchitectural quantification of subchondral cortical shell

Figure 8. Quantification of subchondral bone tissues
a) The 4-mm thick proximal tibiae were micro-CT scanned for quantification of 3-D microarchitecture of subchondral bone plate. Then the 3-mm thick cancellous-cortical bone complex specimen produced 0.5 mm beneath subchondral bone plate was micro-CT scanned for quantification of 3-D microarchitecture of both cancellous bone (b) and cortical bone (c) (VII, VII, IX)

lar thickness (TbTh*, μm) [**82**] were determined. *Structure model index* (SMI) [**83**] was based on a differential analysis of the triangulated bone surface of a structure. The quantification of *architectural anisotropy* (DA), preferential orientation of trabeculae, was based on the mean intercept length method. The degree of anisotropy was defined as the ratio between two eigenvalues, e.g. the ratio of the eigenvalue of the primary direction divided by the eigenvalue of the tertiary direction (MIL_{max}/MIL_{min}) [**72**]. Quantification of *connectivity density* (CD), the number of multiple connected trabeculae per volume (mm^{-3}), was based on a topological approach [**132**]. *Bone surface-to-volume ratio* in mm^{-1} (BS/BV, bone surface area per bone volume), *Bone surface density* (BS/TV, bone surface area per total volume of specimen, mm^{-1}), and 3-D *trabecular separation* (TbSp*, μm) were also calculated[131]. These calculations were done first on total subchondral cancellous bone, then on medial and lateral condyles (Figure 8).

c) 3-D microarchitectural properties of subchondral cortical bone: The cortical thickness determined in 3-D datasets in μm, cortex volume fraction (bone volume per total specimen volume, %) [**49**], cortex surface density (bone surface area per total volume of specimen, mm^{-1}) [**82**], and cortex porosity (cavity/perforation, %) were calculated [**131**]. The cross sectional area (mm^2) of cortex was the mean value obtained from subchondral cortical bone (Figure 8). A detailed description for quantification 3-D microarchitecture of cortical bone has been presented [**43**].

4) Osteoarthrotic grading (V–IX)

Articular cartilage of tibial condyle including subchondral plate was embedded in methylmethacrylate (MMA) and sectioned with a universal heavy-duty microtome (Reichert-Jung, Cambridge Instruments GmbH, Germany). The cartilage sections were stained with Safranin O. Three sections from each medial condyle and lateral condyle were examined. Degree of osteoarthrosis was defined as macroscopically fibrillated cartilage, and this finding was confirmed histologically, the grading was using Mankin's criteria. Mankin's histological-histochemical grading ranges between 0 and 14 (for structure 0–6, cells 0–3, Safranin-O staining 0–4, and tidemark integrity 0–1), where 0 is normal and 14 is severe arthrosis [**116**].

5) Mechanical tests

Human bone samples (III–VI)

After micro-CT scanning, cylindrical cancellous bone speci-

mens were tested in compression to failure to determine its mechanical properties by the method described in detail previously [**39**]. The tests were performed on an 858 Bionix MTS hydraulic material testing machine (MTS Systems Co., Minneapolis, Minnesota, USA), using a 1 kN load cell. *Ultimate stress* (bone strength) was calculated from the first maximal point with maximal stress; *ultimate strain* was defined as the strain corresponding to the maximal stress; *failure energy* (fracture toughness) was calculated as the area underneath the stress-strain curve between zero strain and *ultimate strain*; and *Young's modulus* was calculated as the tangent to the linear portion of the stress-strain curve between 0.4 and 0.6 bone strain.

Guinea pig bone samples (VII–IX)

Mechanical testing of guinea pig proximal tibial bone sample was performed on an 858 Bionix MTS hydraulic material testing machine (MTS Systems Co., Minneapolis, Minnesota), using a 1 kN load cell. After 10 preconditioning cycles, compression test was first performed using a so-called "*reduced platen testing*" in which the central cancellous bone was only compressed in the axial direction to 10% bone strain, thus keeping the remaining peripheral cancellous bone and cortical bone intact[84]. Compression test to failure was performed again on the cortical shell mainly (including a brim of cancellous bone) (Figure 7).

For cancellous bone, Young's modulus, ultimate stress (strength), ultimate strain and failure energy were calculated [**39**]. The cross sectional area of cancellous bone was the same as that of the testing column (Figure 7).

For cortical bone, the same calculation was done as for cancellous bone. The actual cortical cross sectional area was calculated as the mean cross sectional area of proximal and distal ends of the specimen (measured from micro-CT images) minus the contact areas of testing columns for reduced platen test.

6) Determination of bone density, collagen and mineral

Human bone samples (I, IV, VI)

After mechanical testing, the marrow was removed from the specimens by air jet and tap water. The specimens were then defatted in a 1:1 mixture of alcohol and acetone for 48 hours, cleaned once more by air jet and evaporated at room temperature for 24 hours before being freeze-dried. The dry weight (DW) of the freeze-dried specimens was recorded. To determine the tissue density (ρ_{tiss}), each sample was rehydrated under vacuum in Ringer's solution adding a wetting agent (Pervitro 75%) and the submerged weight (μ_s) of the sample was recorded in a Mettler AT250 balance (Mettler Instruments AG, Greifensee, Switzerland) equipped with a density determination kit. Determination of submerged weight and dry weight was repeated once. From the mean weights, the apparent density (ρ_{app}) was calculated from the dry weight of the defatted specimen divided by its original volume, and the tissue density was calculated as:

$$\rho_{tiss} = DW \times \rho_L/(DW - \mu_s)$$

where ρ_L = 1.00 g/cm^3 is the density of the submersion liquid. Porosity was derived as $(1-\rho_{app}/\rho_{tiss})$, and volume fraction as (1–porosity).

To account for inhomogeneity of the specimens, we performed duplicate determinations of ash and hydroxyproline on both a distal and a proximal piece (Figure 6), and the specimens were cut into four pieces. The collagen content of the specimens was estimated by measuring hydroxyproline, assuming a content of hydroxyproline in collagen of 13.4% (w/w) [**128**]. After hydrolysis of the specimens in 6 M HC1 at 100°C for 16 hours, hydroxyproline was estimated according to the procedure of Woessner [**192**] with a slight modification of the reagent concentration [**73**] as described by Danielsen and Andreassen [**24**]. The collagen (tissue) concentration was calculated to be the amount of collagen divided by the dry weight, and the collagen (apparent) density was the collagen weight divided by whole specimen volume. The bone specimens were then ashed in a muffled oven at 100°C for 2 hours and 580° for 18 hours, and the dry weight of the ash determined. The mineral concentration was the amount of mineral divided by the dry weight, and the apparent ash density was the mineral weight divided by whole specimen volume.

Guinea pig bone samples (VII–IX)

After mechanical testing, the 3-mm-thick proximal tibial specimen was defatted using the same procedure as described above. Dry weight was measured and submerged weight of specimens was determined (Mettler AT250 balance, Mettler Instruments AG, Greifensee, Switzerland) using Archimedes' principle [**39**]. The determination of dry weight and submerged weight was repeated once. Due to irregular shape of specimens, total specimen volume was calculated from micro-CT images. Bone tissue density (g/cm^3), and apparent density (g/cm^3) were determined [**39**].

Proximal tibial bone specimens were sectioned into the medial and lateral condyle sub-specimens. The dry weights of the two pieces from each condyle were determined, and then they were used for collagen and mineral determinations by the same procedures applied for human samples as described above.

7) Statistical analyses

Human cancellous bone

All the statistical analyses were based on data from all specimens using statistical software SPSS version 10.0.7 (SPSS Inc. Chicago, Illinois, USA). A p value <0.05 was considered to be significant.

a) For study of the accuracy and precision of micro-CT scanning, liner regression analysis was used to assess different methods and paired t-tests were used to compare discrepancy between groups (I).

b) For assessing age-related changes, all the statistical analyses were based on data from all specimens, and only the mean value for each tibia was used in analyses of age-related variations and in regression analyses. Each individual was represented by one set of values; thus data obtained from individuals are independent from one to another. The paired t-test was first performed to compare the properties between the medial and lateral condyles. Linear regression analyses were further used to assess the association between the overall properties, and the properties of the medial and the lateral condyle versus age. Then the slopes and intercepts of the linear regressions were tested to assess whether there were significant differences in age-related trends in the microstructural properties between the condyles. Linear and multiple regression analyses based on mean value for each tibia were used to assess the associations between Young's modulus and microstructural properties (II-III).

c) For evaluating the multiple associations among various microstructural, physical/compositional, and mechanical properties, the mean value for each tibia was used in analysis. Each individual was represented by one set of values, thus all observations were independent. Bivariate correlation analysis was done to obtain Pearson's correlation coefficient (R) among various properties. Linear regression analyses were used to assess the associations between one of the primary microstructural properties (bone volume fraction, structure model index, anisotropy, connectivity and trabecular thickness) or Young's modulus and all other properties. Assuming that the structure model index or bone volume fraction was a good predictor for Young's modulus, the degree of anisotropy was added in a multiple regression model to test the hypothesis that it could significantly improve the explanation for the variance of Young's modulus. Because of the skewness of data in linear regression analysis, connectivity density and marrow space volume were logarithmically transformed to obtain normal distribution. These data were further divided into three age groups: young (16 to 39 years), middle (40 to 59 years) and old age (60 to 85 years) to assess the multiple associations among properties in different age groups. The correlation coefficient (R) or determination coefficient (R^2) was used to express the proportional variation due to linear or multiple regressions (IV).

d) Normality and equal variance were checked first, then paired or 2-sample t-tests, as appropriate, were done to assess the differences in mechanical and physical/compositional properties between the osteoarthrosis and 3 control groups. Linear regression analyses were used to assess the associations between mechanical properties and physical/compositional properties. Stepwise multiple linear regression analyses were used to evaluate the associations between each of the mechanical properties as dependent variables and all physical/compositional properties measured as independent variables. The determination coefficient (R^2) was used to express proportional variation due to linear or multiple regression (V).

e) Two-way analyses of variance were carried out for repeated measurements of the microstructural properties. Comparing OA and normal groups determined the between-subjects factor and the medial and lateral groups, the within-subjects factor. All the tests were first checked for normality and equal variance. When significant main effects or an interaction between the main effects were found, particular posthoc multiple comparisons between groups were made using the Bonferroni test. Linear regression analyses assessed associations between mechanical and microstructural properties. The slopes and intercepts of the linear regressions were tested to assess whether there were significant differences in the relationship between the best predictors from the mechanical and microstructural properties in the four groups (VI).

Guinea pig subchondral bone

The results (mean with SD) were analyzed statistically. Firstly, normality and equal variance of the data were examined. One-way analyses of variance (ANOVA) were performed among the groups in each experimental period. The post hoc multiple comparisons were adjusted using Bonferroni test or Dunnett's test as appropriate. Paired t-tests were used to compare differences in properties between the medial and lateral condyles (VII–IX).

Results of own studies

Accuracy and precision of micro-CT scanning (I)

Underestimation of volume fraction (small, yet significant) was found by using method I (2%, p = 0.03), using the Archimedes-based volume fraction as reference. Linear regression of volume fractions obtained by applying individual thresholds from method I and method II showed that the slopes of the two regression lines were significantly different ($p < 0.001$).

For method I, the constant coefficient (y-intercept) of the linear model was significantly different from zero, and the slope was significantly different from unity (both $p<0.001$). Due to its definition, method II resulted in a y-intercept equal to 0, and a slope equal to 1 (p=0.37 and p=0.75 respectively). Thus, method II generated accurate values of bone volume fraction (Figure 9).

A 4% underestimation of the volume fractions was seen for the 20 specimens segmented by using the mean threshold (272) from method I (p = 0.001), whereas there was no difference from the Archimedes-based measures of the volume fractions by using the mean threshold (262) from method II (p=0.80). The y-intercept of the linear model of method I was not significantly different from zero, and the slope was not significantly different from unity (p = 0.85 and p = 0.09 respectively). The y-intercept of the linear model of method II was not significantly different from zero, and the slope was not significantly different from unity (p = 0.73 and p = 0.63 respectively) (Figure 9). The mean connectivity densities of the 20 specimens using thresholds 272 and 262 were 7.25 ± 2.29 mm^{-3} and 7.02 ± 2.17 mm^{-3}, respectively ($p<0.002$).

Human aging

Human age-related changes in 3-D microarchitecture (II–III)

Significant decline in bone volume fraction and trabecular thinning after 60 years of age and a change in microarchitecture of cancellous bone from plate-like toward more or less rod-like are observed (Figures 2 and 10). The degree of anisotropy (Figures 10 and 11), structure model index, mean marrow space volume and bone surface-to-volume ratio of human tibial cancellous bone increased significantly with age. Connectivity density did not change significantly with age. Bone volume fraction and bone surface density decreased significantly with age (Figures 10 and 11). In general, analysis in decade groups showed that these changes are not apparent between 20 and 59 years. Typical changes occurred after 60 years of age (Figures 10 and 11). All the microarchitectural properties from the medial and lateral condyles had the same age-related trends.

Mutual association among the properties of cancellous bone (IV)

Based on the entire human tibial cancellous bone datasets, linear regression analysis revealed that the structure model index was the best predictor for Young's modulus ($R^2 = 0.45$). Degree of anisotropy increased this explanation to 53% in a multiple regression model. Bone apparent ash density or volume fraction together with the degree of anisotropy could

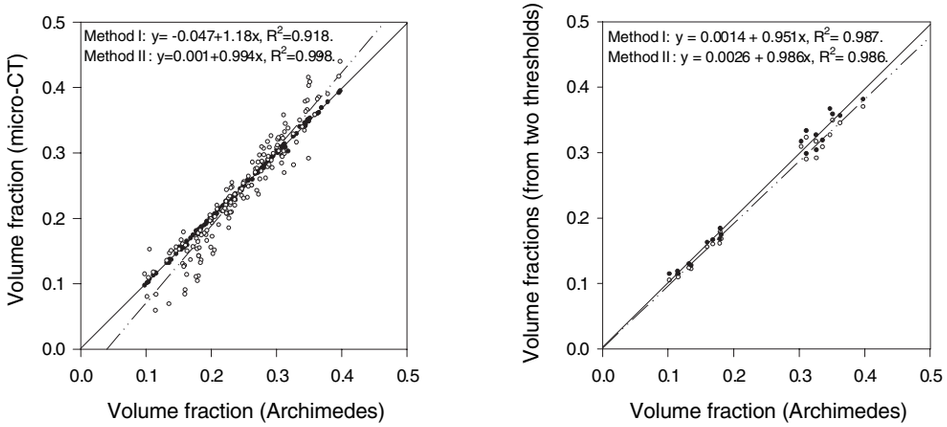

Figure 9. Correlations of bone volume fractions determined by different methods
Left: Correlations of volume fractions (micro-CT vs. Archimedes) of all specimens obtained by applying individual thresholds from method I (dashed line & open circles) and method II (solid line & filled circles). Right: Correlations between volume fractions: Archimedes vs. the mean thresholds from method I (dashed line & open circles) and method II (solid line & filled circles) (I).

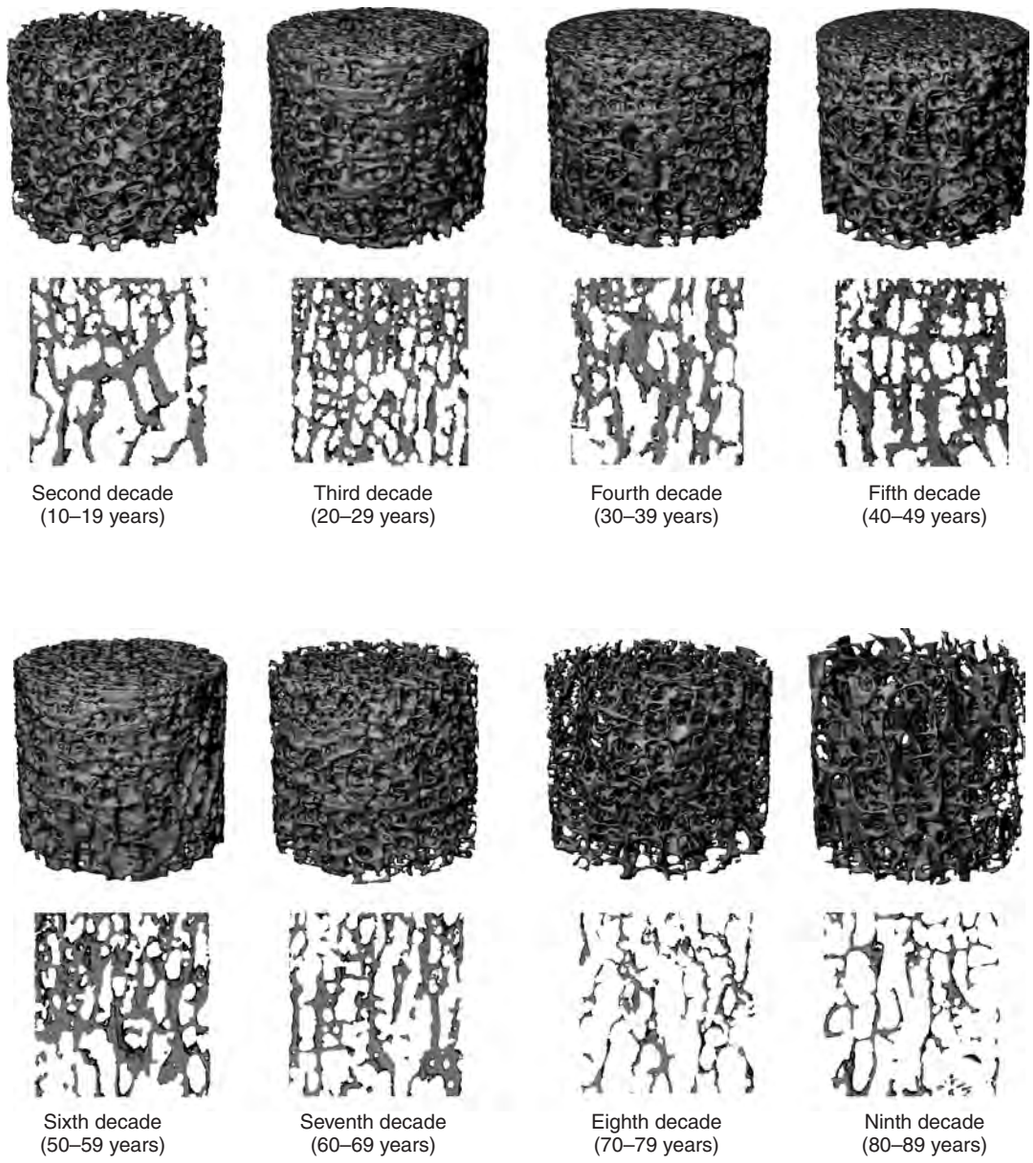

Figure 10. 3-D reconstruction of cancellous bone
Three-dimensional micro-CT image reconstructions and renderings of human tibial cancellous bone specimens randomly selected from medial or lateral condyle in each decade. The renderings are produced from 10 image slices (215 micron in thickness). A significant decline in bone volume fraction, thinning of trabeculae after 60 years, and a change in microstructure of cancellous bone from plate-like to more or less rod-like are seen (II, III).

explain the variance of Young's modulus by 46% or 45%, respectively.

Apparent density, collagen density (Figure 12), and apparent ash density were highly correlated with bone volume fraction ($R^2 > 0.96$). The variance of the structure model index was strongly explained by the apparent ash density or bone volume fraction ($R^2 = 78\%$ and $R^2 = 77\%$, respectively). The variance of the degree of anisotropy was well explained by the marrow space volume by 42%. Bone volume fraction alone could explain 37% of the variance of the degree of anisotropy. The variance of connectivity was highly explained by the marrow space volume ($R^2 = 0.92$). The variance of trabecular thickness was highly explained by the bone surface-to-volume ratio ($R^2 = 0.81$) (Figure 12).

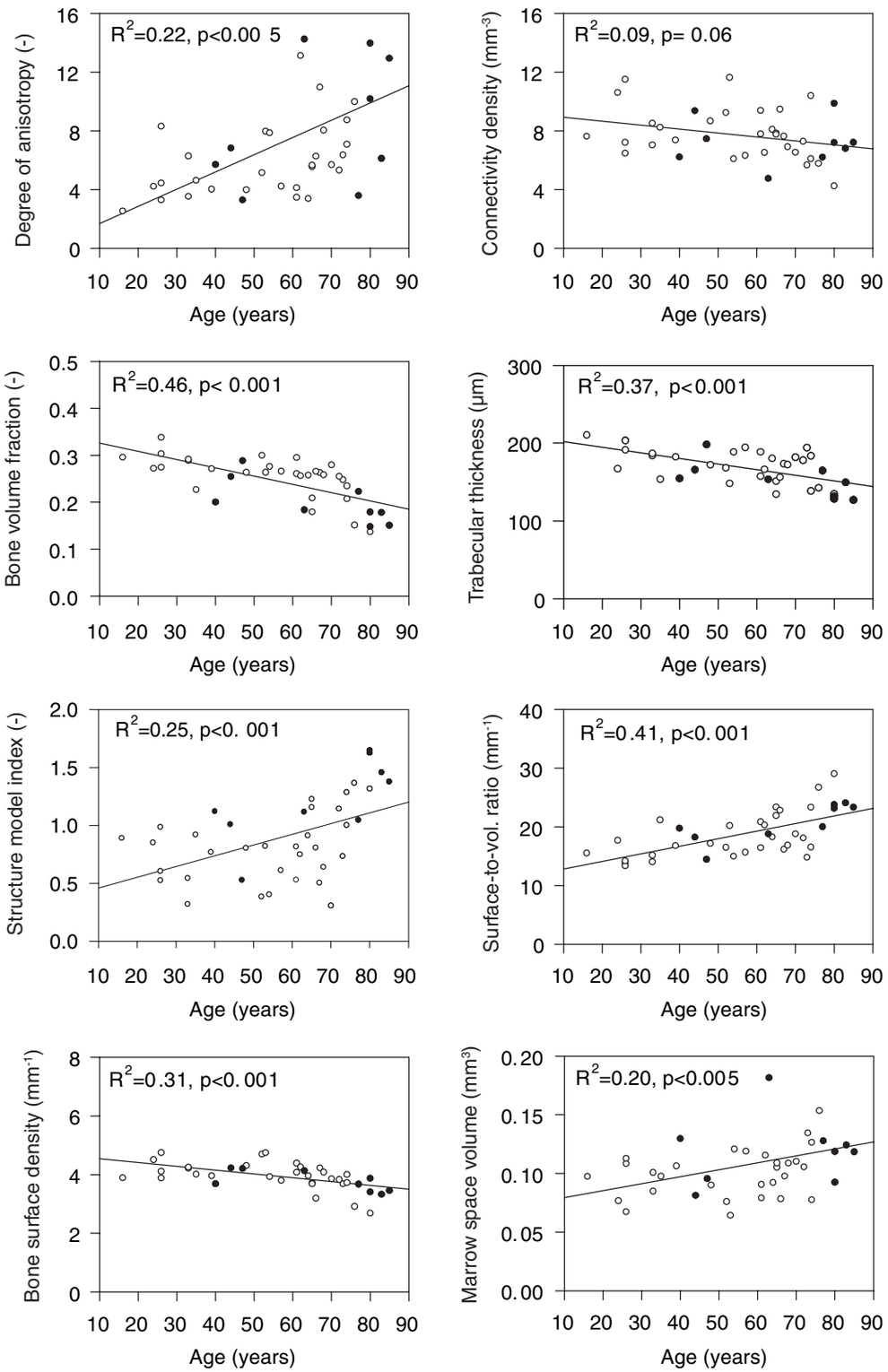

Figure 11. Age-related microarchitectural changes in human cancellous bone (II, III)
Microarchitectural properties in relation to age are illustrated using the overall value of each knee (filled circles=female (n_1=10), open circles=male (n_2=30)). The determination coefficients R^2 and p-values were derived from linear regression.

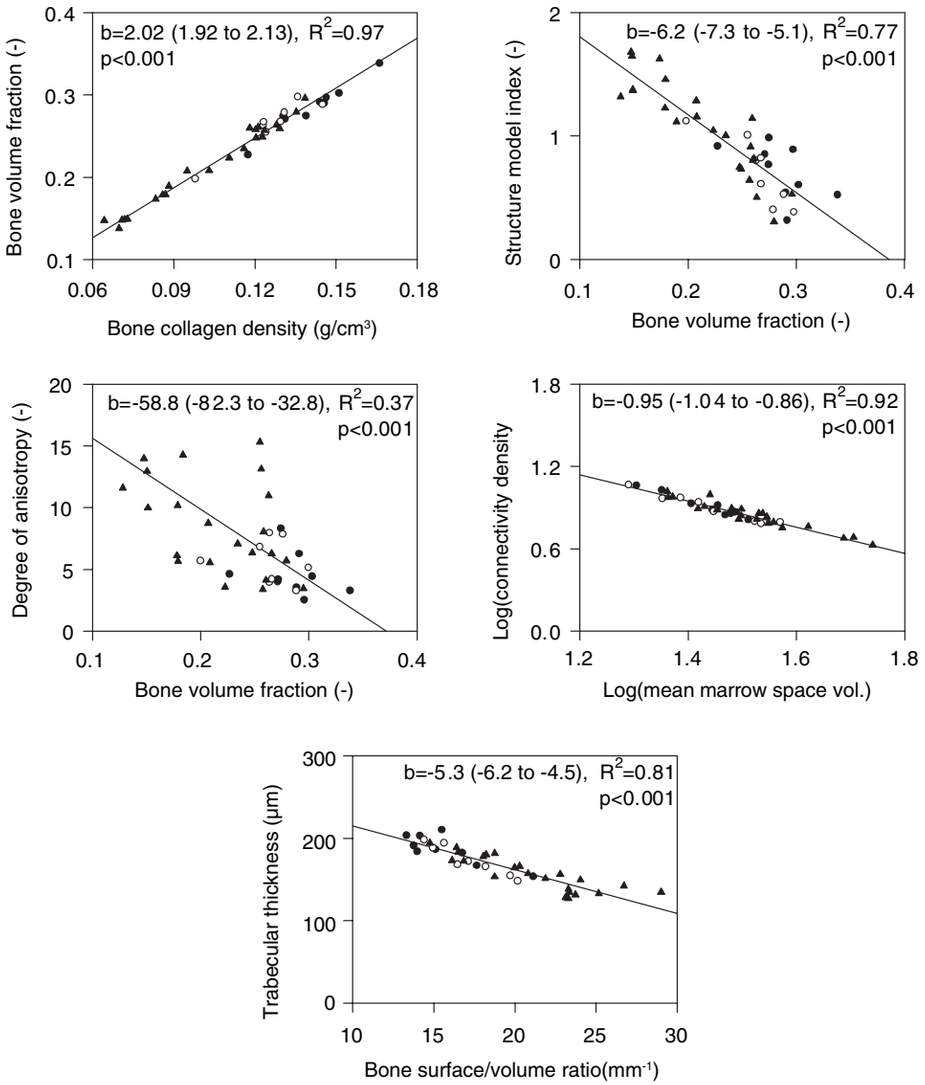

Figure 12. Mutual association among the microarchitectural properties of cancellous bone (IV)
The significant predictors for the primary microarchitectural properties of normal human cancellous bone are illustrated. The data are presented as slope (b) (95% confidence interval), determination coefficient (R^2) and p value derived from linear regression analysis (● = young age, ○ = middle age, ▲ = old age).

Human early OA

Early OA grading was done according to Mankin's criteria [**116**]. Early human OA was seen as degeneration, with slight fissures in the cartilage surface (superficial zone) of the medial condyle in osteoarthrotic tibiae, but the cartilage surface of the lateral condyle was intact. The medial osteoarthrosis was graded as 4.9 (3–7), lateral control as 1.7 (1.5–3), normal medial as 0.8 (0–2), and normal lateral as 0.5 (0–1), respectively (V).

The 3-D reconstructions of cancellous bone from micro-CT images for the four groups are presented in Figure 13. Significant microarchitectural changes of OA cancellous bone can be observed. OA cancellous bone has a very heterogeneous architecture. Compared with normal medial control, osteoarthrotic trabecular bone are significantly thicker and denser, and unusually plate-like, but have lower mechanical strength (Figure 13).

Two-way analyses of variances did not show significant OA/normal and medial/lateral interactions (p = 0.537 to 0.974). Bone volume fraction was greater in the OA groups (both OA and lateral control) than in the normal groups (normal medial and lateral, p = 0.001 for the group effect in the analysis of variance), and was greater medially than laterally (p=0.002 for the effect of condyle in the analysis of variance). OA speci-

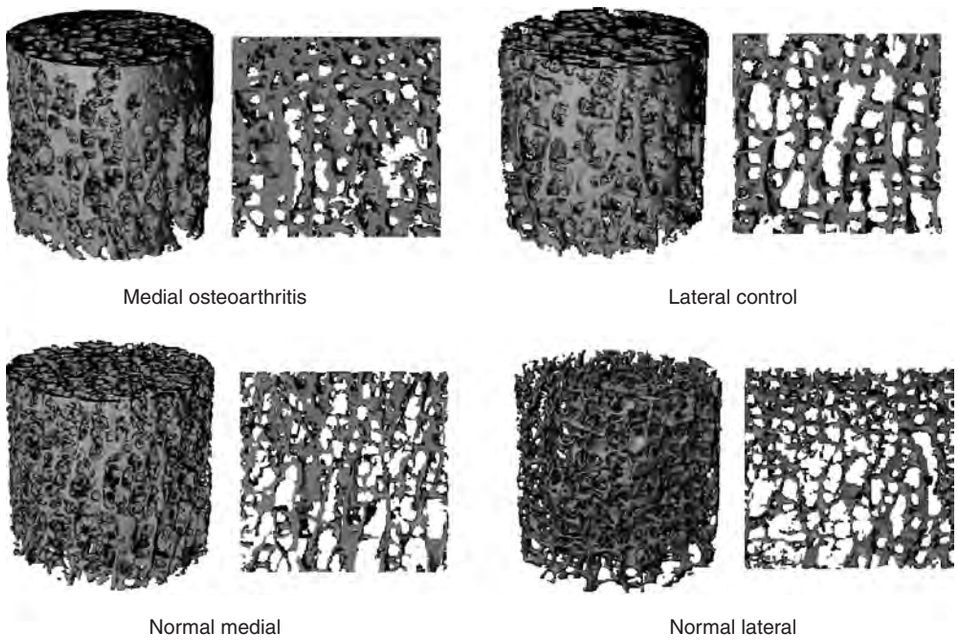

Figure 13. 3-D reconstructions of subchondral cylindrical cancellous bone specimens
Comparing the four specimens obtained from cancellous bone of tibiae with early OA, medial specimens (upper left) had the highest bone volume fraction and trabecular thickness, typical plate-like structure and the lowest bone strength and lateral specimens (upper right) had higher bone volume fraction and trabecular thickness, more plate-like structure and lower bone strength. Of the specimens obtained from normal tibiae, medial specimens (lower left) had lower bone volume fraction and trabecular thickness, more rod-like structure and the highest bone strength, and lateral specimens (lower right) had the lowest bone volume fraction and trabecular thickness, typical rod-like structure and relatively higher bone strength (VI).

mens had a 20% greater bone volume fraction than that of the normal medial (p = 0.049). The structure model index was lower in the OA groups than in the normal groups (p = 0.006), and was smaller medially than laterally (p = 0.001). Medial OA had a 25% lower the structure model index relative to that of the normal medial (Figure 14).

Trabecular thickness was greater in the OA specimens than in the normal specimens (p = 0.002), and was greater medially than laterally (p = 0.002). OA specimens had a 12.5% greater trabecular thickness than that of the normal medial, and the lateral intact samples had a 23% greater trabecular thickness relative to the normal lateral. Bone-surface-to-volume ratio was lower in the OA specimens than in the normal specimens (p= 0.002), and was greater laterally than medially (p = 0.03) (Figure 14).

Bone volume fraction, apparent density, apparent ash density, and collagen density of early OA cancellous bone were significantly greater than those of the 3 controls (p = 0.04–0.001, Figure 14). Neither the mean tissue density, mineral concentration nor collagen concentration of early OA cancellous bone did differ significantly from those of normal controls (not shown).

The ultimate stress of OA cancellous bone was best explained by its linear relationship with the structure model index. The determination coefficient (R^2) of ultimate stress in OA cancellous bone was largely reduced compared with that of the normal medial (Figure 15); only 48% of the variation of ultimate stress could be explained. However, in normal medial controls, 71% of the variation of ultimate stress could be explained by the structure model index, and 54% by the bone volume fraction. More importantly, the slopes of two linear regression lines were significantly different (p = 0.001). For the OA group, the y-intercept of the linear model was significantly different from that of the normal medial (p = 0.001, Figure 15).

Likewise, failure energy of OA cancellous bone was best explained by its linear relationship with the structure model index. The determination coefficient of failure energy in OA was significantly reduced compared with that in the normal medial control (Figure 15), and 54% variation of failure energy of cancellous bone in OA could be explained. In the normal medial control, 69% of the variation of failure energy could be explained by the structure model index alone. The slopes of two linear regression lines were also significantly different (p = 0.001). For the OA group, the y-intercept of the linear model was significantly different from that of the normal medial group (p=0.001, Figure 15).

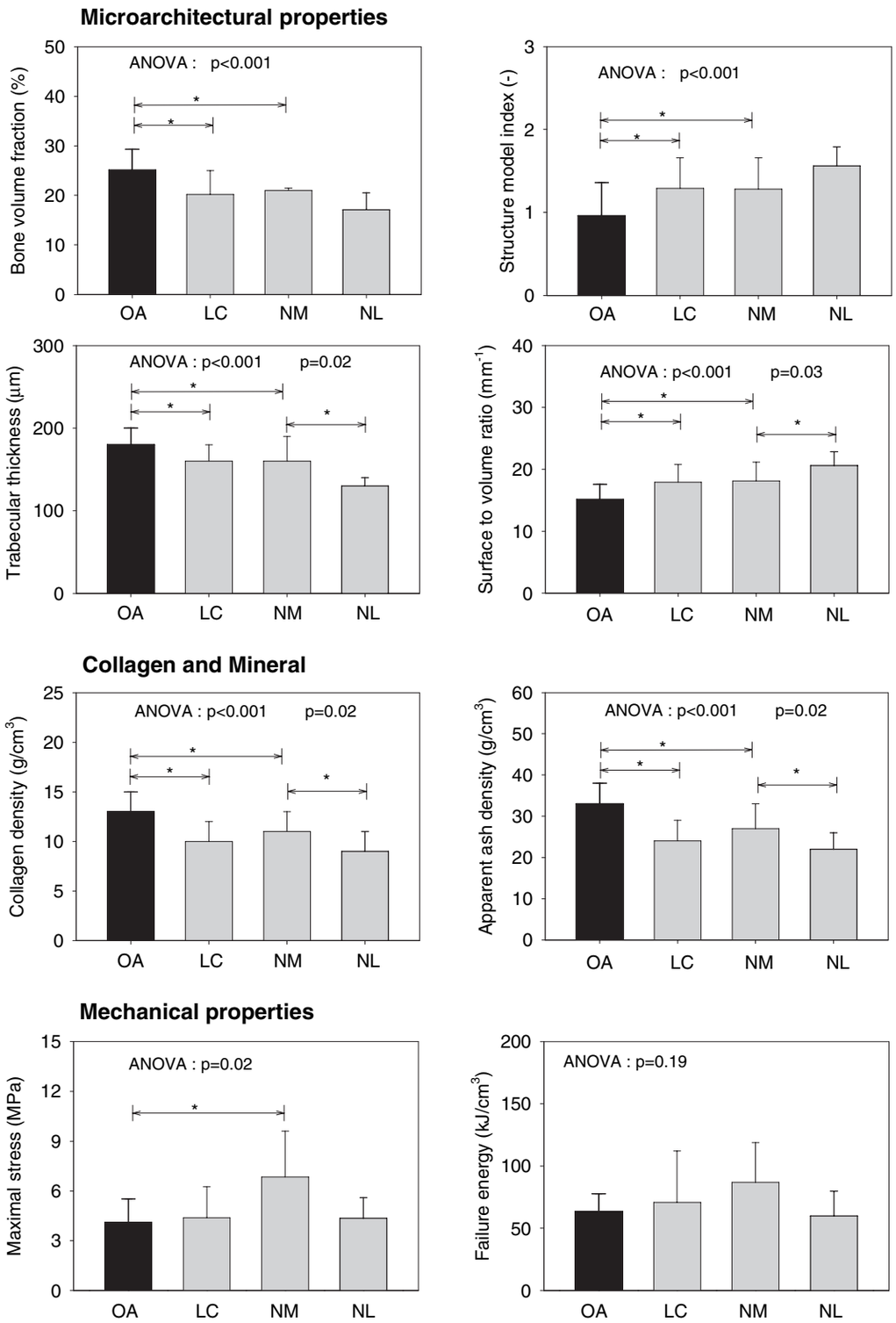

Figure 14. 3-D microarchitectural properties, bone collagen and mineral and mechanical properties of subchondral cancellous bone in 4 groups (V, VI).

OA = medial osteoarthrosis, LC = lateral control, NM = normal medial, and NL = normal lateral. Mean and SD (vertical bar). Two-way ANOVA was performed among the 4 groups, and the resulting p-values for group and condyle effects as well as p-values resulting from post-hoc multiple comparisons are indicated.

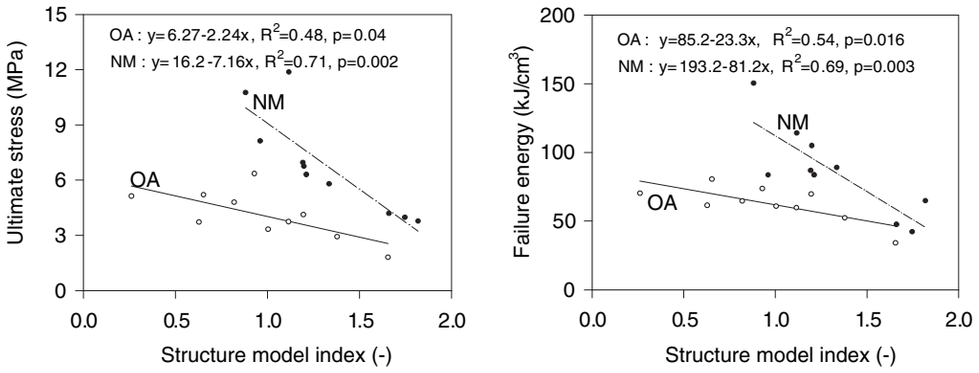

Figure 15. Associations between microarchitectural properties (SMI) and mechanical properties (strength and failure energy) (VI)

Guinea pig osteoarthrosis

Age-related changes (VII)

Examples of the 3-D reconstruction of cancellous bone from micro-CT images for the 5 age groups are shown in Figure 16. Significant microarchitectural changes with age in cancellous bone of guinea pig can be observed. These subchondral bone tissues have very heterogeneous microarchitecture.

OA grading: Progressive cartilage degenerations with age in guinea pig were seen in both condyles, and this was particularly pronounced in the medial condyle. Chondrocyte death and proteoglycan loss with cartilage fibrillation were seen on the medial tibial plateau as early as at 6 months of age. Incidence and severity of the cartilage lesions increased with age: by 12 months of age, all animals had moderate degeneration of the medial tibial plateau, and by 24 months, all animals had severe degeneration of the medial tibial plateau and moderate degeneration of the lateral tibial plateau (Figure 17).

For subchondral plate, bone volume fraction and thickness were increased markedly from 3 to 6 months of age ($P<0.001$), and they remained fairly constant thereafter. This trend was also true for both the medial and lateral condyles. For proximal tibial cortex, cortical thickness showed minimal values at 3 months of age and cortical cross-sectional area increased gradually with age to a maximal value at 24 months (Figures 16 and 17).

For subchondral cancellous bone, apart from an initial high value at 3 months of age, bone volume fraction was the lowest at 6 months and increased thereafter gradually with age. The increase was only statistically significant in the medial condyle. Trabecular thickness was lowest at 3 months and increased with age. Similar trends for property changes were also observed for both condyles. The structure model index decreased significantly with age, reflecting a change of trabeculae from rod-like toward plate-like structure. The same trend was observed for both condyles. Connectivity density was the highest at 3 months and remained fairly constant from 6 months (Figures 16 and 18).

Bone collagen concentration of proximal tibia increased with age in the lateral condyle but not in the medial condyle. Collagen concentration was greater in the medial tibial condyle than in the lateral condyle. Mineral concentration was maximal at 3 months and relatively constant after 6 months of age (Figure 18).

For cancellous bone, ultimate stress increased with age, with maximal values at 24 months. For proximal cortical bone, ultimate stress was maximal at 6 months and nearly constant after 9 months of age (Figure 18).

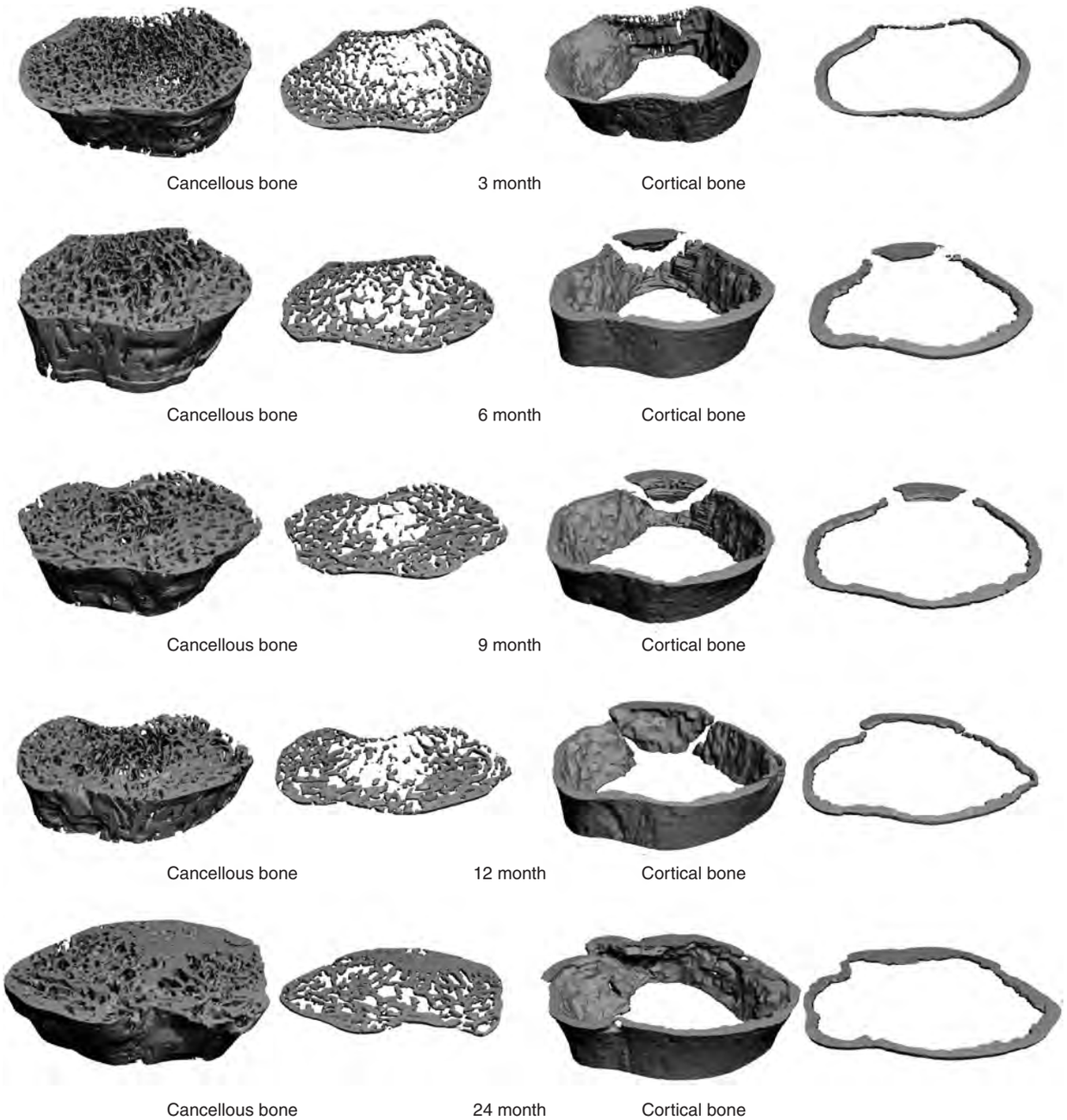

Figure 16. Age-related microarchitectural changes in guinea pig subchondral cancellous bone (left) and cortical bone (right) (VII)
Three-dimensional reconstructions of micro-CT images for guinea pig left proximal tibial cancellous bone and cortical bone 0.5 mm beneath subchondral bone plate in the five age groups are presented. The sample selection was based on the median value of bone volume fraction.

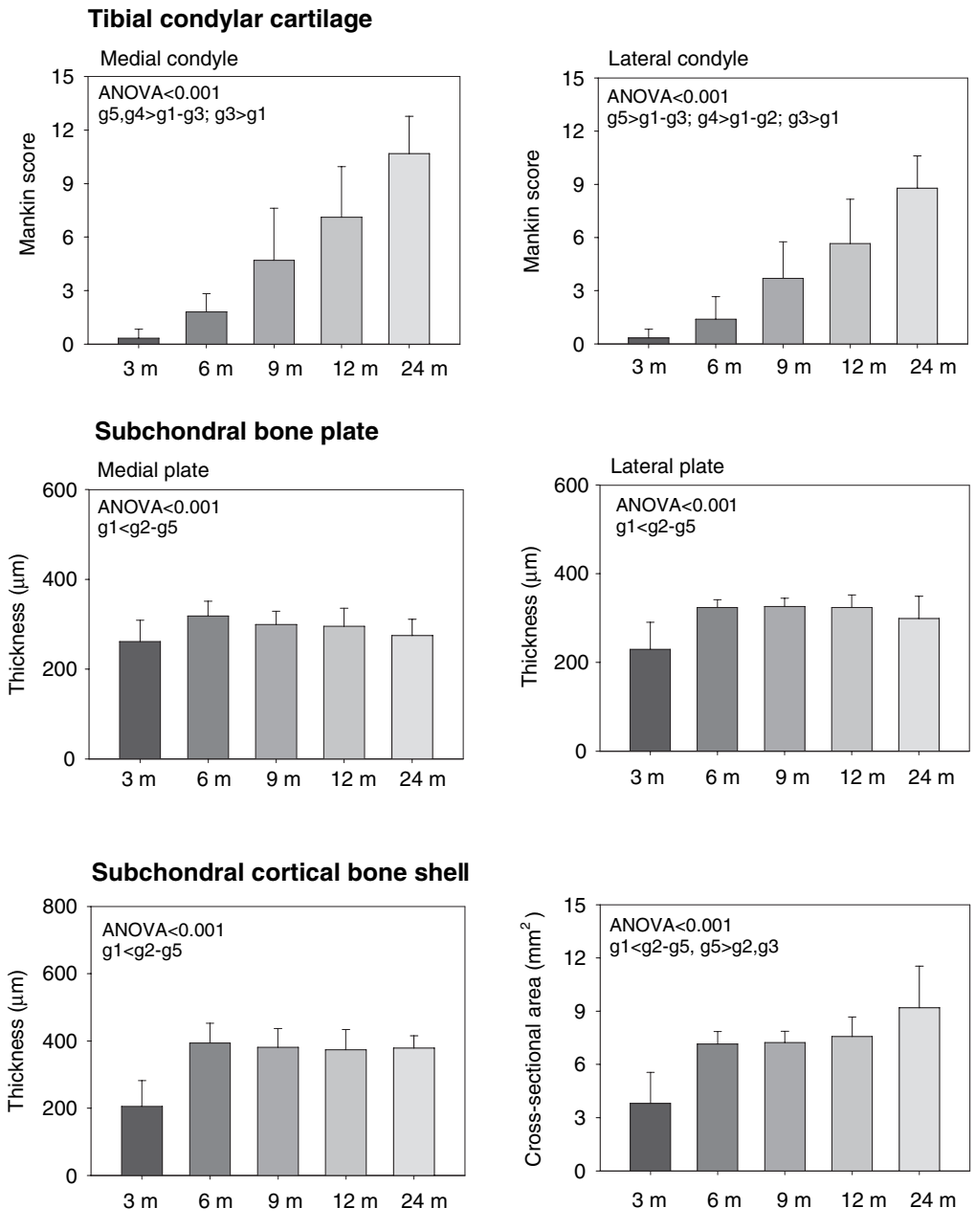

Figure 17. Mankin score for medial and lateral condylar cartilage, subchondral bone plate thickness of medial and lateral condyles, and thickness and cross-sectional area of subchondral cortex.
Mean and SD (vertical bar). One-way ANOVA was performed among the 5 age groups, and the resulting p values from post-hoc multiple comparisons are indicated (g1:3m, g2:6m, etc) (VII)

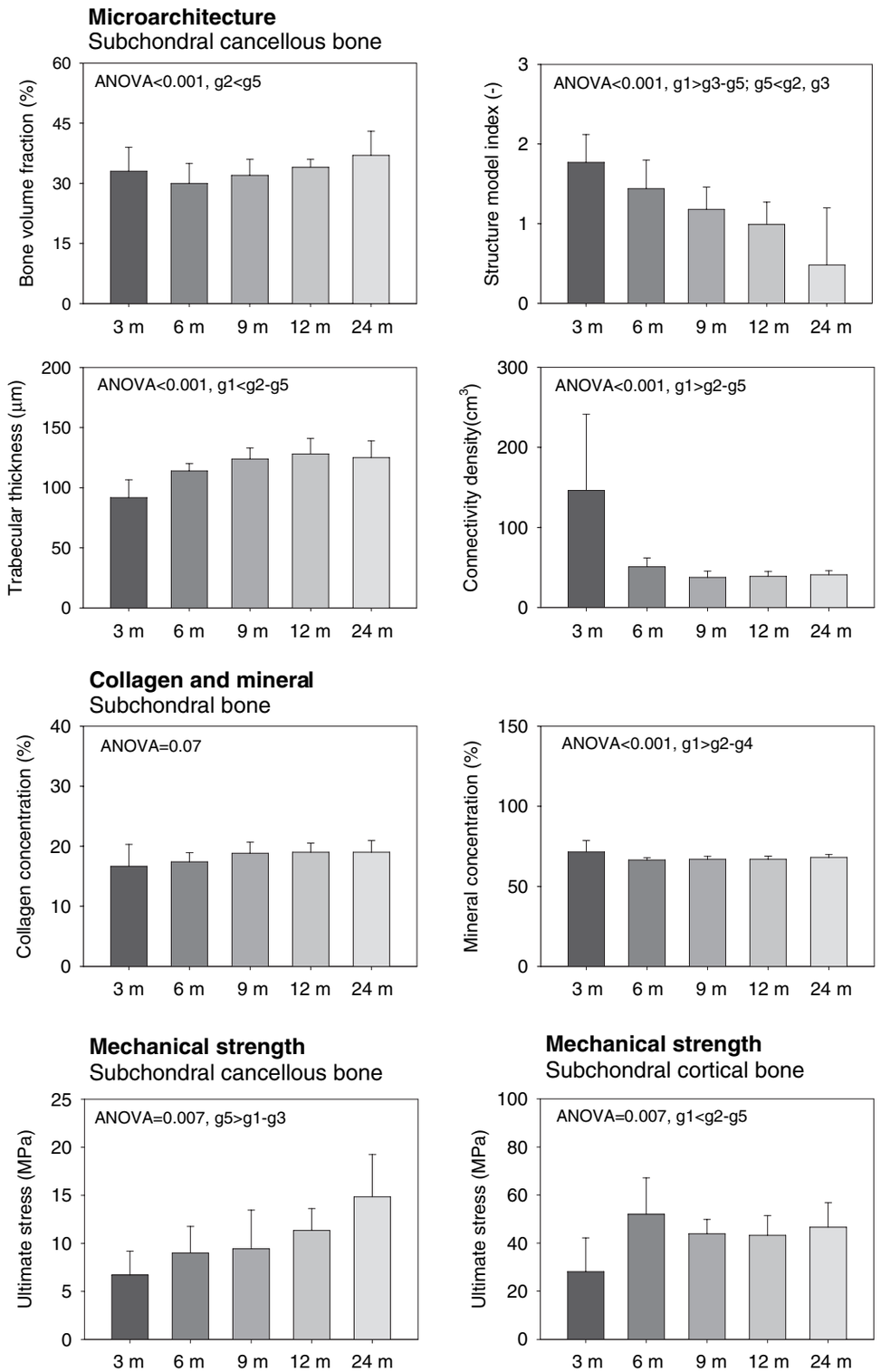

Figure 18. Microarchitectural properties of subchondral cancellous bone, bone collagen and mineral, and mechanical strength of subchondral cancellous and cortical bone.

Mean and SD (vertical bar). One-way ANOVA was performed among the 5 age groups, and the resulting p values from post-hoc multiple comparisons are indicated (g1:3m, g2:6m, etc) (VII)

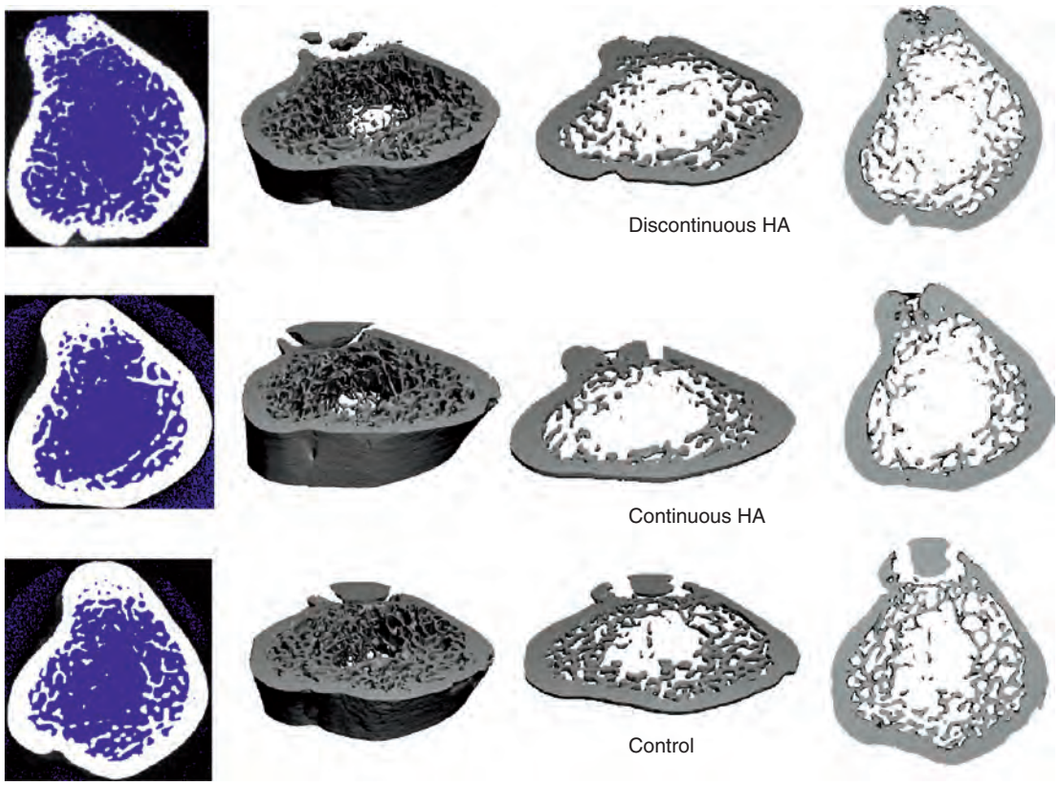

Figure 19. Effect of hyaluronan on 3-D microarchitecture of subchondral bone tissues (VIII)
Examples of 3-D reconstruction of micro-CT imaging for the HA discontinuation, the HA repetition and the control 5.5-month experimental groups. Marked differences in the microarchitecture of subchondral bone are seen. Samples represent the median values of the bone volume fraction.

Effects of hyaluronan (VIII)

Examples of the 3-D reconstruction of cancellous bone from micro-CT images for the 5 experimental groups are illustrated (Figure 19). Significant microarchitectural changes after hyaluronan treatment in subchondral cancellous bone of guinea pig can be observed.

The Mankin score for the medial and lateral condyles are illustrated (Figure 20). Progressive cartilage degenerations are observed in both condyles of 9 and 12 months control groups and the degeneration was particularly significant in the medial condyle. Chondrocyte death and proteoglycan loss with cartilage fibrillation were observed on the medial tibial plateau in both age groups. Incidence and severity of the cartilage lesions increased with age, and by 12 months of age, all animals in the control group had moderate degeneration of the medial tibial plateau. In contrast, all the HA-treated groups after both experimental periods had only slight articular cartilage fibrillation in the medial condyles, and the lateral condyles were almost normal (Figure 20).

There were no significant differences in the properties between the HA repetition and HA discontinuation groups, although there were significant differences in the properties between 2.5-month and 5.5-month HA groups. The subchondral plate thickness was significantly lower in the medial condyle of 2.5-month HA group compared with the control group. No significant differences in the properties of subchondral plate in the 5.5-month HA groups compared to the control group were revealed. Both 5.5-month HA groups had greater plate thickness compared with the 2.5-month HA group, and changes was particularly pronounced in the medial condyle (Figure 20).

Treatment with HA had pronounced effects on the 3-D microarchitecture of subchondral cortical bone. Both 5.5-month HA groups had significantly greater cortical thickness compared with the control and compared with the 2.5-month HA group (Figure 20).

Treatment with HA had striking effects on the 3-D microarchitecture of subchondral cancellous bone. In the 2.5-month HA group, cancellous bone had significantly lower bone volume fraction, and greater structure model index compared with the control group. Both 5.5-month HA groups had significantly lower bone volume fraction, connectivity density and greater structure model index compared with the control

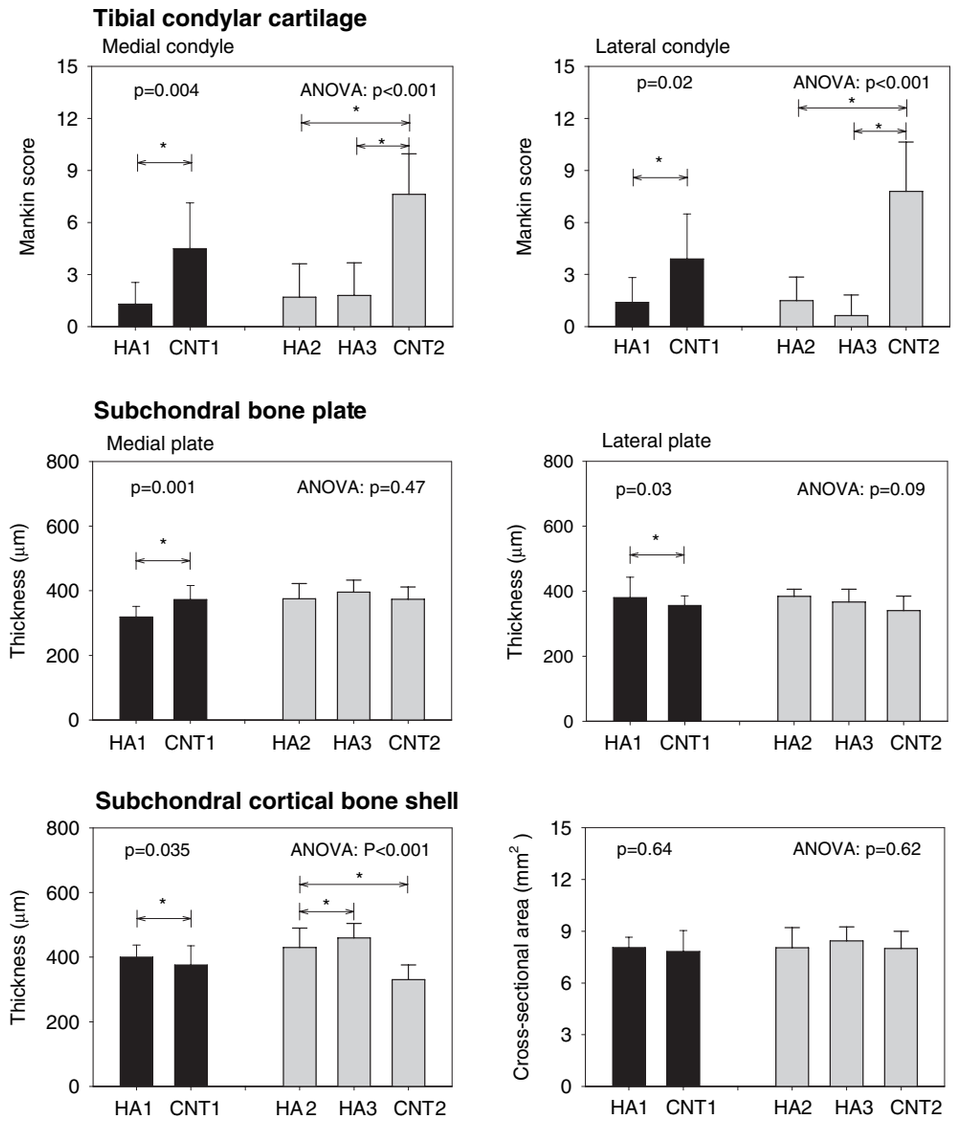

Figure 20. Mankin score for medial and lateral condylar cartilage, subchondral bone plate thickness of medial and lateral condyles, and thickness and cross-sectional area of subchondral cortex (VIII)
Mean and SD (vertical bar). Two sample t-test was performed between the two groups in the phase one; and one-way ANOVA was performed among the three groups in the phase 2. The resulting p values are indicated (post-hoc multiple comparisons; *p<0.05).

and lower structure model index compared with the 2.5-month HA group (Figure 21).

After HA treatment, no significant effect on bone collagen and mineral in the 2.5-month HA group was apparently found, whereas both 5.5-month HA groups had significantly increased bone mineral concentration, mineral density, collagen to mineral ratio and tissue density overall, and in the medial and lateral condyles. Furthermore, HA groups also had significantly greater apparent density in the medial condyle in both HA repetition and discontinuation groups. No significant differences in the properties for the 2.5-month HA group compared with the 5.5-month HA groups were apparently found (Figure 21).

Treatment with HA had neither influence on the mechanical properties of the cancellous bone nor the cortical bone in the 2.5-month HA group. Neither were the mechanical properties of cancellous bone in the two 5.5-month HA groups found to be different from control. In contrast to cancellous bone, cortical bone showed significantly changed mechanical properties with decreased Young's modulus in both 5.5-month HA groups. However, HA treatment had no effect on the ultimate stress of the cortical bone (Figure 21).

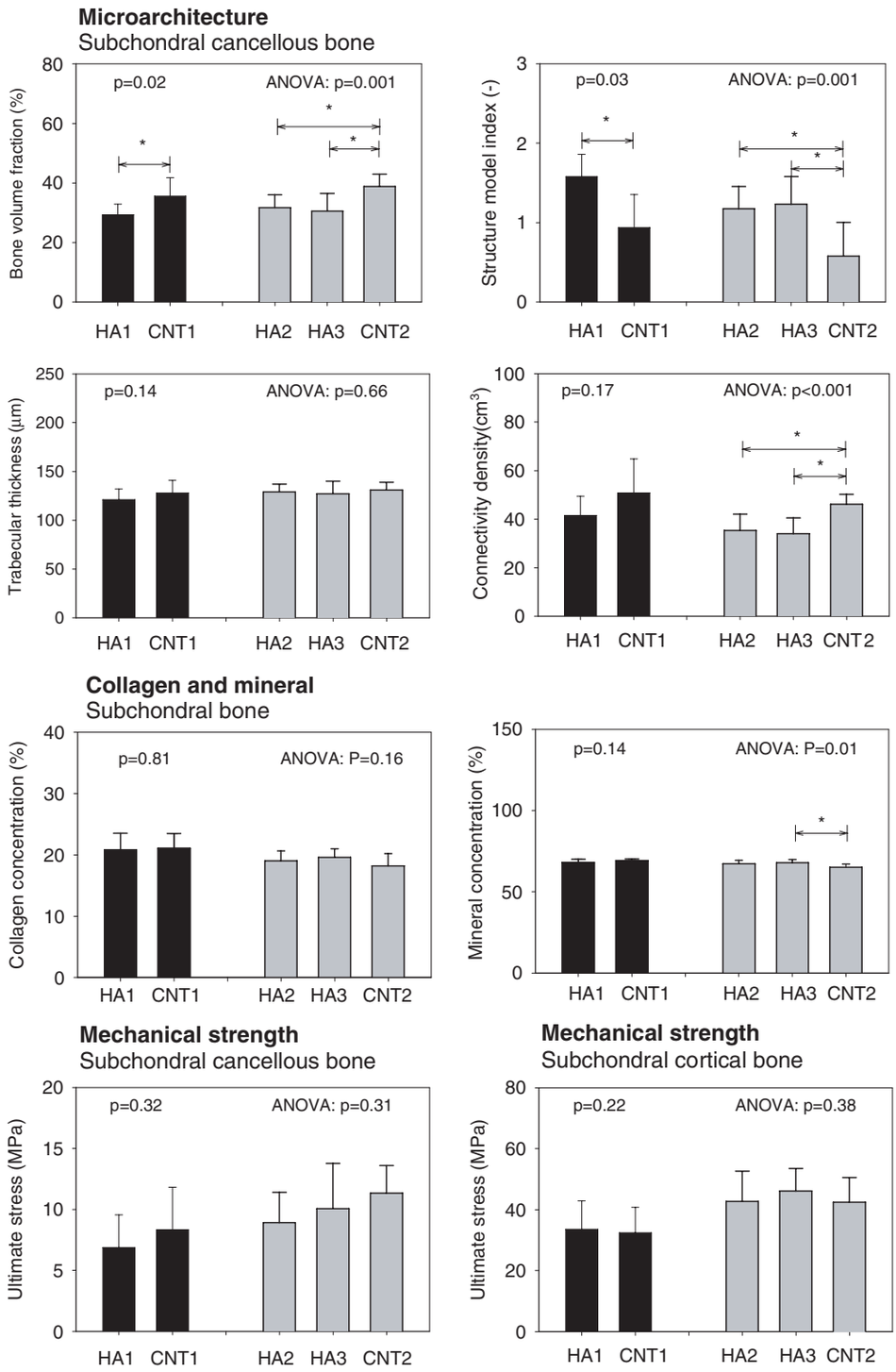

Figure 21. Microarchitectural properties of subchondral cancellous bone, bone collagen and mineral, and mechanical strength of subchondral cancellous bone and cortical bone (VIII)

Mean and SD (vertical bar). Two sample t-test was performed between the two groups in the phase one; and one-way ANOVA was performed among the three groups in the phase 2. The resulting p values are indicated (post-hoc multiple comparison); *p<0.05.

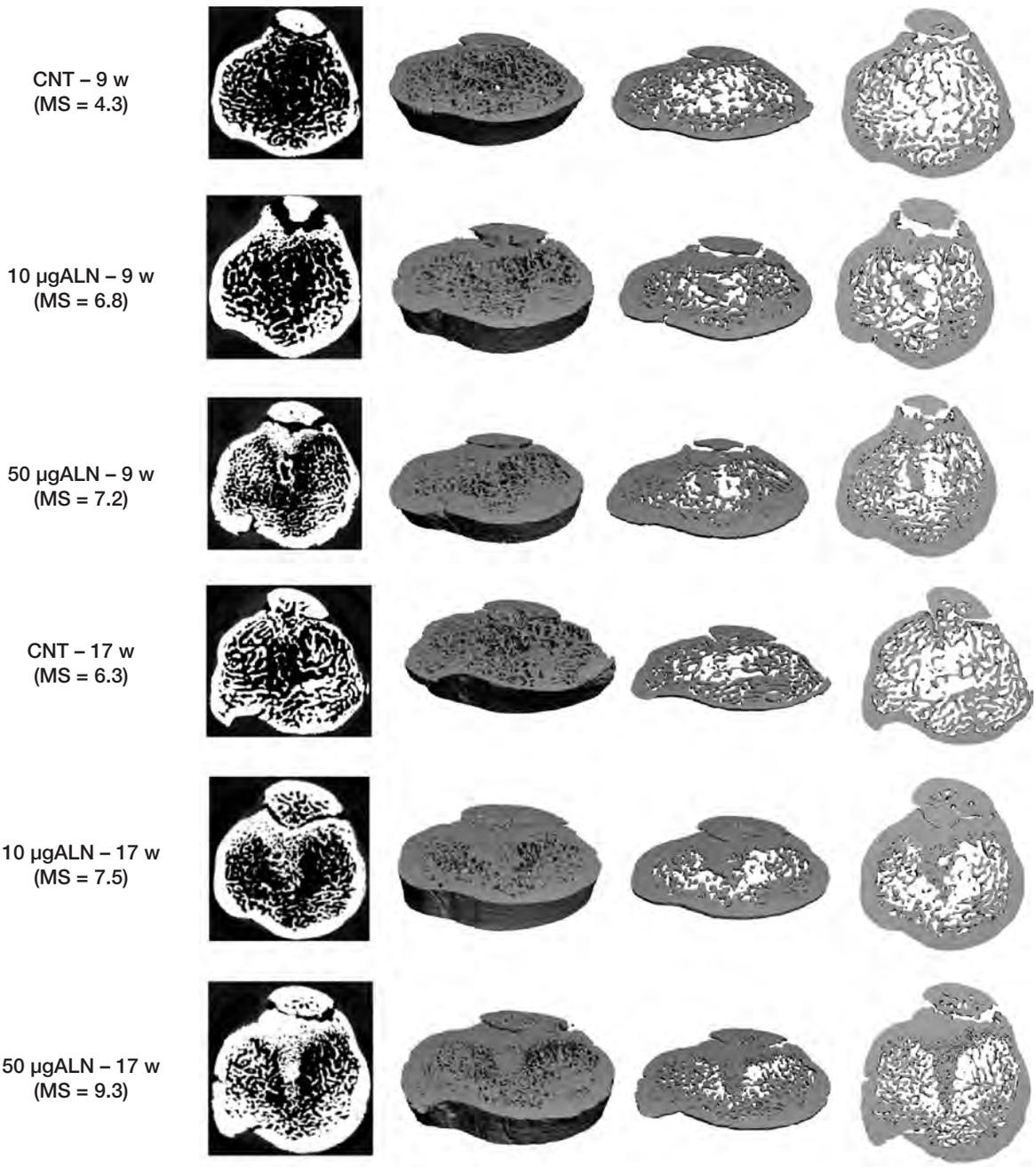

Figure 22. The effects of bone remodeling inhibition by alendronate on 3-D microarchitecture (IX)
Three-dimensional reconstruction of proximal tibial subchondral bone tissues from micro-CT imaging is illustrated. Significant microarchitectural changes by inhibition of bone remodeling with ALN in guinea pig primary osteoarthrosis can be observed. These changes are significant in all the ALN groups, where bone density was increased, with more densely packed and extremely plate-like trabeculae and thicker cortex. MS, Mankin score.

Effects of alendronate (IX)

Three-dimensional reconstruction of proximal tibial subchondral bone tissues in 6 groups is demonstrated in Figure 22. Significant microarchitectural changes by inhibition of bone remodeling with ALN can be seen.

Progressive cartilage degenerations were observed in both tibial condyles of the guinea pigs. Both the 9 months and the 12 months guinea pigs developed typical osteopathy that was similar to human OA. Thus, chondrocyte death and proteoglycan loss with cartilage fibrillation were observed on

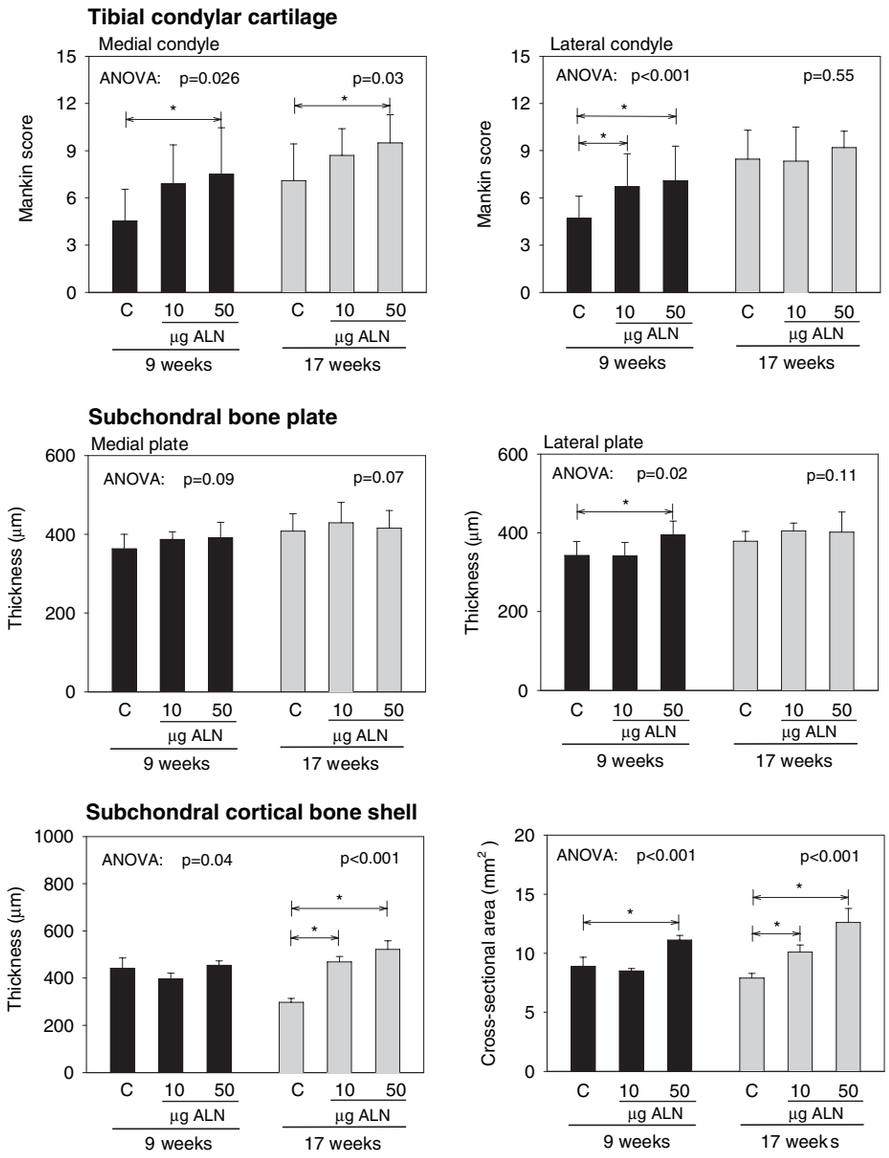

Figure 23. Mankin score for medial and lateral condylar cartilage, subchondral bone plate thickness of medial and lateral condyles, and thickness and cross-sectional area of subchondral cortex (IX)
Mean and SD (vertical bar). One-way ANOVA was performed among the three 9-week groups and the three 17-week groups, and the resulting p values are indicated. *p<0.05 when 10 mg and 50 mg ALN groups were compared with controls (C) of the same age (post-hoc multiple comparisons).

the medial tibial plateau in all 6 groups. The incidence and severity of the cartilage lesions increased with age, and at 12 months of age, the control animals had moderate degeneration in both the medial and the lateral tibial condylar cartilage. The ALN-treated groups had more severe cartilage degeneration in the medial condyle and also in the lateral condyle in the 9-week groups when compared with the controls (Figure 22). In the 9-week groups, the 50 µg/kg ALN treatment resulted in significantly increased lateral subchondral bone plate thickness compared with the controls (Figures 22 and 23).

The most outstanding changes in the 3-D microarchitecture of subchondral cortical bone following ALN treatment were a larger cortical thickness and cross-sectional area with an effect of ALN that appeared to increase with both ALN dose and treatment period (Figure 23).

The most striking features after ALN treatments were microarchitectural changes in the subchondral cancellous bone (Figures 22 and 24). Thus, ALN treatments resulted in significantly increased cancellous bone volume fraction and connectivity density. In addition, the trabeculae became more

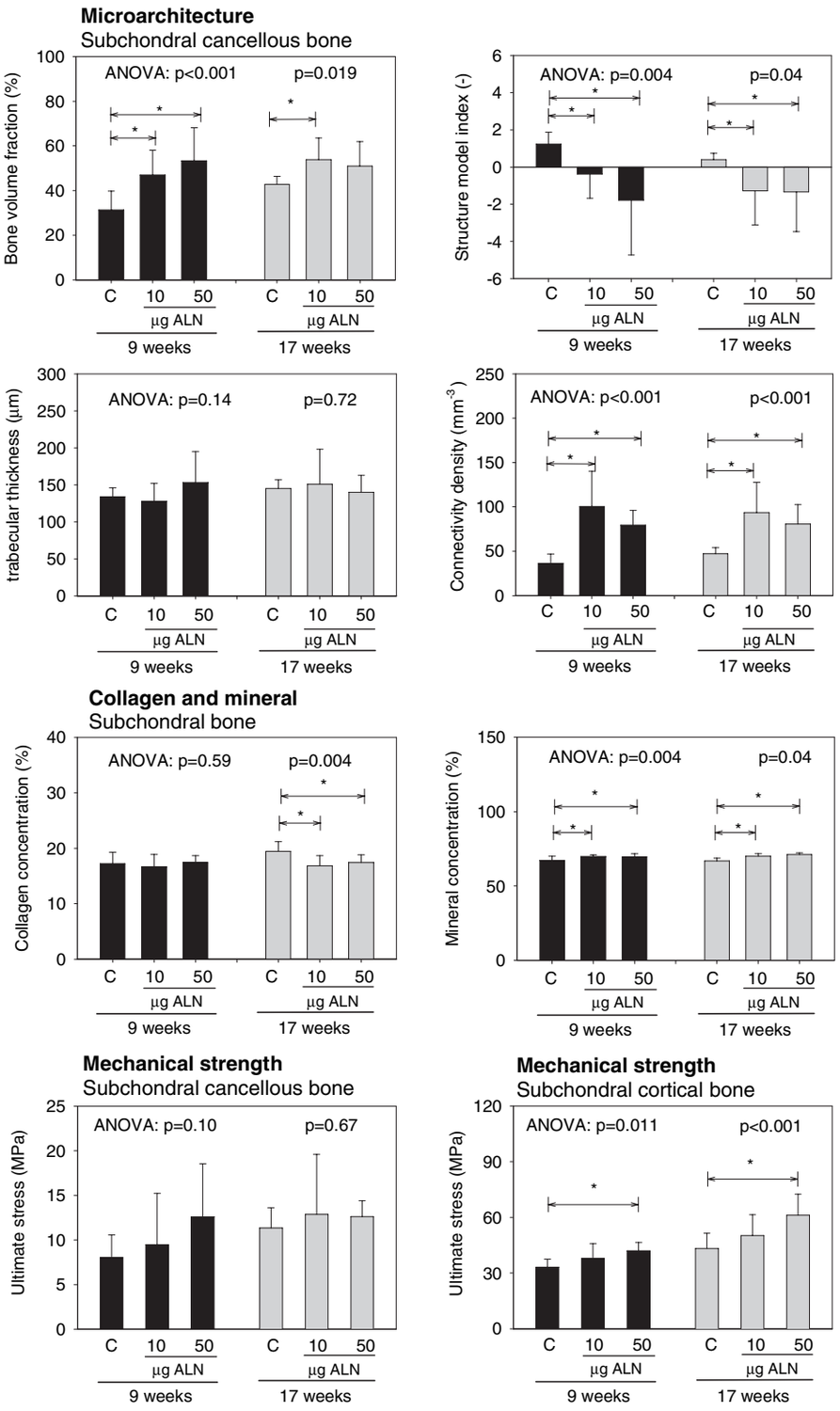

Figure 24. Microarchitectural properties of subchondral cancellous bone, bone collagen and mineral, and mechanical strength of subchondral cancellous and cortical bone (IX)

Subchondral cancellous bone volume fraction, structure model index, trabecular thickness, and connectivity density; bone collagen and mineral; and the mechanical strength of cancellous bone and cortical bone are illustrated. *p<0.05 when 10 mg and 50 mg ALN groups were compared with controls (C) of the same age (post-hoc multiple comparisons).

plate-like in structure. The changes in trabecular bone appeared after 9 weeks of treatment with only minor dose response of the doses given, and prolonged ALN treatment did not accentuate the difference between the ALN-treated and the controls (Figure 24).

ALN treatment resulted in compositional changes. Bone collagen concentration was reduced and mineral concentration was increased. These changes were mirrored in a reduced collagen/mineral ratio and an increased tissue density (not shown). Furthermore, the apparent density was increased (not shown). These observed changes appeared to be more pronounced after 17 weeks of treatment but were minimally influenced by the does of ALN (Figure 24).

Treatment with ALN did not significantly influence the normalized mechanical properties of the cancellous bone. In cortical bone, the high-dose ALN treatment increased ultimate stress in both the 9-week and 17-week groups (Figure 24).

Discussion

Advantages and limitations of current methods for quantification of cancellous bone properties

Despite the considerable progress made over the past two decades in advanced bone imaging techniques, which made 3-D quantification of trabecular microstructure possible in a true, unbiased and assumption-free manner [**82, 83, 131, 132**] (I–IV), there remain certain challenges. These changes include the important balances between spatial resolution and sampling size, or between signal-to-noise and radiation exposure or acquisition time, or between the complexity and expense of the imaging technologies vs. their availability and accessibility [**62**]. Based on the standardized methods, various physical/compositional properties can be measured with accuracy and precision [**25, 39, 73, 128, 165**]. Furthermore, the well-established compressive mechanical testing methods have provided a powerful tool for the evaluation of bone's mechanical properties [**82, 83, 131, 132, 134**]. However, one should bear in mind that the mechanical testing of biological samples is not without problem [**96**].

Precision and accuracy of micro-CT measurements

The precision (reproducibility) of micro-CT has been demonstrated to be excellent. Accurate 3-D datasets can be generated by applying correct segmentation technique with optimal threshold corresponding to the Archimedes-based volume fraction (I). However, traditional 2-D histomorphometry based on plate model provides volume fraction dependent biased results, especially when populations with different volume fractions are compared [**29**], and the trabecular thickness and connectivity are underestimated (II). Our data suggest that it must be careful when applying thresholds in generating 3-D data. An optimal fixed global threshold may be determined from the Archimedes-based volume fraction of a subgroup of specimens. This optimal fixed global threshold can be applied to obtain reliable volume fraction data. We emphasize that the optimal threshold always depends on the material studied, therefore it should be determined whenever a study series is performed (I).

Comparison of microstructure data from Micro-CT and conventional histomorphometry was reported. Micro-CT is apparently an interesting method providing reliable morphometric results in less time than conventional histomorphometry. However, the correlation coefficient is not sufficient to study the agreement between techniques in histomorphometry. The architectural analysis is influenced by calculation algorithms and thresholds used in segmentation [**18**].

Quantification of trabecular and cortical bone microarchitecture

Microarchitectural properties of cancellous bone, such as architectural anisotropy, connectivity, structure type, and trabecular thickness; and of cortical bone, such as porosity, cortical thickness can be calculated directly from 3-D micro-CT images. These imaging techniques, which are unbiased and free of assumptions, enable a detailed and versatile quantification of 3-D microarchitecture of bone tissues [**49, 83, 131, 171**], and a better understanding of bone microarchitecture, its relationships with mechanical properties, and its role as determinant of bone quality (I–IV).

Quantification of microarchitecture of cancellous bone can be divided in three main aspects: trabecular scale, trabecular topology, and trabecular orientation [**190**]. Trabecular scale quantifies parameters such as bone volume fraction, trabecular thickness, number and separation. Trabecular topology analyses trabecular integrity, shape, connectively and marrow space using parameters such as Euler number, structure model index, and marrow star volume. Trabecular orientation assesses trabecular anisotropy and trabecular orientation along stress lines and differential loss of horizontal or vertical trabeculae.

Quantification of microarchitecture of cortical bone is also of great interesting for its role as major determinant of mechanical competence include thickness of the cortex, cortical cross-sectional area and area moment of inertia. Cortical porosity, crystallinity or the presence of microdamages also contribute to bone's mechanical competence [**6**].

Quantification of physical/compositional properties

Bone matrix is a two-phase system: collagen and mineral. The collagen fibers provide the ductility and ability to absorb energy (i.e., the toughness). Changes of collagen properties affect the mechanical properties of bone and increase fracture susceptibility. Differences in the quality of the collagenous matrix, including the nature and extent of its posttranslational modifications, may be related to bone strength. Different determinants of bone quality are interrelated, especially the mineral and collagen, and analysis of their specific roles in bone strength is difficult. Different processes of maturation of collagen occur in bone, which can result either from enzymatic or nonenzymatic processes. The enzymatic process involves activation of lysyl oxidase, which leads to the formation of immature and mature crosslinks that stabilize the collagen fibrils. The modifications of collagen are age-related and may impair the mechanical properties of bone [**184**].

The mineral phase of bone matrix provides its stiffness. However, besides the mere amount of the mineral phase,

size and shape of carbonated apatite crystals are postulated to affect bone's mechanical properties. Crystallinity is able to explain to certain extent the variation in monotonic mechanical strength and fatigue properties. Recent results showed that the tissue-level strength and stiffness increased with increasing crystallinity while the ductility reduced. Thus, the crystal properties are considered an important bone quality factor and aberrations in these properties may contribute to senile osteoporotic fractures [**194**].

Physical properties, such as collagen density, apparent density and volume fraction are considered to be major determinants of mechanical properties [**39, 71, 135**]. Compositional properties, such as collagen and mineral concentrations, provide additional information to the changes in mechanical properties [**25, 26, 39**] (IV-V). Bone collagen cross-links have been widely used to assess bone resorption levels in many metabolic bone diseases, and used as a convenient measure of matrix degradation. Collagen cross-links are of significant importance for the biomechanical integrity of bone [**100, 140, 141**].

Quantification of mechanical properties

The conventional mechanical testing allows us easily to acquire the mechanical properties of bone. By using the combined testing technique [**158**], it has been possible to investigate the mechanical properties of the cartilage-bone complex simultaneously [**40, 41**]. Despite a simple approach, numerous inherent problems exist by using these testing techniques. The major problem is end-plate error, which accounts for a systematic underestimation of the Young's moduli by 20 to 40% [**108, 136**] and a random error of about 12.5% [**97**]. Other problems include unknown friction between the end platens [**110**], specimen geometry [**95, 111**], structural end phenomena [**133, 195**], continuum assumption [**79**], storage [**113**], effect of drying [**17, 108**], and effect of temperature [**108**]. Bone has been demonstrated to be a structure rather than a material, which makes it impossible to remove small samples for testing without disrupting its structural integrity. One must realize that it is impossible to perform mechanical testing *in vivo*, and none of the mechanical testing *in vitro* is perfect, even though it has been argued that artifacts of testing can be reduced by improving testing technique [**94**]. Despite these limitations, the precision of various mechanical tests is generally excellent, although accuracy is somewhat uncertain. Therefore, studies based on the same methods are at least comparable. In general, these well-established mechanical testing methods are still considered as "golden standard" and have provided a strong tool for the evaluation of bone's mechanical properties [**87-89, 111-113**] (IV-V).

Cancellous bone is a complex material with substantial heterogeneity. Bone's elastic and strength properties vary widely with animal species, across anatomic sites, and with aging and disease. Although these mechanical properties depend very much on density, architecture and tissue material properties play important roles. It is of interest to note that the strains at which the bone fails are almost independent of density [**96**]. With continued progress in this field of bone mechanics, substantial insight will be gained into important problems as ageing diseases: osteoporosis and related bone fracture, osteoarthrosis, bone remodeling, and design and survival of orthopaedic implants.

Aging and the most common aging-related bone diseases – osteoarthrosis, osteoporosis and rheumatoid arthritis

Aging is a major risk factor for osteoarthrosis (osteoarthritis) [**3**] and osteoporosis [**163**]. Although, they are not necessary outcomes of aging, and the relationship between age-related changes in bone and development of disease is not clear. The etiology of osteoarthritis and osteoporosis is multifactorial, and these factors include both constitutional and environmental, e.g. genetic susceptibility, endocrine and metabolic status, mechanical and traumatic injury [**33**]. Osteoarthritis and osteoporosis are common musculoskeletal disorders that frequently coexist in the same patient population. OA and OP have been observed and studied for more than 30 years, the potential relationship between these two processes in a given individual is controversial and less well understood. Although most previous case-control studies suggest an inverse relationship between the presence of OA and OP [**33**], other data from cotwin control studies indicate that these two processes are not mutually exclusive and that the prevalence of osteoporosis in the OA population is virtually identical to that seen in the "normal" population [**4**].

Rheumatoid arthritis (RA) among elderly people has also been an increasingly important health concern. Elderly-onset rheumatoid arthritis (EORA) is defined as rheumatoid arthritis starting after 60 years of age, that is different from the RA in younger patients and it more frequently has an acute onset accompanied by constitutional symptoms [**137**].

The relation between structure and mechanical strength has attracted increasing interest, and the knowledge of 3-D microarchitectural properties of cancellous bone is essential for a better understanding of the age-related changes of bone properties. The following discussion focuses on the current understanding of the microarchitectural adaptation of bone tissues in aging and these most common age-related musculoskeletal diseases.

Age-related microarchitectural changes in cancellous bone

The microarchitectural characteristics of human aging cancellous bone are thinning of trabeculae, decrease of bone volume fraction (density), loss of connectivity, transformation of trabeculae from plate-like into rod-like, increase of trabecular

separation and bone marrow spacing, and increase of anisotropy [**51**] (II–III).

During aging, the net amount of bone lost is determined by the difference between the amount of bone removal and formation. The bone removal occurs from the endocortical, trabecular and intracortical components of its endosteal (inner) envelope, and bone formation is beneath its periosteal (outer) envelope. Bone loss already happens slowly in young adult of both genders. At menopause, bone loss accelerates in women because remodeling intensity increases, and the bone remodeling balance becomes more negative (i.e. bone resorption greater than formation) and the high remodeling rate also reduces bone mineral content [**163**].

The bone loss with aging accompanies systemic microarchitectural changes of cancellous bone, i.e. both the axial and peripheral cancellous bone deterioration. In the human spine, from age 20 to 80 years, the decline in ash density was 48–50% compared to a 75–80% decrease in vertical stiffness and strength [**127**], and in human tibia, from 20 to 83 years, the decline in ash density is 46% compared to the 33%–57% decrease in loading axial stiffness and strength [**39**]. Cancellous bone structure type changes towards more rod-like in the elderly with decreased trabecular thickness. These changes become significant after 80 years of age for human tibial cancellous bone, whereas structure type and trabecular thickness seem to remain relatively unchanged between 20 and 80 years (II). However, trabeculae rearrange volume orientation through remodeling process to best support mechanical loading as evidenced by the facts of increased anisotropy in the aging cancellous bone. In the aging cancellous bone, trabeculae align more preferentially to the primary direction – parallel to the tibial longitudinal loading axis (III).

Although bone collagen may have less effect on bone's strength and stiffness than does bone mineral, bone collagen characteristics contribute to bone biomechanical properties and may have a profound effect on bone fragility [**13**]. The changes of collagen that occur with aging and reduce bone's toughness may be an important risk factor of fracture in older women with low bone mass. Type I collagen may have an impact on skeletal fragility [**184**]. Reduced concentration of collagen reducible cross links in human trabecular bone are associated with aging and osteoporosis [**141**].

Aging-induced osteopenia results in two to fourfold of vertebral fragility fracture for both women and men during the last 30 years [**125**]. This dramatic increase in fracture risk is strongly related to a deterioration of bone's mechanical competence and bone quality. The reduction of bone strength is determined by whole bone microarchitectural properties and intrinsic material properties. The anti-resorption agents are therefore focusing on reestablishment of mechanical competence, microarchitecture and bone quality.

Recently, a novel method has been developed allowing quantification of trabecular bone on an elemental (rod/plate) level [**114, 171, 182**]. The trabecular structures were decomposed into rods and plates for the analysis with local morphometry. This method is able to decompose the trabecular structures into rods and plates and measure local morphometric parameters such as thickness or orientation directly on the extracted rods and plates. Age-related changes of trabecular microarchitecture can thus be investigated on an elemental level, which may help to improve our understanding of age-related bone failure mechanism as well as the effect of pharmaceutical intervention in the prevention of such fractures, thus the combination of local and global morphometry is one of the useful methods for a detailed and quantitative description of age-related changes in bone microstructure [**170**].

Age-related microarchitectural changes in cortical bone

Like cancellous bone, cortical bone is also a heterogeneous material with a complex hierarchical microstructure. The microarchitectural characteristics of human aging cortical bone can be described as thinning of cortex, increase of intracortical porosity, and decrease of cortical cross-sectional area. These aging-related alternations of microarchitecture accompanying with changes in crystallinity, collagen fibre orientation, degree of mineralization, and/or the presence of microdamages contribute to bone's mechanical competence and integrity.

Aging is associated with a decline of cortical bone mass and with a deterioration of cortical microarchitecture that contributes to fracture risk, independently of bone mass. These changes are more pronounced in women than in men and are exaggerated in patients with fracture [**32**]. Ideally for bone strength, there should be minimal porosity within cortical bone, with only those cavities required for the living tissues. Porosity in the endocortex has less impact on bone strength than porosity on the outer diameter or periosteal surface. Cortical porosity generally originates on the endosteal surface and progressively expands toward the periosteal surface [**5**]. Cortical bone porosity and the amount of haversian bone increase with age. Changes in porosity account for 76% of the reduction in strength [**123**]. Small increases in porosity lead to disproportionately large losses in bone strength [**176**], and increase of cortical porosity and decrease of cortical thickness are associated with hip fracture. Cortical microarchitectural changes are highly correlated with porosity [**123**]. Age-related changes in porosity contribute to the decline in mechanical properties. From 20 to 100 years, ultimate stress, ultimate strain, and energy absorption decrease by 5%, 9%, and 12% per decade, respectively [**123**].

In cortical bone, all new remodeling basic multicellular units (BMUs) are initially targeted to bone needing replacement [**120**], and it is likely (but unproven) that the same can be applied to cancellous bone [**145**]. Because a new BMU can only arise from an existing blood vessel [**144**], this requires it to travel some minimum distance in the right direction to

accomplish its purpose. In cortical bone, collagen network reduces up to 50% in its capability to absorb energy during aging that is likely due to an increase in the percentage of denatured collagen [**186**]. Degree of mineralization increases with aging reflecting an increase in mineral content of cortical bone tissue [**22**]. With aging, microcracks in cortical bone accumulate and there is a concomitant progressive increase in microcrack density [**160**] that weaken the cortical bone tissue.

With aging, cortical bone becomes increasingly brittle and fractures with less energy. Alterations in bone's mechanical competence are explained by functional adaptation of bone structure and age-related deterioration of intrinsic mechanical properties. This deterioration is directly related to the bone remodeling process that affects collagen fiber orientation, degree of mineralization, and the amount of unrepaired fatigue damage [**119**]. Like cancellous bone, cortical bone's mechanical competence and its fragility in particular depend largely on the structure and microstructure of the cortical bone compartment.

Increased bone turnover disturbs bone structure that may result in fracture. Osteocyte apoptosis and decrease are suggested to be major factors in the bone loss and fracture associated with aging. Both the osteocyte and periosteal cell layer are assumed to be of greater importance in the process of maintaining skeletal integrity, and they might be a target for pharmacological agents to reduce fracture especially in cortical bone [**53**].

Microcrack accumulation in cortical bone has been implicated in skeletal fragility and stress fractures. Microdamages in particular not only weaken the cortical bone tissue but also provide an effective mechanism for energy dissipation, and the microcracks affect the mechanical and material properties of cortical bone. The growth of microcrack has been related to osteocyte apoptosis and the initiation of the remodeling process [**130**]

Osteoarthrosis-related adaptation in subchondral bone

The microarchitectural characteristics of human osteoarthrotic subchondral cancellous bone are thickening of subchondral plate and cancellous bone, increased bone volume fraction (density), transformation of trabeculae from rod-like into plate-like, decrease of trabecular separation and bone marrow spacing (VI,VII).

Traditionally, osteoarthrosis has been considered a disease whose central pathological feature is hyaline articular cartilage loss where damages are clearly visible. However, more evidence accumulates that OA is not a disease of cartilage [**11, 56, 151, 153**]. OA has also been conceptualized as a whole organ disease, because OA involves not only eburnation and osteophytes, but also enthesophytes, ossification at the insertion sites of ligaments, tendons, and joint capsules to bone [**156**]. However, the role of bone, in particular underlying subchondral bone, in the pathophysiology, initiation and progression of OA is not fully elucidated and is still controversial. Although articular cartilage is avascular, there is evidence that vascular pathology may also play a role in the initiation and progression of OA [**57**].

OA is a chronic joint disease and develops and changes very slowly, which makes it difficult to follow over any length of time in human. The recent investigations have suggested that subchondral cancellous bone may be involved, and plays a significant role in the cartilage degeneration of OA (V, VI). Subchondral bone sclerosis may not be required for initiation of cartilage fibrillation, but may be necessary for OA progression, and only the changes in bone and calcified cartilage close to the joint are important for the disease process [**15**]. Epidemiological studies also report that subchondral bone sclerosis increases accompanying OA progression [**78**]. More investigations have shown that specific changes in the microarchitecture of subchondral cancellous bone in OA are consistent with an acceleration of bone turnover [**104**], and an increasing severity of OA is correlated with joint space narrowing [**35**] and with changes of trabecular surface and shape [**55**]. Subchondral bone and overlying cartilage are closely related, and function as a unit to withstand mechanical loading [**41**]. The microarchitectural changes already occur in the early human tibial OA subchondral cancellous bone (VI) resulting in the disruption of the unit function of the cartilage and bone to mechanical loading [**40**], and the disruption of normal equilibrium between cartilage properties, bone tissue properties and bone volume fraction early in the development of osteoarthritis [**30**].

In human early OA, the increase in bone density in early OA cancellous bone did not make up for the loss of mechanical properties, which suggests deterioration in the quality of OA cancellous bone (V). In early OA, subchondral cancellous bone reveals a low collagen density and apparent ash (mineral) density, but relatively unchanged collagen and mineral concentrations (V), and a reduced mechanical matrix tissue properties and an increase in denatured collagen content were observed in human early OA subchondral bone [**31**].

In human severe OA, the stiffness of subchondral bone increases more slowly as apparent density increases than does the stiffness for normal subchondral bone. This suggests higher bone turnover rates and lower mineralization of bone tissue in OA [**104**]. Severe OA has an abnormal low mineralization pattern [**74**], and an abnormal trabecular bone collagen metabolism [**117**]. Subchondral bone collagen metabolism is increased in OA. The greatest changes in cancellous bone collagen metabolism and the hypomineralization of deposited collagen are found within the subchondral zone of osteoarthrotic femoral heads [**117, 118**]. These data suggest that bone collagen metabolism may be an important factor in the pathogenesis of OA, which deserves further investigation.

Bone loss with aging in OA is lower, and this is explained by lower bone turnover. Although subchondral bone is slightly hypomineralized because of local increased turnover, the increase in number of trabeculae and bone volume compensates for this, resulting in a stiffer structure. Bone turnover in the subchondral region of established OA is increased, but the general bone turnover is reduced. Further reduction of bone turnover, however, may lead to overmineralized (aged) osteons and loss of bone quality, resulting in increased fragility [**33**]. OA bone has greater apparent and tissue density, and also wider geometrical measures of the skeleton, diameters of long bones and trabeculae, which contribute positively to better strength and fewer fragility fractures. However, OA bone strength does not increase proportionally to the bone density increase as expected.

Despite human studies have not confirmed the hypothesis that the increasing bone metabolism primarily initiates cartilage destruction or vice versa. Recent studies on animal models, such as macaque, have demonstrated that thickening of subchondral bone precedes fibrillation of the cartilage, which might be the results of increased bone resistance to compression [**16**].

These findings show that severe osteoarthritis or a related factor may change the age dependences of both the structural parameters and the mechanical properties usually reported for normal cancellous bone. These results suggest for this pathology to have a protective role against the age-related decrease in density, the age-related deterioration of the microarchitecture and the age-related decrease of the failure strength for the cancellous bone in the principal compressive region of the human femoral head.

Due to ethical reasons, it is difficult to obtain tissue samples from human early-stage OA. Investigations on the earliest pathological changes and in particular on the pharmaceutical interventions have been focused on animal models. The male Dunkin-Hartley strain guinea pig has been documented as a convenient experimental model that develops spontaneous primary age-related knee joint OA [**8, 188**] (VII). Our current study reveals pronounced alterations of the microarchitecture and bone matrix composition of the subchondral bone, which may help to gain new insights into the nature development of OA and to promote novel approaches for the intervention and treatment of OA (VII).

Recently, Hyaluronan (HA) has attracted increasing interest as a potential agent in therapeutic intervention in osteoarthrosis (OA). HA has been shown possible to reduce arthritic lesions in experimental animal models of articular cartilage injury. High molecular weight HA intra-articular injection of guinea pig knee joint clearly shows effectively protects against cartilage degeneration. This change is accompanied with decreased subchondral bone density and thickness, changed trabecular structure toward rod-like, so that subchondral bone becomes more compliant and thereby reduces cartilage stress during impact loading. HA preserves cancellous bone mechanical properties by increasing bone mineralization. Early HA administration is effective for intervention of OA initiation and progression, and short-term early HA treatment is sufficient to maintain treatment effects (VIII).

Using this guinea pig OA model, we have tested the Radin's hypothesis [**152, 153**] that whether increase of subchondral bone density enhancing cartilage stress during impact loading could lead to progressive cartilage degeneration and accelerated OA progression (IX). By inhibition of bone remodeling with alendronate (ALN), significantly increased subchondral bone mass, changed microarchitecture, and increased bone mineral content and density are fond in the subchondral bone. More interestingly, accelerated articular cartilage degeneration is observed at the medial condyle and, to some extent, at the lateral condyle (IX). These results suggest that increased subchondral bone density promotes OA progression and call for circumspection in using bone density–enhancing drugs for intervention of primary OA (IX).

Evidence is increasing for bone changes during progression of OA, such as increase of turnover in the subchondral bone, changing of the trabecular structure, osteophytes, bone marrow lesions and sclerosis of the subchondral plate. Furthermore, investigations has reported secondary positive effects on cartilage health when bone resorption was suppressed, or deterioration of the cartilage when resorption is increased. It is thus suggested that an optimal treatment for OA might include targeting both the bone and cartilage compartments [**91**].

Our data are in favour of the concept that subchondral bone plays a centre role in the pathogenesis of OA initiation and progression [**152, 153**] (VI–IX). However, evidence for an essential role in the etiology has never been proven. Recent investigations showing reduced chemical and mechanical properties of subchondral bone in various stages of the disease have inspired interest in the role of subchondral bone in the development and progression of the disease. Until now, little is known about the interaction between the cartilage and bone in the etiology of osteoarthritis. Recent research indicates that bone is intimately involved and plays a vital role in disease progression. While there is currently little evidence of a direct cause and effect relation between subchondral bone sclerosis and degeneration of the overlying cartilage.

There are certain limitations using guinea pigs as OA model. Firstly, the initiation and development of guinea pig primary OA may not reflect exactly human primary OA. Secondly, the animal models can not replace clinical trials. Thirdly, guinea pig is a small animal, thus its small bone size limits the application of orthopaedic implant or biomaterial research. Furthermore, other factors like genetic, environmental, methodological factors might affect the results of animal data. Therefore, interpretation of animal results should be careful. Nevertheless, male Dunkin–Hartley guinea pigs Charles River strain displays a spontaneous onset of progressive degenerative changes in the knee joint similar to human OA [**8**].

Osteoporosis-related microarchitectural changes in bone

Osteoporosis is a systemic skeletal disorder affecting both axial and peripheral bone tissues. The distinct characteristics of OP cancellous bone can be described by compromised bone strength that predisposes individuals to increased fracture risk. The deterioration of properties in OP cancellous bone is similar to human aging, but to a much greater extent. Typical microarchitectural characteristics of OP cancellous bone can be described as decrease of bone volume fraction (density), loss of connectivity with fewer and thinner trabeculae, transformation of cancellous bone structure into extremely rod-like, increase of trabecular separation and bone marrow spacing, and increase of anisotropy. A typical OP cortical bone can be described as thinning of cortex, decrease of cortical cross sectional area and increase of porosity.

Osteoporosis, which leads to loss of bone strength, results in fragility fractures, where bone strength is determined by its material and structural properties. The fundamental pathogenetic mechanisms underlying this disorder include: failure to achieve a skeleton of optimal strength during growth and development; excessive bone resorption resulting in loss of bone mass and disruption of architecture; and failure to replace lost bone due to defects in bone formation [**154**]. Estrogen deficiency plays a critical role in the development of osteoporosis; other factors like calcium and vitamin D deficiencies and secondary hyperparathyroidism also contribute. The mechanisms underlying the regulation of bone remodeling involve not only the osteoblastic and osteoclastic cell lineages but also other marrow cells, in addition to the interaction of systemic hormones, local cytokines, growth factors, and transcription factors [**154**].

Osteoporosis has long been considered a disease of the aging female skeleton. However, it is now clear that men are also at risk for this disorder [**161**]. Due to the heterogeneity of the disease, the pathophysiology of primary OP is not clearly defined. Others suggest that primary OP is due to a greater biological aging rather than a specific disease process [**20**]. With aging and osteoporosis, a process of progressive reduction of bone formation rather than increase of bone resorption occurs. This process results in reduction of bone mass, deterioration of microarchitecture, and hence decrease of mechanical strength, which are disproportionate to the reduction in bone mass alone.

Significant microarchitectural changes occur in OP cancellous bone compared with normal control, despite only a slight reduction in bone volume fraction [**172**]. These microarchitectural changes are suggested to be a consequence of trabecular plate perforations. The prevailing opinion is that bone loss in the vertebral centrum is accompanied by a reduction in total number of trabeculae, by preferential resorption of horizontal trabeculae, and by hypertrophy of the remaining vertical trabeculae [**126, 142, 143**].

Bones adapt to the loads falling on them, and are adapted to resist fracture. Bones become fragile with aging. There are many factors that contribute to bone fragility. These factors including fatigue damage accumulation and microarchitectural deterioration had been definitely established as qualitative (nonmass) contributing factors. Higher than necessary bone remodeling cycles, and osteocyte deficiency are also contributing factors [**146**]. The changes in the material and structural properties may result in bone fragility. These changes include abnormal collagen, mineral content, composition and distribution, diseases of high remodeling and low remodelling [**19**]. Evidence indicates that bone mass alone is insufficient to satisfactorily explain the skeletal fragility of osteoporosis. Bone quality needs to be considered in the diagnosis and treatment of the disease. Bone quality includes trabecular and cortical microarchitecture, morphology, bone turnover, degree of mineralization of the bone matrix, and the amount of microdamage accumulated in the bone tissue.

Fracture is the final clinical outcome of the osteoporotic process [**179**]. Osteoporosis would have little significance were it not for the associated fracture that may occur as a result of minimal trauma or even spontaneously. The ability of a bone to resist fracture depends on bone mass and its spatial distribution, the cortical and trabecular microarchitecture, and the intrinsic properties of the materials that comprise the bone [**10**]. The remaining tissue seems to be normal in composition of osteoporotic bone, beside the reduction in bone mass [**129**]. Loss of bone mass, deterioration in bone macro- and microstructure, and changes of quality in bone matrix play a significant role in the pathogenesis of osteoporotic fractures [**143, 147, 179**].

Current clinical treatments of osteoporosis concentrate on the inhibition of osteoclast activity to maintain bone mass. However, osteoclast cells have a major role in removing existing microcracks from the bone matrix, and hence the use of bone resorption-inhibiting drugs may lead to insufficient bone repair and therefore an increase of microdamage accumulation and loss of bone quality [**122, 130**].

Rheumatoid arthritis related microarchitectural changes in bone

Rheumatoid arthritis (RA) is a major cause of secondary osteoporosis and is frequently associated with both paraarticular osteoporosis and generalized osteoporosis. Thus, RA bears similar characteristics of microarchitectural changes in cancellous bone that compromise bone strength predisposing RA patients to increased fracture risk. More importantly, focal bone erosions, the radiographic hallmark of rheumatoid arthritis, are typically localized at the joint margins and also in subchondral bone, where focal bone resorption can be detected in the subchondral bone adjacent to the bone marrow space into which the synovial inflammatory tissues have extended.

The erosions progress throughout the course of disease and are generally related to disease severity [**68**].

In early-stage RA patients, disease activity and impairment of daily physical activity are considered a significant determinant of deterioration of bone structure [**90**]. Women with RA have decreased bone mineral density in both the appendicular and axial skeleton, and they have lower appendicular and axial bone mass that is not attributable to the use of steroids. Patients currently taking steroids have even lower appendicular and axial bone mass, which may reflect their poorer functional outcome and is likely to increase the risk of fractures [**103**]. RA patients have a reduced bone volume and decreased bone turnover, which is further aggravated by microarchitectural deterioration stressing the severe osteoporosis associated with the disease [**148**]. Others reported that, unlike postmenopausal osteoporosis, osteoporosis in rheumatoid arthritis is characterized by relatively preserved bone mass in the axial bone (lumbar spine) and marked loss in the peripheral bone. Furthermore, bone loss in RA occurs early in the disease process, emphasizing that osteoporosis management should be considered early in the disease [**166**]. The complex risk factors of osteoporosis in rheumatoid arthritis include primary osteoporosis risk factors in addition to inflammation, immobilization, and use of corticosteroids [**80**].

Osteopenia in RA patients is an important factor in the surgical management of joint disease. Bone loss stimulated by inflammatory arthritis results in increased bone remodeling and altered bone microarchitecture. The subchondral bone plate near the joint surface is narrow and perforated by vascular inflammatory invasion, and in the shaft the thin cortices are weakened by giant resorption defects [**9**]. The cortical defects are suggested to be responsible for the experimentally observed loss of strength, and these defects may explain the increased femoral fracture risk in rheumatoid arthritis. Osteoclast is demonstrated in increased number and activity in rheumatoid arthritis and in animal models [**9**].

The progressive destruction of the periarticular bone contributes significantly to joint dysfunction and disability in RA patients. There becomes increasing interest in developing a better understanding of the pathologic mechanisms involved in the disease process and in developing therapies that can arrest these events. From sites of bone erosion joint, tissue sections reveal multinucleated cells with phenotypic characteristics of osteoclasts that are responsible for bone resorption during physiologic remodeling associated with the rheumatoid synovial lesion. Analysis of the rheumatoid synovium may find factors known to directly or indirectly induce osteoclast differentiation and activation. Quantitative assessment of periarticular and generalized bone loss in rheumatoid arthritis may provide reliable indicators of future disease course and potential response variables in disease intervention. Osteoclast plays a crucial role in the development of erosions and periarticular and generalized osteoporosis [**80**]. Recent findings suggest that targeting of osteoclasts and osteoclast mediated bone resorption represent a rational approach to develope targeted therapies that can specifically inhibit or slow the progressive focal bone destruction associated with the rheumatoid synovial lesion [**69, 70**]. With the improvement of understanding pathogenesis of rheumatoid arthritis, better treatment strategy could be obtained.

Conclusions of own studies

Human aging and OA

The precision of micro-CT measurement is excellent. To generate accurate 3-D micro-CT image datasets, care must be taken when applying thresholds. A fixed threshold may be used to obtain reliable volume fraction data, and this fixed threshold may be determined from the Archimedes-based volume fraction of a subgroup of specimens. The threshold may vary between different materials, and so it should be determined whenever a study series is performed (I).

Based on accurately generated micro-CT datasets, age-related microarchitectural changes of human tibia cancellous bone have been demonstrated (II, III). Apart from connectivity, all measured microarchitectural properties correlate significantly with age, and the same age-related trends in these properties are observed for both condyles. However, age-related changes in the properties of human tibial cancellous bone do not follow the same pattern, nor do they occur at the same age. The observed increase of anisotropy and the constant nature of connectivity suggest an important bone remodeling mechanism that normal aging tibia may orient trabecular volume orientation. The aging trabeculae align more strongly and preferentially to the primary loading direction to compensate bone loss (III). Age-related changes in trabecular thickness and structure type become significant first after 80 years of age (II). With regards to type of trabeculae, the plate-like structure reflects high mechanical stress and the rod-like structure reflects low mechanical stress. Trabecular structure type and bone volume fraction correlates strongly. Trabecular structure type together with anisotropy correlates well with the Young's modulus. The most effective microarchitectural properties for predicting the mechanical properties of cancellous bone seem to differ with age (IV).

In early human OA subchondral cancellous bone, none of the mechanical properties of cancellous bone can be predicted by the measured physical/compositional properties (V). The increased trabecular thickness and density, but relatively decreased connectivity suggests a mechanism of bone remodeling in early OA as a process of filling trabecular cavities. This process leads to a progressive change of trabeculae from rod-like to plate-like, the opposite to that of normal ageing. The increase in bone tissue accompanied with deteriorated microarchitecture in early-stage OA cancellous bone does not account for the loss of mechanical properties, which suggests deterioration in the quality of OA cancellous bone (VI).

Guinea pig OA

Age-related pronounced alterations of the microarchitecture and bone matrix composition of the subchondral bone tissues in guinea pig have been demonstrated. These alterations do not appear to follow the same pattern as in normal aging and may have different influences on the resulting mechanical properties. The microarchitectural and compositional changes in OA subchondral bone tissues show patterns different from those of normal aging bone (VII).

Intra-articular injection of hyaluronan effectively protects against cartilage degeneration in guinea pig primary OA. The decrease of subchondral bone density and thickness and change of trabecular structure toward rod-like result in more compliant subchondral bone and thereby reduces cartilage stress during impact loading. Moreover, hyaluronan maintains the mechanical properties of cancellous bone likely through increasing its mineralization. Early administration of hyaluronan is effective for intervention of OA initiation and progression, and short-term early HA treatment is sufficient to maintain treatment effects in OA guinea pig model (VIII).

The inhibition of bone remodeling by ALN results in significant increase of subchondral bone mass and bone mineral content, and markedly changes of microarchitecture. Furthermore, the resulting increased bone mass accelerates articular cartilage degeneration at the medial condyle and, to some extent, at the lateral condyle. These results suggest that increased subchondral bone density promotes OA progression and call for circumspection in using bone density–enhancing drugs for intervention of primary OA (IX).

Summary

Bone, a living material capable of self-repair, has evolved over several hundred million years to become a remarkable tissue. Bone is a two phase porous structure composed of organic matrix and mineral components. The organic matrix is composed primarily of the protein collagen (10% of adult bone mass) that provides flexibility. The mineral component is composed of hydroxyapatite (65% of adult bone mass), which is an insoluble salt of calcium and phosphorus, and small amounts of magnesium, sodium and bicarbonate. About 25% of adult bone mass is comprised of water. There are two major kinds of bone, cancellous (trabecular or spongy) and cortical (compact or solid) bone, and their principal function is to resist mechanical forces and withstand fractures.

With aging, inevitable bone loss occurs in both genders, which is frequently the cause of osteoporosis; and inevitable bone and joint degeneration happens, which often results in osteoarthrosis and elderly-onset rheumatoid arthritis. Aging-related musculoskeletal diseases have become major social and economic burdens as people live longer. Over the last a few decades, much significant research on the properties has been carried out on diseases such as age-related bone fracture, prosthetic loosening, bone remodeling, and degenerative bone diseases on both axial central vertebra and peripheral bone tissues. We have now achieved great deal of knowledge on normal aging- and diseases-related changes in bone properties (Table 1). These alterations are of major importance for the understanding of degenerative bone diseases, and for the design, fixation and durability of total joint prosthesis. Understanding the microarchitectural properties, mechanical adaptations, and collagen and mineral qualities of subchondral bone tissues highlighted in these studies may help to gain more insights into the pathogenesis of degenerative bone diseases and to target and develop novel approaches for the intervention and treatment.

Table 1. Summary of property changes in aging and the most common aging-related bone diseases

	Aging	Osteoarthrosis	Osteoporosis	Rheumatoid arthritis
Bone turnover	Increased at menopause [162]	Increased at local [33, 104] & reduced in general [33]	Heterogeneous: low, normal or increased [172]	Decreased [148]
Bone mass/density	Decreased [39, 127]	Increased [103](V)	Reduced [129, 154]	Reduced [103]
Bone collage	Unchanged in content [39], reduced collagen reduciable cross link [141]	Unchanged (V), but denatured [31] in early OA, abnormal in severe OA [117, 118]	Abnormal bone collagen [184]	Cross-linking density & degradation depend on the disease activity [93]
Mineral content	Relative unchanged [39] or reduced at menopause [163]	Unchanged in early OA(V), slightly decreased in severe OA [74, 104]	Relative unchanged [129]	Decreased at both appendicular and axial skeleton [103]
Microarchitecture	Systemic deterioration at both axial and peripheral sites [124, 125] (III)	Deterioration in early OA(VI), and severe OA [55]	Systemic deterioration at both axial & peripheral sites [143, 172, 179]	Deterioration at affected joints [9, 90]
Mechanical properties	Reduced [39, 127]	Decreased in early OA(V), increased to less extent than bone mass increase [104]	Reduced to greater extent [167]	Reduced to greater extent [9]
Bone quality	Reduced [160]	Reduced (VI) [54]	Reduced markedly [172]	Reduced markedly [9, 103]
Microdamage	Accumulated [14, 160]	Accumulated markedly [54]	Accumulated [14, 173]	
Bone fragility	Increased [162, 184]	Increased [33]	Increased greatly [14, 146]	Increased greatly [9, 103]
Risk of fracture	Increased [125]	Decreased [33, 105]	Increased greatly [14, 179]	Increased greatly [103]
Suggestion for therapeutic target	Regulate bone modeling & remodeling; prevent & treat bone fragility & loss [121]	Cartilage, subchondral bone & all tissues involved [34, 86]	Reduce bone formation & increase bone resorption [163]; preserve & build strength through bone quality [98]	Osteoclast & osteoblast mediated bone resorption to prevent and reduce focal bone loss [68]

Suggestions for future studies

Advanced micro-CT imaging techniques, mechanical testing, collagen and mineral measurements, and histomorphometry have been standard procedures for the assessment of bone tissues. Using these techniques, we have obtained much knowledge regarding cancellous bone and cortical bone properties relating to aging and diseases. It is now possible to quantify bone's properties at different scales: e.g. macrostructure, microstructure, and nanostructure *in vivo* and *in vitro*; and to quantify bone at different levels: such as organ level (e.g. viewing whole bone as an organ), apparent level (e.g. microarchitecture), tissue level (e.g. bone tissue elastic modulus by finite element analysis), element level (e.g. rod or plate trabecula) and cell level (e.g. osteoblast, osteoclast and stem cells). With these advanced techniques, future research directions are proposed.

1) Pathogenesis of aging-related musculoskeletal bone diseases such as osteoarthrosis, osteoporosis, and rheumatoid arthritis

Enormous amount of imaging data generated from theses studies need to be further analyzed using newly developed imaging techniques. e.g. i) volumetric spatial decomposition of trabecular bone into rods and plates that allows an element based description of bone microarchitecture [**114, 171, 182**]; ii) a large-scale finite element model that simulates mechanical testing to assess bone's mechanical modulus in a non-destructive manner [**23, 181**].

2) Tissue engineering and biomatrials

Tissue engineering in orthopaedic implant fixation [**139, 168, 174**] and spine fusion [**106, 107**] with bone marrow cells; and biomaterial research [**183**] in normal, osteoporotic [**37**] and osteoarthritic animal model [**36, 44**]; potential application of bioreactors in culturing cells; and eventually clinical trial of biomaterials in human.

3) Stimulation of bone defect healing and fracture repair with mesenchymal stem cells

Many adult tissues contain a population of stem cells that have the ability to regenerate after trauma, disease or aging. There has been great interest in mesenchymal stem cells (MSCs) and their roles in regenerating tissues and defect repair. MSCs are present in the bone marrow and have enormous clinical potential and are able to differentiate into cell types such as osteoblasts, chondrocytes, and endothelial cells. MSCs population can be expanded ex vivo to regenerate tissues not only of the mesenchymal lineage, such as bone and cartilage tissues, but also other types of tissues [**92**]. The use of autologous bone marrow stromal cells in repair of large bone defects in human has been reported [**150**]. Therefore, future research efforts might be focused on the potential use of this cell population in tissue engineering, such as implant fixation, spine fusion and fracture repair in combination with bone substitute.

4) In vivo micro-CT for animal researches and for human

Micro-CT in vitro scanning has been widely used for bone samples obtained from all sizes of animal, such as mouse [**2, 75-77**], rat [**175**], guinea pig [**44**], rabbit [**52, 149**], dog [**28, 46, 85, 101, 102**], pig [**106, 107**] sheep [**7, 37**], and human [**29, 51, 64-67**]. In vivo micro-CT imaging can now also be applied to all sizes of animals depending on the location to be scanned. In vivo monitoring microarchitectural changes e.g. during disease process (e.g. guinea pig OA, rat OP) or fracture repair is of particular importance [**61, 185**]. A 3-D high resolution peripheral quantitative CT scanner is now also applicable at lower extremities [**115**] that allow detecting microarchitectural changes during treatment in human.

5) Radiostereometry in monitoring orthopaedic implant migration

Radiostereometry (RSA) is a method for the study of the kinematics of the skeletal system. Since its introduction in 1974 [**164**], RSA has been widely used in the assessment of joint replacements. RSA is a highly accurate, true 3-D method of quantifying the motion between an implant and the host bone, for assessment of motion between bony structures that have been fixed and for measuring wear [**180**]. This method is of particular importance for clinical long-term follow-up after joint replacement in severe aging-related diseases, and evaluation of implant migration.

Dansk resumé

Det humane skelet optimerer dets mikroarkitektur ved at tilpasse sig til mekanisk belastning gennem vækst og udvikling. Mekanismerne for tilpasningen involverer en kaskade af processer: cellulær mekanotransduktion, som stimulerer knoglemodellering og -remodellering samt resulterer i enten knogleformation eller -resorption. Denne proces medfører hensigtsmæssige mikroarkitektoniske ændringer, som forsøger at justere og optimere knoglestrukturen til dets aktuelle mekaniske miljø.

Normale individer opnår deres maksimale knoglemasse i 25 til 30 års alderen, og herefter falder knoglemassen med alderen for begge køn. Knogletabet ledsages af mikroarkitektoniske forringelser, som resulterer i reduceret mekanisk styrke, der øger sandsynligheden for lavenergi-frakturer. Der vil med alderen ske et uundgåeligt knogletab, som hyppigt resulterer i osteoporose. Med alderen indtræder ofte knogle- og leddegeneration, som hyppigt resulterer i osteoarthrose (OA). Disse sygdomme er blandt de største sundhedsproblemer betragtet ud fra socioøkonomiske omkostninger.

De overordnede mål for denne doktordisputats var at undersøge alders- og OA-relaterede forandringer i 3-D mikroarkitekturen, de mekaniske egenskaber samt kollagen og mineral kvaliteten af det subchondrale trabekulære og kortikale knoglevæv. Studierne består af 2 dele. En human del, hvor alders- (I–IV) og tidlig OA-relateret (V–VI) forandringer i det trabekulære knoglevævs egenskaber blev bestemt. En dyrestudie del, hvor tre aspekter i en OA marsvin-model (VII-IX) blev studeret: Først blev den spontane aldersrelaterede OA-udvikling i marsvinene undersøgt. Dernæst undersøgtes de potentielle effekter af hyaluronan på subchondralt knoglevæv ved OA. Sidst men ikke mindst, undersøgtes effekten af forøget subchondral knogledensitet på OA-udvikling, hvor den forøgede knogledensitet blev induceret ved at hæmme knogleremodelleringen med bisfosfonat. Studierne har til formål at opnå større indsigt i alders- og OA-relaterede subchondrale knogletilpasninger.

Mikroarkitektonisk tilpasning af human trabekulær knogle med alderen

Præcisionen af mikro-CT målinger er god. Nøjagtige 3-D mikro-CT datasæt kan opnås ved at anvende passende sort/hvid tærskelværdier. Faste tærskelværdier kan bruges til at opnå pålidelige knogle volumen fraktioner. De faste tærskelværdier er baseret på knogle volumen fraktioner opnået ved Archimedes princip anvendt på en undergruppe af prøver (I).

Ved brug af nøjagtige mikro-CT datasæt har vi påvist aldersrelaterede mikroarkitektoniske forandringer i trabekulær knogle i humane tibia (II, III). Bortset fra konnektiviteten, korrelerede alle målte mikroarkitektoniske egenskaber signifikant til alder. Imidlertid følger de aldersrelaterede forandringer i egenskaberne for trabekulær knogle i humane tibia ikke det samme udviklingsmønster og indtræder heller ikke ved samme alder som i det overtale skelet. Den observerede stigning i anisotropi og den uforandrede konnektivitet, tyder på en vigtig knogleremodelleringsmekanisme, så normal aldrende tibia tilpasser sig trabeklernes orientering i rummet til belastninger. Især retter de aldrende trabekler ind efter belastningsretningen for at kompensere for knogletabet (III). Aldersrelaterede forandringer i trabekeltykkelse og strukturtype bliver først signifikant efter 80 års alderen. Den pladeformede strukturtype afspejler høj mekanisk belastning, mens den stavformede strukturtype afspejler lav mekanisk belastning (II). Den trabekulære strukturtype og knogle volumen fraktion er højsignifikant korrelerede. Den trabekulære strukturtype viser sammen med anisotropien en god korrelation med Young's modulus. De mikroarkitektoniske egenskaber, der bedst forudsiger de mekaniske egenskaber i trabekulær knogle, ser ud til at variere med alderen (IV).

Mikroarkitektonisk tilpasning af human osteoarthrotisk subchondral knogle

I subchondral trabekulær knogle ved tidlig stadie af human OA kan ingen af de mekaniske egenskaber af trabekulær knogle forudsiges ved at måle densitet/sammensætning af knoglematrix (V). Den forøgede trabekel tykkelse og densitet af knoglevævet med en samtidigt observeret relativ reduktion i konnektivitet tyder på, at knogle-remodellering i tidlig stadie af OA resulterer i udfyldning af de trabekulære hulrum. Denne proces leder til en progressiv ændring af trabekler fra en stavformet til en pladeformet strukturtype, hvilket er det modsatte af ændringerne ved normal aldring. Stigningen i mængden af trabekulært knoglevæv samtidig med en forringet mikroarkitektur af dette i tidligt stadie af OA kan dog ikke forklare reduktionen af de mekaniske egenskaber, hvilket tyder på en forringelse af kvaliteten af trabekulær knogle ved OA (IV).

Mikroarkitektonisk tilpasning af osteoartrotisk subchondral knogle i marsvin

Der er påvist tydelige aldersrelaterede forandringer af mikroarkitektoniske egenskaber og sammensætning af knoglematrix i det subchondrale knoglevæv i marsvin. Disse ændringer ser ikke ud til at følge samme mønster som ved normal aldring og kan således influere anderledes på de mekaniske egenskaber (VII).

Intraartikulære injektioner af hyaluronan beskytter effektivt mod brusk-degeneration ved primær OA. Reduktionen af subchondral knogledensitet og -tykkelse, samt ændringen af den trabekulære strukturtype til stavformede, resulterer i en mere

eftergivelig subchondral knogle med deraf følgende reduktion af brusk belastning under stødbelastning. Derudover medfører hyaluronan-behandling en opretholdelse af de mekaniske egenskaber i trabekulær knogle ved at øge mineraliseringen. Tidlig behandling med hyaluronan er en effektiv intervention ved begyndende OA samt ved progression af OA. Tidlig, kortvarig hyaluronan-behandling er nok til at opnå en varig effekt af behandlingen i OA marsvin-modellen (VIII).

Hæmningen af knogleremodellering ved hjælp af bisfosfonatet, Alendronat, fører til en signifikant stigning i den subchondrale knoglemasse og knoglemineralindhold, og udtalte ændringer i mikro-arkitekturen. Derudover resulterer den øgede knoglemasse i en acceleration af artikulær brusk-degeneration på den mediale kondyl, og til en vis grad også på den laterale kondyl. Disse resultater tyder på, at øget subchondral knogle-densitet fremmer OA progression og maner til forsigtighed i brugen af medicin, som virker ved at øge knogledensiteten, i intervention af tidlig OA (IX).

Konklusion

Incidensen af alders-relaterede muskuloskeletale sygdomme øges som et resultat af den stigende ældrepopulation samt af livsstilsændringer. Gennem de sidste par dekader er der lavet meget vigtig sygdomsforskning på trabekulær knogle inden for aldersrelateret knoglefraktur, proteseløsning, knogleremodellering og degenerative knoglesygdomme i både axiale (vertebrae) og perifere knogler. Vi har nu opnået stor viden om normale alders- og sygdomsrelaterede forandringer i knogleegenskaber og -kvalitet. Denne viden er af stor vigtighed for forståelsen af degenerative knoglesygdomme og for design, fiksering og funktionstid af proteser, værtsknogles funktionelle tilpasning samt for anvendelse af biomaterialer med henblik på implantat/væv interaktion og opheling af fraktur og knogledefekter. Forståelsen af mikroarkitektoniske egenskaber, mekaniske tilpasninger samt kollagen og mineral kvalitet i subchondrale knoglevæv, belyst i denne doktordisputats kan bidrage til en større indsigt i patogenesen af degenerative knoglesygdomme, og målrette og bidrage til udviklingen af nye tiltag for forebyggelse og behandling.

Reference list

[1] Aaron JE, Makins NB, Sagreiya K. The microanatomy of trabecular bone loss in normal aging men and women. Clin Orthop 1987; 215: 260-71.

[2] Abdallah BM, Ding M, Jensen CH, Ditzel N, Flyvbjerg A, Jensen TG et al. Dlk1/FA1 is a novel endocrine regulator of bone and fat mass and its serum level is modulated by growth hormone. Endocrinology 2007; 148: 3111-21.

[3] Aigner T, Haag J, Martin J, Buckwalter J. Osteoarthritis: aging of matrix and cells--going for a remedy. Curr Drug Targets 2007; 8: 325-31.

[4] Antoniades L, MacGregor AJ, Matson M, Spector TD. A cotwin control study of the relationship between hip osteoarthritis and bone mineral density. Arthritis Rheum 2000; 43: 1450-5.

[5] Atkinson PJ. Changes in resorption spaces in femoral cortical bone with age. J Pathol Bacteriol 1965; 89: 173-8.

[6] Augat P, Schorlemmer S. The role of cortical bone and its microstructure in bone strength. Age Ageing 2006; 35 Suppl 2: ii27-ii31.: ii27-ii31.

[7] Augat P, Schorlemmer S, Gohl C, Iwabu S, Ignatius A, Claes L. Glucocorticoid-treated sheep as a model for osteopenic trabecular bone in biomaterials research. J Biomed Mater Res 2003; 66A: 457-62.

[8] Bendele AM, Hulman JF. Spontaneous cartilage degeneration in guinea pigs. Arthritis Rheum 1988; 31: 561-5.

[9] Bogoch ER, Moran E. Abnormal bone remodelling in inflammatory arthritis. Can J Surg 1998; 41: 264-71.

[10] Bouxsein ML. Technology insight: noninvasive assessment of bone strength in osteoporosis. Nat Clin Pract Rheumatol 2008; 4: 310-8.

[11] Brandt KD, Radin EL, Dieppe PA, van de Putte L. Yet more evidence that osteoarthritis is not a cartilage disease. Ann Rheum Dis 2006; 65: 1261-4.

[12] Bullough PG. The role of joint architecture in the etiology of arthritis. Osteoarthritis Cartilage 2004; 12 Suppl A: S2-9.: S2-S9.

[13] Burr DB. The contribution of the organic matrix to bone's material properties. Bone 2002; 31: 8-11.

[14] Burr DB, Forwood MR, Fyhrie DP, Martin RB, Schaffler MB, Turner CH. Bone microdamage and skeletal fragility in osteoporotic and stress fractures. J Bone Miner Res 1997; 12: 6-15.

[15] Burr DB, Schaffler MB. The involvement of subchondral mineralized tissues in osteoarthrosis: quantitative microscopic evidence. Microsc Res Tech 1997; 37: 343-57.

[16] Carlson CS, Loeser RF, Purser CB, Gardin JF, Jerome CP. Osteoarthritis in cynomolgus macaques. III: Effects of age, gender, and subchondral bone thickness on the severity of disease. J Bone Miner Res 1996; 11: 1209-17.

[17] Carter DR, Hayes WC. The compressive behavior of bone as a two-phase porous structure. J Bone Joint Surg Am 1977; 59: 954-62.

[18] Chappard D, Retailleau-Gaborit N, Legrand E, Basle MF, Audran M. Comparison insight bone measurements by histomorphometry and microCT. J Bone Miner Res 2005; 20: 1177-84.

[19] Chavassieux P, Seeman E, Delmas PD. Insights into material and structural basis of bone fragility from diseases associated with fractures: how determinants of the biomechanical properties of bone are compromised by disease. Endocr Rev 2007; 28: 151-64.

[20] Croucher PI, Garrahan NJ, Compston JE. Structural mechanisms of trabecular bone loss in primary osteoporosis: specific disease mechanism or early ageing? Bone Miner 1994; 25: 111-21.

[21] Cruz-Orive LM, Karlsson L, Larsen S. Characterizing anisotropy: a new concept. Micron Microscopica Acta 1992; 23: 75-6.

[22] Currey JD, Brear K, Zioupos P. The effects of ageing and changes in mineral content in degrading the toughness of human femora. J Biomech 1996; 29: 257-60.

[23] Dalstra M, Huiskes R, van Erning L. Development and validation of a three-dimensional finite element model of the pelvic bone. J Biomech Eng 1995; 117: 272-8.

[24] Danielsen CC, Andreassen TT. Mechanical properties of rat tail tendon in relation to proximal-distal sampling position and age. J Biomech 1988; 21: 207-12.

[25] Danielsen CC, Andreassen TT, Mosekilde L. Mechanical properties of collagen from decalcified rat femur in relation to age and in vitro maturation. Calcif Tissue Int 1986; 39: 69-73.

[26] Danielsen CC, Mosekilde L, Svenstrup B. Cortical bone mass, composition, and mechanical properties in female rats in relation to age, long-term ovariectomy, and estrogen substitution. Calcif Tissue Int 1993; 52: 26-33.

[27] Davison KS, Siminoski K, Adachi JD, Hanley DA, Goltzman D, Hodsman AB et al. Bone strength: the whole is greater than the sum of its parts. Semin Arthritis Rheum 2006; 36: 22-31.

[28] Day JS, Ding M, Bednarz P, van der Linden JC, Mashiba T, Hirano T et al. Bisphosphonate treatment affects trabecular bone apparent modulus through micro-architecture rather than matrix properties. J Orthop Res 2004; 22: 465-71.

[29] Day JS, Ding M, Odgaard A, Sumner DR, Hvid I, Weinans H. Parallel plate model for trabecular bone exhibits volume fraction-dependent bias. Bone 2000; 27: 715-20.

[30] Day JS, Ding M, van der Linden JC, Hvid I, Sumner DR, Weinans H. A decreased subchondral trabecular bone tissue elastic modulus is associated with pre-arthritic cartilage damage. J Orthop Res 2001; 19: 914-8.

[31] Day JS, van der Linden JC, Bank RA, Ding M, Hvid I, Sumner DR et al. Adaptation of subchondral bone in osteoarthritis. Biorheology 2004; 41: 359-68.

[32] Dempster DW. The pathophysiology of bone loss. Clin Geriatr Med 2003; 19: 259-vi.

[33] Dequeker J, Aerssens J, Luyten FP. Osteoarthritis and osteoporosis: clinical and research evidence of inverse relationship. Aging Clin Exp Res 2003; 15: 426-39.

[34] Dieppe P. Subchondral bone should be the main target for the treatment of pain and disease progression in osteoarthritis. Osteoarthritis Cartilage 1999; 7: 325-6.

[35] Dieppe P, Cushnaghan J, Young P, Kirwan J. Prediction of the progression of joint space narrowing in osteoarthritis of the knee by bone scintigraphy. Ann Rheum Dis 1993; 52: 557-63.

[36] Ding M. Microarchitectural adaptations of primary osteoarthrotic subchondral bone. In: Qin L, Genant HK, Griffith JF, Leung KS, editors. Advanced Bioimaging technologies in assessment of the quality of bone and scaffold materials: Springer-Verlag; 2007; p. 641-55.

[37] Ding M, Cheng L, Bollen P, Schwarz P, Overgaard S. Glucocorticoid Induced Osteopenia in Cancellous Bone of Sheep - Validation of Large Animal Model for Spine Fusion and Biomaterial Research. Spine 2010; 35: Accepted for publication.

[38] Ding M. Age variations in the properties of human tibial trabecular bone and cartilage. Acta Orthop Scand Suppl 2000; 292: 1-45.

[39] Ding M, Dalstra M, Danielsen CC, Kabel J, Hvid I, Linde F. Age variations in the properties of human tibial trabecular bone. J Bone Joint Surg Br 1997; 79: 995-1002.

[40] Ding M, Dalstra M, Linde F, Hvid I. Changes in the stiffness of the human tibial cartilage-bone complex in early-stage osteoarthrosis. Acta Orthop Scand 1998; 69: 358-62.

[41] Ding M, Dalstra M, Linde F, Hvid I. Mechanical properties of the normal human tibial cartilage-bone complex in relation to age. Clin Biomech (Bristol , Avon) 1998; 13: 351-8.

[42] Ding M, Danielsen CC, Hvid I. Bone density does not reflect mechanical properties in early-stage arthrosis. Acta Orthop Scand 2001; 72: 181-5.

[43] Ding M, Danielsen CC, Hvid I. Effects of hyaluronan on three-dimensional microarchitecture of subchondral bone tissues in guinea pig primary osteoarthrosis. Bone 2005; 36: 489-501.

[44] Ding M, Danielsen CC, Hvid I. Age-related three-dimensional microarchitectural adaptations of subchondral bone tissues in guinea pig primary osteoarthrosis. Calcif Tissue Int 2006; 78: 113-22.

[45] Ding M, Danielsen CC, Hvid I. The effects of bone remodeling inhibition by alendronate on three-dimensional microarchitecture of subchondral bone tissues in Guinea pig primary osteoarthrosis. Calcif Tissue Int 2008; 82: 77-86.

[46] Ding M, Day JS, Burr DB, Mashiba T, Hirano T, Weinans H et al. Canine cancellous bone microarchitecture after one year of high-dose bisphosphonates. Calcif Tissue Int 2003; 72: 737-44.

[47] Ding M, Hvid I. Quantification of age-related changes in the structure model type and trabecular thickness of human tibial cancellous bone. Bone 2000; 26: 291-5.

[48] Ding M, Odgaard A, Danielsen CC, Hvid I. Mutual associations among microstructural, physical and mechanical properties of human cancellous bone. J Bone Joint Surg Br 2002; 84: 900-7.

[49] Ding M, Odgaard A, Hvid I. Accuracy of cancellous bone volume fraction measured by micro-CT scanning. J Biomech 1999; 32: 323-6.

[50] Ding M, Odgaard A, Hvid I. Changes in the three-dimensional microstructure of human tibial cancellous bone in early osteoarthritis. J Bone Joint Surg Br 2003; 85: 906-12.

[51] Ding M, Odgaard A, Linde F, Hvid I. Age-related variations in the microstructure of human tibial cancellous bone. J Orthop Res 2002; 20: 615-21.

[52] Eckardt H, Ding M, Lind M, Hansen ES, Christensen KS, Hvid I. Recombinant human vascular endothelial growth factor enhances bone healing in an experimental nonunion model. J Bone Joint Surg Br 2005; 87: 1434-8.

[53] Epstein S. Is cortical bone hip? What determines cortical bone properties? Bone 2007; 41: S3-S8.

[54] Fazzalari NL, Forwood MR, Smith K, Manthey BA, Herreen P. Assessment of cancellous bone quality in severe osteoarthrosis: bone mineral density, mechanics, and microdamage. Bone 1998; 22: 381-8.

[55] Fazzalari NL, Parkinson IH. Fractal properties of subchondral cancellous bone in severe osteoarthritis of the hip. J Bone Miner Res 1997; 12: 632-40.

[56] Felson DT, Neogi T. Osteoarthritis: is it a disease of cartilage or of bone? Arthritis Rheum 2004; 50: 341-4.

[57] Findlay DM. Vascular pathology and osteoarthritis. Rheumatology (Oxford) 2007; 46: 1763-8.

[58] Fisher NL, Lewis TL, Embleton BJ. Statistical analysis of spherical data. Cambridge: Cambridge University Press; 1987, p. 1-329.

[59] Friedman AW. Important determinants of bone strength: beyond bone mineral density. J Clin Rheumatol 2006; 12: 70-7.

[60] Frost HM. Wolff's Law and bone's structural adaptations to mechanical usage: an overview for clinicians. Angle Orthod 1994; 64: 175-88.

[61] Gasser JA, Ingold P, Grosios K, Laib A, Hammerle S, Koller B. Noninvasive monitoring of changes in structural cancellous bone parameters with a novel prototype micro-CT. J Bone Miner Metab 2005; 23 Suppl: 90-6.

[62] Genant HK, Engelke K, Prevrhal S. Advanced CT bone imaging in osteoporosis. Rheumatology (Oxford) 2008; 47 Suppl 4: iv9-16.

[63] Genant HK, Jiang Y. Advanced imaging assessment of bone quality. Ann N Y Acad Sci 2006; 1068: 410-28.: 410-28.

[64] Giesen EB, Ding M, Dalstra M, van Eijden TM. Mechanical properties of cancellous bone in the human mandibular condyle are anisotropic. J Biomech 2001; 34: 799-803.

[65] Giesen EB, Ding M, Dalstra M, van Eijden TM. Architectural measures of the cancellous bone of the mandibular condyle identified by principal components analysis. Calcif Tissue Int 2003; 73: 225-31.

[66] Giesen EB, Ding M, Dalstra M, van Eijden TM. Reduced mechanical load decreases the density, stiffness, and strength of cancellous bone of the mandibular condyle. Clin Biomech (Bristol , Avon) 2003; 18: 358-63.

[67] Giesen EB, Ding M, Dalstra M, van Eijden TM. Changed morphology and mechanical properties of cancellous bone in the mandibular condyles of edentate people. J Dent Res 2004; 83: 255-9.

[68] Goldring SR. Bone and joint destruction in rheumatoid arthritis: what is really happening? J Rheumatol Suppl 2002; 65: 44-8.

[69] Goldring SR. Pathogenesis of bone erosions in rheumatoid arthritis. Curr Opin Rheumatol 2002; 14: 406-10.

[70] Goldring SR, Gravallese EM. Pathogenesis of bone lesions in rheumatoid arthritis. Curr Rheumatol Rep 2002; 4: 226-31.

[71] Goldstein SA, Goulet R, McCubbrey D. Measurement and significance of three-dimensional architecture to the mechanical integrity of trabecular bone. Calcif Tissue Int 1993; 53 Suppl 1: S127-S132.

[72] Goulet RW, Goldstein SA, Ciarelli MJ, Kuhn JL, Brown MB, Feldkamp LA. The relationship between the structural and orthogonal compressive properties of trabecular bone. J Biomech 1994; 27: 375-89.

[73] Grant RA. Estimation of hydroxyproline by the AutoAnalyzer. J Clin Pathol 1965; 18: 686.

[74] Grynpas MD, Alpert B, Katz I, Lieberman I, Pritzker KP. Subchondral bone in osteoarthritis. Calcif Tissue Int 1991; 49: 20-6.

[75] Hald A, Ding M, Egerod K, Hansen RR, Konradsen D, Jorgensen SG et al. Differential effects of repeated low dose treatment with the cannabinoid agonist WIN 55,212-2 in experimental models of bone cancer pain and neuropathic pain. Pharmacol Biochem Behav 2008; 91: 38-46.

[76] Hald A, Hansen RR, Thomsen MW, Ding M, Croucher PI, Gallagher O et al. Cancer-induced bone loss and associated pain-related behavior is reduced by risedronate but not its phosphonocarboxylate analog NE-10790. Int J Cancer 2009; 125: 1177-85.

[77] Hald A, Nedergaard S, Hansen RR, Ding M, Heegaard AM. Differential activation of spinal cord glial cells in murine models of neuropathic and cancer pain. Eur J Pain 2009; 13: 138-45.

[78] Hannan MT, Anderson JJ, Zhang Y, Levy D, Felson DT. Bone mineral density and knee osteoarthritis in elderly men and women. The Framingham Study. Arthritis Rheum 1993; 36: 1671-80.

[79] Harrigan TP, Jasty M, Mann RW, Harris WH. Limitations of the continuum assumption in cancellous bone. J Biomech 1988; 21: 269-75.

[80] Haugeberg G, Orstavik RE, Kvien TK. Effects of rheumatoid arthritis on bone. Curr Opin Rheumatol 2003; 15: 469-75.

[81] Hernandez CJ, Keaveny TM. A biomechanical perspective on bone quality. Bone 2006; 39: 1173-81.

[82] Hildebrand T, Rüegsegger P. A new method for the model-independent assessment of thickness in three-dimensional images. J Micro 1997; 185: 67-75.

[83] Hildebrand T, Rüegsegger P. Quantification of bone microarchitecture with the structure model index. CMBBE 1997; 1: 15-23.

[84] Hogan HA, Ruhmann SP, Sampson HW. The mechanical properties of cancellous bone in the proximal tibia of ovariectomized rats. J Bone Miner Res 2000; 15: 284-92.

[85] Hu JH, Ding M, Soballe K, Bechtold JE, Danielsen CC, Day JS et al. Effects of short-term alendronate treatment on the three-dimensional microstructural, physical, and mechanical properties of dog trabecular bone. Bone 2002; 31: 591-7.

[86] Hunter DJ. Are there promising biologic therapies for osteoarthritis? Curr Rheumatol Rep 2008; 10: 19-25.

[87] Hvid I. Mechanical strength of trabecular bone at the knee. Dan Med Bull 1988; 35: 345-65.

[88] Hvid I. Trabecular bone strength at the knee. Clin Orthop 1988; 227: 210-21.

[89] Hvid I, Hansen SL. Trabecular bone strength patterns at the proximal tibial epiphysis. J Orthop Res 1985; 3: 464-72.

[90] Inaba M, Nagata M, Goto H, Kumeda Y, Kobayashi K, Nakatsuka K et al. Preferential reductions of paraarticular trabecular bone component in ultradistal radius and of calcaneus ultrasonography in early-stage rheumatoid arthritis. Osteoporos Int 2003; 14: 683-7.

[91] Karsdal MA, Leeming DJ, Dam EB, Henriksen K, Alexandersen P, Pastoureau P et al. Should subchondral bone turnover be targeted when treating osteoarthritis? Osteoarthritis Cartilage 2008; 16: 638-46.

[92] Kassem M. Stem cells: potential therapy for age-related diseases. Ann N Y Acad Sci 2006; 1067: 436-42.

[93] Kaufmann J, Mueller A, Voigt A, Carl HD, Gursche A, Zacher J et al. Hydroxypyridinium collagen crosslinks in serum, urine, synovial fluid and synovial tissue in patients with rheumatoid arthritis compared with osteoarthritis. Rheumatology (Oxford) 2003; 42: 314-20.

[94] Keaveny TM, Guo XE, Wachtel EF, McMahon TA, Hayes WC. Trabecular bone exhibits fully linear elastic behavior and yields at low strains. J Biomech 1994; 27: 1127-36.

[95] Keaveny TM, Hayes WC. A 20-year perspective on the mechanical properties of trabecular bone. J Biomech Eng 1993; 115: 534-42.

[96] Keaveny TM, Morgan EF, Niebur GL, Yeh OC. Biomechanics of trabecular bone. Annu Rev Biomed Eng 2001; 3: 307-33.: 307-33.

[97] Keaveny TM, Pinilla TP, Crawford RP, Kopperdahl DL, Lou A. Systematic and random errors in compression testing of trabecular bone. J Orthop Res 1997; 15: 101-10.

[98] Kleerekoper M. Osteoporosis prevention and therapy: preserving and building strength through bone quality. Osteoporos Int 2006; 17: 1707-15.

[99] Kleerekoper M, Villanueva AR, Stanciu J, Rao DS, Parfitt AM. The role of three-dimensional trabecular microstructure in the pathogenesis of vertebral compression fractures. Calcif Tissue Int 1985; 37: 594-7.

[100] Knott L, Bailey AJ. Collagen cross-links in mineralizing tissues: a review of their chemistry, function, and clinical relevance. Bone 1998; 22: 181-7.

[101] Kold S, Bechtold JE, Ding M, Chareancholvanich K, Rahbek O, Soballe K. Compacted cancellous bone has a spring-back effect. Acta Orthop Scand 2003; 74: 591-5.

[102] Kold S, Rahbek O, Toft M, Ding M, Overgaard S, Soballe K. Bone compaction enhances implant fixation in a canine gap model. J Orthop Res 2005; 23: 824-30.

[103] Lane NE, Pressman AR, Star VL, Cummings SR, Nevitt MC. Rheumatoid arthritis and bone mineral density in elderly women. The Study of Osteoporotic Fractures Research Group. J Bone Miner Res 1995; 10: 257-63.

[104] Li B, Aspden RM. Composition and mechanical properties of cancellous bone from the femoral head of patients with osteoporosis or osteoarthritis. J Bone Miner Res 1997; 12: 641-51.

[105] Li B, Aspden RM. Material properties of bone from the femoral neck and calcar femorale of patients with osteoporosis or osteoarthritis. Osteoporos Int 1997; 7: 450-6.

[106] Li H, Zou X, Woo C, Ding M, Lind M, Bunger C. Experimental anterior lumbar interbody fusion with an osteoinductive bovine bone collagen extract. Spine 2005; 30: 890-6.

[107] Li H, Zou X, Woo C, Ding M, Lind M, Bunger C. Experimental lumbar spine fusion with novel tantalum-coated carbon fiber implant. J Biomed Mater Res B Appl Biomater 2006; .

[108] Linde F. Elastic and viscoelastic properties of trabecular bone by a compression testing approach. Dan Med Bull 1994; 41: 119-38.

[109] Linde F, Gothgen CB, Hvid I, Pongsoipetch B. Mechanical properties of trabecular bone by a non-destructive compression testing approach. Eng Med 1988; 17: 23-9.

[110] Linde F, Hvid I. The effect of constraint on the mechanical behaviour of trabecular bone specimens [see comments]. J Biomech 1989; 22: 485-90.

[111] Linde F, Hvid I, Madsen F. The effect of specimen geometry on the mechanical behaviour of trabecular bone specimens. J Biomech 1992; 25: 359-68.

[112] Linde F, Norgaard P, Hvid I, Odgaard A, Soballe K. Mechanical properties of trabecular bone. Dependency on strain rate. J Biomech 1991; 24: 803-9.

[113] Linde F, Sorensen HC. The effect of different storage methods on the mechanical properties of trabecular bone. J Biomech 1993; 26: 1249-52.

[114] Liu XS, Sajda P, Saha PK, Wehrli FW, Bevill G, Keaveny TM et al. Complete volumetric decomposition of individual trabecular plates and rods and its morphological correlations with anisotropic elastic moduli in human trabecular bone. J Bone Miner Res 2008; 23: 223-35.

[115] Macneil JA, Boyd SK. Improved reproducibility of high-resolution peripheral quantitative computed tomography for measurement of bone quality. Med Eng Phys 2007.

[116] Mankin HJ, Dorfman H, Lippiello L, Zarins A. Biochemical and metabolic abnormalities in articular cartilage from osteo-arthritic human hips. II. Correlation of morphology with biochemical and metabolic data. J Bone Joint Surg Am 1971; 53: 523-37.

[117] Mansell JP, Bailey AJ. Abnormal cancellous bone collagen metabolism in osteoarthritis. J Clin Invest 1998; 101: 1596-603.

[118] Mansell JP, Tarlton JF, Bailey AJ. Biochemical evidence for altered subchondral bone collagen metabolism in osteoarthritis of the hip. Br J Rheumatol 1997; 36: 16-9.

[119] Martin B. Aging and strength of bone as a structural material. Calcif Tissue Int 1993; 53 Suppl 1: S34-S39.

[120] Martin RB. Is all cortical bone remodeling initiated by microdamage? Bone 2002; 30: 8-13.

[121] Martin TJ, Seeman E. New mechanisms and targets in the treatment of bone fragility. Clin Sci (Lond) 2007; 112: 77-91.

[122] Mashiba T, Hirano T, Turner CH, Forwood MR, Johnston CC, Burr DB. Suppressed bone turnover by bisphosphonates increases microdamage accumulation and reduces some biomechanical properties in dog rib [see comments]. J Bone Miner Res 2000; 15: 613-20.

[123] McCalden RW, McGeough JA, Barker MB, Court BC. Age-related changes in the tensile properties of cortical bone. The relative importance of changes in porosity, mineralization, and microstructure. J Bone Joint Surg Am 1993; 75: 1193-205.

[124] Mosekilde L. Age-related changes in vertebral trabecular bone architecture--assessed by a new method. Bone 1988; 9: 247-50.

[125] Mosekilde L. Vertebral structure and strength in vivo and in vitro. Calcif Tissue Int 1993; 53 Suppl 1: S121-S125.

[126] Mosekilde L. The effect of modelling and remodelling on human vertebral body architecture. Technol Health Care 1998; 6: 287-97.

[127] Mosekilde Li, Mosekilde Le, Danielsen CC. Biomechanical competence of vertebral trabecular bone in relation to ash density and age in normal individuals. Bone 1987; 8: 79-85.

[128] Neuman RE, Logan MA. The determination of collagen and elastin in tissues. J Biol Chem 1950; 186: 549-56.

[129] Nevitt MC. Epidemiology of osteoporosis. In: Lane NE, editor. Rheumatic Disease Clinics of North America: Osteoporosis. Philadelphia: W.B.Saunders Company; 1994; p. 535-59.

[130] O'Brien FJ, Brennan O, Kennedy OD, Lee TC. Microcracks in cortical bone: how do they affect bone biology? Curr Osteoporos Rep 2005; 3: 39-45.

[131] Odgaard A. Three-dimensional methods for quantification of cancellous bone architecture. Bone 1997; 20: 315-28.

[132] Odgaard A, Gundersen HJ. Quantification of connectivity in cancellous bone, with special emphasis on 3-D reconstructions. Bone 1993; 14: 173-82.

[133] Odgaard A, Hvid I, Linde F. Compressive axial strain distributions in cancellous bone specimens. J Biomech 1989; 22: 829-35.

[134] Odgaard A, Jensen EB, Gundersen HJ. Estimation of structural anisotropy based on volume orientation. A new concept. J Microsc 1990; 157: 149-62.

[135] Odgaard A, Kabel J, van Rietbergen B, Dalstra M, Huiskes R. Fabric and elastic principal directions of cancellous bone are closely related [see comments]. J Biomech 1997; 30: 487-95.

[136] Odgaard A, Linde F. The underestimation of Young's modulus in compressive testing of cancellous bone specimens. J Biomech 1991; 24: 691-8.

[137] Olivieri I, Palazzi C, Peruz G, Padula A. Management issues with elderly-onset rheumatoid arthritis: an update. Drugs Aging 2005; 22: 809-22.

[138] Overgaard S. Calcium phosphate coatings for fixation of bone implants - Evaluated mechanically and histologically by stereological methods. Acta Orthop Scand 2000; 71: 1-74.

[139] Overgaard S, Soballe K, Jorgen H, Gundersen G. Efficiency of systematic sampling in histomorphometric bone research illustrated by hydroxyapatite-coated implants: optimizing the stereological vertical-section design. J Orthop Res 2000; 18: 313-21.

[140] Oxlund H, Barckman M, Ortoft G, Andreassen TT. Reduced concentrations of collagen cross-links are associated with reduced strength of bone. Bone 1995; 17: 365S-71S.

[141] Oxlund H, Mosekilde L, Ortoft G. Reduced concentration of collagen reducible cross links in human trabecular bone with respect to age and osteoporosis. Bone 1996; 19: 479-84.

[142] Parfitt AM. Age-related structural changes in trabecular and cortical bone: cellular mechanisms and biomechanical consequences. Calcif Tissue Int 1984; 36 Suppl 1: S123-S128.

[143] Parfitt AM. Trabecular bone architecture in the pathogenesis and prevention of fracture. Am J Med 1987; 82: 68-72.

[144] Parfitt AM. The bone remodeling compartment: a circulatory function for bone lining cells. J Bone Miner Res 2001; 16: 1583-5.

[145] Parfitt AM. Targeted and nontargeted bone remodeling: relationship to basic multicellular unit origination and progression. Bone 2002; 30: 5-7.

[146] Parfitt AM. What is the normal rate of bone remodeling? Bone 2004; 35: 1-3.

[147] Parfitt AM, Mathews CH, Villanueva AR, Kleerekoper M, Frame B, Rao DS. Relationships between surface, volume, and thickness of iliac trabecular bone in aging and in osteoporosis. Implications for the microanatomic and cellular mechanisms of bone loss. J Clin Invest 1983; 72: 1396-409.

[148] Perez-Edo L, ez-Perez A, Marinoso L, Valles A, Serrano S, Carbonell J. Bone metabolism and histomorphometric changes in rheumatoid arthritis. Scand J Rheumatol 2002; 31: 285-90.

[149] Qin L, Zhang G, Sheng H, Yeung KW, Yeung HY, Chan CW et al. Multiple bioimaging modalities in evaluation of an experimental osteonecrosis induced by a combination of lipopolysaccharide and methylprednisolone. Bone 2006; 39: 863-71.

[150] Quarto R, Mastrogiacomo M, Cancedda R, Kutepov SM, Mukhachev V, Lavroukov A et al. Repair of large bone defects with the use of autologous bone marrow stromal cells. N Engl J Med 2001; 344: 385-6.

[151] Radin EL, Abernethy PJ, Townsend M, Rose RM. The role of bone changes in the degeneration of articular cartilage in osteoarthrosis. Acta Orthop belg 1987; 44: 55-63.

[152] Radin EL, Paul IL, Rose RM. Role of mechanical factors in pathogenesis of primary osteoarthritis. Lancet 1972; 1: 519-22.

[153] Radin EL, Rose RM. Role of subchondral bone in the initiation and progression of cartilage damage. Clin Orthop 1986: 34-40.

[154] Raisz LG. Pathogenesis of osteoporosis: concepts, conflicts, and prospects. J Clin Invest 2005; 115: 3318-25.

[155] Riggs BL. Overview of osteoporosis. West J Med 1991; 154: 63-77.

[156] Rogers J, Shepstone L, Dieppe P. Is osteoarthritis a systemic disorder of bone? Arthritis Rheum 2004; 50: 452-7.

[157] Røhl L, Larsen E, Linde F, Odgaard A, Jorgensen J. Tensile and compressive properties of cancellous bone. J Biomech 1991; 24: 1143-9.

[158] Røhl L, Linde F, Odgaard A, Hvid I. Simultaneous measurement of stiffness and energy absorptive properties of articular cartilage and subchondral trabecular bone. Proc Inst Mech Eng H 1997; 211: 257-64.

[159] Rüegsegger P, Koller B, Muller R. A microtomographic system for the nondestructive evaluation of bone architecture. Calcif Tissue Int 1996; 58: 24-9.

[160] Schaffler MB, Choi K, Milgrom C. Aging and matrix microdamage accumulation in human compact bone. Bone 1995; 17: 521-5.

[161] Seeman E. Osteoporosis in men. Baillieres Clin Rheumatol 1997; 11: 613-29.

[162] Seeman E. Pathogenesis of bone fragility in women and men. Lancet 2002; 359: 1841-50.

[163] Seeman E. Reduced bone formation and increased bone resorption: rational targets for the treatment of osteoporosis. Osteoporos Int 2003; 14 Suppl 3: S2-S8.

[164] Selvik G. Roentgen stereophotogrammetry. A method for the study of the kinematics of the skeletal system. Acta Orthop Scand Suppl 1989; 232: 1-51.

[165] Sharp DJ, Tanner KE, Bonfield W. Measurement of the density of trabecular bone. J Biomech 1990; 23: 853-7.

[166] Shibuya K, Hagino H, Morio Y, Teshima R. Cross-sectional and longitudinal study of osteoporosis in patients with rheumatoid arthritis. Clin Rheumatol 2002; 21: 150-8.

[167] Silva MJ. Biomechanics of osteoporotic fractures. Injury 2007; 38 Suppl 3: S69-S76.

[168] Soballe K. Hydroxyapatite ceramic coating for bone implant fixation. Mechanical and histological studies in dogs. Acta Orthop Scand Suppl 1993; 255: 1-58.

[169] Sogaard CH, Danielsen CC, Thorling EB, Mosekilde L. Long-term exercise of young and adult female rats: effect on femoral neck biomechanical competence and bone structure. J Bone Miner Res 1994; 9: 409-16.

[170] Stauber M, Muller R. Age-related changes in trabecular bone microstructures: global and local morphometry. Osteoporos Int 2006; 17: 616-26.

[171] Stauber M, Muller R. Volumetric spatial decomposition of trabecular bone into rods and plates--a new method for local bone morphometry. Bone 2006; 38: 475-84.

[172] Steiniche T. Bone histomorphometry in the pathophysiological evaluation of primary and secondary osteoporosis and various treatment modalities. APMIS Suppl 1995; 51: 1-44.

[173] Stepan JJ, Burr DB, Pavo I, Sipos A, Michalska D, Li J et al. Low bone mineral density is associated with bone microdamage accumulation in postmenopausal women with osteoporosis. Bone 2007; 41: 378-85.

[174] Sumner DR, Turner TM, Urban RM, Virdi AS, Inoue N. Additive enhancement of implant fixation following combined treatment with rhTGF-beta2 and rhBMP-2 in a canine model. J Bone Joint Surg Am 2006; 88: 806-17.

[175] Turner AS. Animal models of osteoporosis--necessity and limitations. Eur Cell Mater 2001; 1: 66-81.: 66-81.

[176] Turner CH. Biomechanics of bone: determinants of skeletal fragility and bone quality. Osteoporos Int 2002; 13: 97-104.

[177] Turner CH, Burr DB. Basic biomechanical measurements of bone: a tutorial. Bone 1993; 14: 595-608.

[178] Turner CH, Pavalko FM. Mechanotransduction and functional response of the skeleton to physical stress: the mechanisms and mechanics of bone adaptation. J Orthop Sci 1998; 3: 346-55.

[179] Vaananen HK. Pathogenesis of osteoporosis. Calcif Tissue Int 1991; 49 Suppl: S11-S14.

[180] Valstar ER, Gill R, Ryd L, Flivik G, Borlin N, Karrholm J. Guidelines for standardization of radiostereometry (RSA) of implants. Acta Orthop 2005; 76: 563-72.

[181] van Rietbergen B, Weinans H, Huiskes R, Odgaard A. A new method to determine trabecular bone elastic properties and loading using micromechanical finite-element models. J Biomech 1995; 28: 69-81.

[182] van Ruijven LJ, Giesen EB, Mulder L, Farella M, van Eijden TM. The effect of bone loss on rod-like and plate-like trabeculae in the cancellous bone of the mandibular condyle. Bone 2005; 36: 1078-85.

[183] Verdonschot N, van Hal CT, Schreurs BW, Buma P, Huiskes R, Slooff TJ. Time-dependent mechanical properties of HA/TCP particles in relation to morsellized bone grafts for use in impaction grafting. J Biomed Mater Res 2001; 58: 599-604.

[184] Viguet-Carrin S, Garnero P, Delmas PD. The role of collagen in bone strength. Osteoporos Int 2006; 17: 319-36.

[185] Waarsing JH, Day JS, van der Linden JC, Ederveen AG, Spanjers C, De CN et al. Detecting and tracking local changes in the tibiae of individual rats: a novel method to analyse longitudinal in vivo micro-CT data. Bone 2004; 34: 163-9.

[186] Wang X, Bank RA, TeKoppele JM, Agrawal CM. The role of collagen in determining bone mechanical properties. J Orthop Res 2001; 19: 1021-6.

[187] Wang X, Puram S. The toughness of cortical bone and its relationship with age. Ann Biomed Eng 2004; 32: 123-35.

[188] Watson PJ, Hall LD, Malcolm A, Tyler JA. Degenerative joint disease in the guinea pig. Use of magnetic resonance imaging to monitor progression of bone pathology. Arthritis Rheum 1996; 39: 1327-37.

[189] Watts NB. Bone quality: getting closer to a definition. J Bone Miner Res 2002; 17: 1148-50.

[190] Wehrli FW. Structural and functional assessment of trabecular and cortical bone by micro magnetic resonance imaging. J Magn Reson Imaging 2007; 25: 390-409.

[191] Whitehouse WJ. The quantitative morphology of anisotropic trabecular bone. J Microsc 1974; 101 Pt 2: 153-68.

[192] Woessner JF. Determination of hydroxyproline in connective tissue. In: Hall DA, editor. The Methodology of Connective Tissue Research. Oxford: Joynson-Bruvvers Ltd; 1976; p. 227-33.

[193] Wolff J. Ueber die innere Architectur der Knochen und ibre Bedeutung fiir die Frage vom Knochenwacbstum. Virchow Arch Pathol Anat Physiol KlinMed 1870; 50: 389-450.

[194] Yerramshetty JS, Akkus O. The associations between mineral crystallinity and the mechanical properties of human cortical bone. Bone 2008; 42: 476-82.

[195] Zhu M, Keller TS, Moeljanto E, Spengler DM. Multiplanar variations in the structural characteristics of cancellous bone. Bone 1994; 15: 251-9.

[196] Zioupos P, Currey JD, Hamer AJ. The role of collagen in the declining mechanical properties of aging human cortical bone. J Biomed Mater Res 1999; 45: 108-16.

ISSN 1745-3674